Co-culture of *Acetobacterium woodii* and *Clostridium drakei* using CO_2 and *in situ* generated H_2 to produce caproic acid via lactic acid

Vom Promotionsausschuss der
Technischen Universität Hamburg
zur Erlangung des akademischen Grades
Doktor-Ingenieur (Dr.-Ing.)

genehmigte Dissertation

von
Jan Herzog

aus
Mühlacker

2024

1. Gutachter: Prof. Dr. rer. nat. An-Ping Zeng
2. Gutachter: Prof. Dr.-Ing. Michael Schlüter
Vorsitzender: Prof. Dr. rer. nat. Johannes Gescher

Tag der mündlichen Prüfung: 19. Dezember 2023

Identifiers
DOI: https://doi.org/10.15480/882.9002
Handle: https://hdl.handle.net/11420/44848
ORCID: https://orcid.org/0000-0002-7555-8805

Abstract

Syngas fermentation processes have been proposed as promising technology for high value chemical production from one carbon compounds including CO_2, reducing both direct carbon emissions and replacing fossil fuels as feedstock in the chemical industry. Among the potential microorganisms able to utilize CO_2 as main carbon source, *Acetobacterium woodii* is one of the most extensively studied and is considered a model organism for acetogens. Its main metabolite is the rather low value product acetic acid; however, recent recombinant strains are capable of producing lactate from CO_2 and H_2. Using the chain-elongating bacteria *Clostridium drakei*, a synthetic co-culture has the potential to produce higher value products such as caproic acid. In this study, a synthetic co-culture with the acetogens *Acetobacterium woodii* and *Clostridium drakei* in a stirred tank bioreactor, using CO_2 and H_2 as substrates for the production of caproic acid via the intermediate lactate was successfully developed and established. The H_2 for the process was generated *in situ* with an All-in-One electrode, which was designed for effective H_2 generation in any standard bioreactor. Caproate concentrations reached a maximum concentration of 0.1 g L^{-1} and a yield from lactate of up to 0.2 g g^{-1}. The co-cultivation was found to be beneficial for *Clostridium drakei* as inhibiting effects observed in pure culture were not noticed during co-cultivations. For the development of the co-culture, both strains were characterized separately. The recently developed strain *Acetobacterium woodii ΔlctBCD ΔpyrE* [p83_P_{bgaL}_NFP] was found to be the most promising in comparison to other *Acetobacterium woodii* strains, reaching 0.5 g L^{-1} of lactate in the bioelectrochemical system with a volumetric productivity of up to 0.2 g L^{-1} d^{-1}. H_2 supply limitation was identified as the major bottleneck for the fermentations with the All-in-One electrode, as conventional gas fermentations with the same *Acetobacterium woodii* strain yielded 8.1 g L^{-1} lactate with a volumetric productivity of up to 2.0 g L^{-1} d^{-1}. Nonetheless, cathode surface enlargement and reduction of Faradaic losses or numbering-up of the All-in-One could increase H_2 production and thus lactate production. To the author's best knowledge, this is the first study to show data of *Clostridium drakei* cultivations in a stirred-tank bioreactor growing on lactate. The maximum caproate concentration added up to 1.5 g L^{-1} with a volumetric productivity of 0.7 g L^{-1} d^{-1}. The inhibitory level of caproic acid was identified at 1.5 g L^{-1}. Lastly, a lactate dependent process control was developed for the co-cultivation process, which can adjust the H_2 production rate dynamically depending on the lactate concentrations measured online during the cultivation.

Acknowledgments

I would like to express my gratitude to the following people, for without them, this project would not have been possible.
First and foremost, I would like to thank my supervisor Prof. Dr. An-Ping Zeng for his invaluable supervision, the helpful scientific discussions, and his patience during my PhD study. I am deeply grateful to him for giving me the opportunity to work on this project at his institute. I would also like to thank Prof. Dr. Michael Schlüter and Prof. Dr. Johannes Gescher for their contribution as second examiner and chair to this thesis and the interesting discussions we had within the DFG priority program and during conferences. Furthermore, I would like to express my deepest gratitude to my project partners Dr. Frank Bengelsdorf and Alexander Mook at the Ulm University. Thank you, Frank, for the invaluable help with the publications, your mentoring and the scientific exchange of ideas as well as fruitful discussions. Alex, you have been the best project partner I could have imagined. Thank you for your excellent bacterial strains, the mutual help with our publications and the good times we had during the priority program. I am also very thankful to Prof. Dr. Dirk Weuster-Botz and Miriam Bäumler from the Technical University of München for the opportunity and the support to test the *A. woodii* strain at their lab with direct gas sparging. I would like to thank my students, Lotta Guhl, Imer Itez and Preethi Gurumoorthi for their invaluable and diligent work on this project. Thank you to all my fellow colleagues at the IBB, especially Yaeseong, Philipp, Tyll, Giovanni, Jonas, and Ludwig for your support over the years. Our fruitful discussions, the help in the lab and in general the good times were priceless and motivated me to pursue my goals. In addition, I would like to thank Sebastian Hofmann for his motivational support throughout this journey and the side projects we did for the priority program. Thanks to him and all my colleagues from the InterZell program, especially Thi, Franzi, Tobi, Simone, Simon, and Karin, for all the good times we had during the InterZell meetings and courses. I am deeply grateful to my wife Paulina, who is my biggest support and motivator. Thank you for your understanding and patience, for your encouragement and for all the sacrifices you had to make during these years. Finally, I would also like to thank my parents for their everlasting support in my life and helping me to realize my dreams.

This project was funded by the Deutsche Forschungsgemeinschaft (DFG – 427864786) as part of the priority program InterZell (SPP 2170). Thank you for funding my research.

Table of Contents

Abbreviations

Abbreviation	Definition
ADP	Adenosine diphosphate
AiO	All in one electrode
ATP	Adenosine triphosphate
ATPase	ATP synthase
BES	Bioelectrochemical system
BCR	Bubble column reactor
CE	Counter electrode
CSTR	Continuous stirred tank reactor
DCW	Dry cell weight
DET	Direct electron transfer
DI	Deionized
DMSO	Dimethyl Sulfoxide
Ech	Energy converting hydrogenase
EFC	Enzymatic fuel cell
Etf	Electron-transferring flavoprotein
FAST	Fluorescence-fusion and absorption-shifting tag
$Fd_{red/ox}$	Ferredoxin in reduced and oxidized form
FISH	Fluorescence *in situ* hybridization
HPLC	High performance liquid chromatography
Hyd	Hydrogenase
IET	Indirect electron transfer
LDH	Lactate dehydrogenase
MFC	Microbial fuel cell
NAD^+/NADH	Nicotinamide adenine dinucleotide
ORP	Oxidation / reduction potential
SHE	Standard hydrogen electrode
THF	Tetrahydrofolate
RE	Reference electrode
Rnf	Ferredoxin:NAD^+-oxidoreductase (*Rhodobacter* nitrogen fixation)
WE	Working electrode
WLP	Wood-Ljungdahl pathway
WT	Wild type strain

Nomenclature

Symbol	Unit	Description
A	cm²	Area
A_e	cm²	Surface area of an electrode
A_I	m²	Area of the interface between a gas and a liquid phase
a	$m^2\ m^{-3}$	Specific interfacial area of a gas bubble
C_i^*	-	Number of carbon atoms of a product compound *i*
C_j^*	-	Number of carbon atoms of a substrate compound *j*
c_{Ac}	$g\ L^{-1}$	Acetate concentration
c_{But}	$g\ L^{-1}$	Butyrate concentration
c_{Cap}	$g\ L^{-1}$	Caproate concentration
c_{Form}	$g\ L^{-1}$	Formate concentration
c_{Fruc}	$g\ L^{-1}$	Fructose concentration
c_i	$mol\ L^{-1}$	Concentration of a compound *i*
$c_{i,G}$	$mol\ L^{-1}$	Concentration of a compound *i* in the gas phase
$c_{i,L}$	$mol\ L^{-1}$	Concentration of a compound *i* in the bulk liquid
c_{Lac}	$g\ L^{-1}$	Lactate concentration
c_{ox}	$g\ L^{-1}$	Concentration of an oxidized species
c_P	$g\ L^{-1}$	Product concentration
c_{red}	$g\ L^{-1}$	Concentration of a reduced species
c_s	$g\ L^{-1}$	Substrate concentration
$c^*_{i,G}$	$mol\ L^{-1}$	Concentration of a compound *i* in the gas film at the interface
$c^*_{i,L}$	$mol\ L^{-1}$	Concentration of a compound *i* in the liquid film at the interface
D_i	$cm^2\ s^{-1}$	Diffusion coefficient of a compound *i*
d	m	Diameter
E	V	Cell potential
E^0	V	Standard cell potential
$E_{p,a}$	V	Anodic peak potential
$E_{p,c}$	V	Cathodic peak potential
F	$C\ mol^{-1}$	Faraday constant ($9.65 \times 10^4\ C\ mol^{-1}$)
g	$m\ s^{-2}$	Gravitational acceleration
H_s^{cp}	$mol\ L^{-1}\ atm^{-1}$	Henry’s solubility constant
h	m	Liquid height above the sparger in a bubble column reactor
I	A	Electrical current

Symbol	Unit	Description
I_{AiO}	mA	Electrical current of the AiO electrode
$I_{p,a}$	A	Anodic peak current
$I_{p,c}$	A	Cathodic peak current
j	A cm^{-2}	Electrical current density
K_s	g L^{-1}	Substrate saturation constant
k_G	m s^{-1}	Mass transfer coefficient in the gas phase
k_L	m s^{-1}	Mass transfer coefficient in the liquid phase
k_La	s^{-1}	Volumetric mass transfer coefficient in the liquid phase
M_{gas}	g mol^{-1}	Molar mass of a gas
N	s^{-1}	Stirrer speed
Ne	-	Newton number
$N_{i,G}$	mol L^{-1} s^{-1}	Mass transfer rate of a compound *i* across the gas boundary layer
$N_{i,L}$	mol L^{-1} s^{-1}	Mass transfer rate compound *i* across the liquid boundary layer
n_i	mol	Amount of a product compound *i*
n_j	mol	Amount of a product compound *j*
OD_{600}	-	Optical density measured at 600 nm
OD_{Ind}	-	OD_{600} of time point of induction
OD_{max}	-	Maximum OD_{600}
P_{vol}	g L^{-1} d^{-1}	Volumetric productivity
$P\ V^{-1}$	W L^{-1}	Volumetric power input
p	atm	Pressure
p_i	atm	Partial pressure of a gas *i*
p_U	Pa	Head space pressure
Q	C	Electrical charge
q_{Cap}	g h^{-1}	Caproate formation rate
q_{H2}	mmol h^{-1}	Hydrogen evolution rate
q_{Lac}	g h^{-1}	Lactate formation rate
$-q_{Lac}$	g h^{-1}	Lactate consumption rate
q_P	g g^{-1} L^{-1}	Specific product formation rate
q_S	g g^{-1} L^{-1}	Specific substrate consumption rate
R	J mol^{-1} K^{-1}	Universal gas constant (8.314 J mol^{-1} K^{-1})
R_C	-	Carbon recovery
Re	-	Reynolds number
R_{elec}	Ω	Electrical resistance

Symbol	**Unit**	**Description**
$R_{e/s}$	mol s^{-1} cm^{-2}	Reaction rate on the electrode-solution interface
r_i	g L^{-1} h^{-1}	Reaction rate of a component *i*
T	K	Temperature
t	h	Time
U	V	Electrical voltage
U_{av}	V	Average voltage of the AiO electrode during an experiment
U_e	V	Applied cell voltage
U_{ref}	V	Voltage between working and reference electrode
V	m^3	Volume
V_0	L	Initial working volume
$\dot{V}_{gas}$	m^3 s^{-1}	Gas flow rate
V_R	m^3	Reactor volume
vvm	L L^{-1} min^{-1}	Volume specific gas flow rate
v/v	L L^{-1}	Volume per volume
$v\%$	L L^{-1}	Volume percent
$w\%$	g g^{-1}	Mass percent
X	g L^{-1}	Biomass concentration
X_0	g L^{-1}	Initial biomass concentration
$Y_{P/S}$	g g^{-1}	Product yield coefficient
$Y_{X/S}$	g g^{-1}	Biomass yield coefficient
z	-	Number of electrons transferred in a redox reaction
χ_i	-	Fraction of a gas *i* in the total gas stream
$\Delta G_0'$	kJ mol^{-1}	Gibb's free energy change
$\Delta OD_{20/40\,h}$	-	Cell density increase during the first 20 or 40 h of fermentation time
η	kg m^{-1} s^{-1}	Dynamic viscosity
η_F	-	Faradic efficiency
μ	h^{-1}	Specific cell growth rate
μ_{max}	h^{-1}	Maximum cell growth rate
ν_{SR}	V s^{-1}	Scan rate
ρ_{gas}	kg m^{-3}	Density of a gas
ρ_L	kg m^{-3}	Density of a liquid

1 Introduction

In 1896, the chemist Svante Arrhenius published a hypothesis based on the previous work of Eunice Newton Foote and John Tyndall (Jackson, 2020), stating that an increase in carbon dioxide (CO_2) in the atmosphere could lead to an increase in global temperatures (Arrhenius, 1896). Half a century later, the increase of CO_2 in the atmosphere was first measured and in 1979, the National Academy of Sciences (USA) reported that the earth's temperature is increasing due to CO_2 emissions caused by humankind (Charney et al., 1979). This was 44 years ago. In 2015, the majority of nations worldwide signed the Paris Agreement, finally pledging to "pursue efforts to limit the global temperature increase to 1.5 °C above pre-industrial levels" (United Nations, 2015). However, global surface temperatures have already reached +1.1 °C and crossing the +1.5 °C mark cannot be averted anymore. With the current efforts of all nations which signed the Paris Agreement to reduce greenhouse gas emissions, global temperatures will likely exceed 2.0 °C above pre-industrial levels by 2050 (Masson-Delmotte et al., 2021). The temperature increase is already causing climate and weather extremes everywhere across the globe and these hazards will intensify if greenhouse gas emissions are not reduced to a net zero margin (Lee et al., 2023). Therefore, the transformation of all major industries towards climate neutral technologies is overdue.

The production of chemicals alone accounted for 925 Mt of CO_2 in 2021 which makes this sector the third largest industrial sector concerning direct CO_2 emissions (IEA, Paris, 2022). This is mostly due to the usage of fossil fuels as feedstocks, which must be replaced with climate neutral alternatives. Modern biotechnological processes are already capable of producing many chemicals, e.g., fuels, from biological sources (Naik et al., 2010). However, these so-called first-generation biofuels are based on food crops such as corn or sugarcane, and many groups have expressed their concerns, regarding the increase in total demand for agricultural land, increased nitrous oxide emissions and furthermore competition with the critical resource food (Daniell et al., 2012). Consequently, the biotechnological industry has developed processes which utilize energy-dense biomass from waste streams, such as agricultural, municipal or food wastes, as feedstock for biofuel and fine chemical production (Naik et al., 2010; Wainaina et al., 2018). Not only do they not compete with human alimentation and the usage of arable land, their abundance and low costs make them especially attractive for utilization as feedstock (Wainaina et al., 2018). Plant materials in these waste streams containing lignocellulose can be transformed directly with cellulolytic microorganisms, however for an industrial application, the conversion rates and productivities still face too many challenges (Brown and Brown, 2013). Most lignocellulose-based processes require therefore a pretreatment step to either break down polysaccharides into fermentable monosaccharides (Haghighi Mood et al., 2013) or transform lignocellulose via gasification into a mixture of carbon monoxide (CO), CO_2, hydrogen (H_2) and nitrogen, so called syngas, which can then be used by anaerobic bacteria in syngas fermentations (Liew et al., 2016). However, these pretreatments are either energy or water intensive, therefore facing high costs as major drawback. A promising solution is the utilization of waste gases directly from their emitters: the steel and cement industry as well as from oil refining or coal and natural gas (Dürre and Eikmanns, 2015). Not only do these waste gases contain high contents of fermentable syngas, but they are also obtainable at low cost and do not need energy intensive pretreatment steps (Abubackar et al., 2011). Furthermore, by consuming the same waste gases which are causing climate change directly as feedstocks instead of releasing them into the atmosphere, a real impact can be contributed towards a circular bioeconomy and a reduction of greenhouse gas emissions (Liew et al., 2016; Bengelsdorf and Dürre, 2017; Takors et al., 2018).

Bacteria such as acetogens which can use CO_2 as carbon source also require H_2 as energy source in large quantities to metabolize CO_2. Although syngas from waste streams usually contains H_2, the amount varies strongly depending on its source (Hiller et al., 2003). If the waste gas only contains CO_2 or insufficient amounts of H_2, the latter must be added to the bioreactor to assure high productivities. Unfortunately, 99 % of the worldwide produced H_2 comes from fossil-based sources such as natural gas or coal, causing associated CO_2 emissions of up to 900 Mt in 2021 (IEA, 2022). Furthermore, it is estimated that only 24 Mt could be produced from low-emission sources by 2030, despite the fact that H_2 will be a critical element in the energy transition (IEA, 2022). This implies that in the near future, no sustainable H_2 grid will be available. One solution to already ensure carbon neutral H_2 for syngas fermentation processes could be using flexible electrolysis units powered from renewable sources like wind or solar energy directly at the fermentation site. Given that cultivation media are water based, electrolysis could even be performed *in situ*, e.g., with the All-in-One (AiO) electrode which can be easily integrated into a bioreactor (Utesch and Zeng, 2018). The AiO electrode has shown effective H_2 generation in various fermentation processes (Arbter et al., 2019; Utesch et al., 2019) and has also the potential for large scale applications. This set up has the potential for a true-low emission syngas fermentation process for the production of value chemicals.

2 Objectives

The goal of this study is to establish a low-emission syngas fermentation process for the production of the value chemical caproic acid. For this, a synthetic co-culture of the acetogens *Acetobacterium woodii* and *Clostridium drakei* in a stirred-tank reactor was chosen, where *A. woodii* uses CO_2 and H_2 to produce the intermediate lactate, while *C. drakei* generates the final product caproic acid from lactate. The H_2 for this process should be generated *in situ* from the AiO electrode.

For the envisaged process development, it is first necessary to investigate cell growth and product formation in a stirred-tank bioreactor of both bacterial strains separately, to reach a deeper understanding of the metabolic processes and to adjust technical parameters if necessary to optimize cell growth and product formation. Thus, pure cultures of different *A. woodii* strains need to be characterized regarding optimal growth and lactate formation in the bioelectrochemical system (BES) utilizing the AiO electrode for H_2 production to identify the most promising strain. Furthermore, it is necessary to compare process performance of the BES to conventional gas fermentations in order to determine possible limitations of the BES and optimize it if applicable.

Pure cultivations of *C. drakei* in a stirred tank reactor should be characterized regarding lactate uptake and caproate production. Furthermore, potential growth inhibition concentrations of caproic acid must be determined and the impacts of co-culture conditions, i.e., culture medium, electric voltages from the AiO electrode and low inoculation cell densities need to be identified.

In a final step, an automatic process control system should be developed to adjust the H_2 generation rate of the AiO electrode based on the concentration of the intermediate lactate in the cultivation medium to limit the extensive use of electricity.

3 Theoretical Background

3.1. Acetogens

Acetogens are a group of obligate anaerobic microorganisms which were defined as being able to use the acetyl-CoA pathway for acetyl-CoA and biomass synthesis from CO_2 as well as for energy conservation (Drake, 1995). The first acetogen, *Clostridium aceticum*, was isolated in 1936 and was found to grow on H_2 and CO_2 (Wieringa, 1936). Since then, a large number of acetogens have been discovered and isolated (see Table 3-1 for a selection of acetogens), the majority being of the genera *Acetobacterium* and *Clostridium*. These microorganisms are usually found in anoxic habitats such as fresh water or marine sediments, sewage sludge or gastrointestinal tracts but also in hypersaline sediments, deep aquifers, oxic soils or plant roots (Drake et al., 2006). However, the group of acetogens vary greatly in their nutritional, morphological and physiological properties (Drake et al., 2008). Most acetogens grow optimally at moderate temperatures in between 30 – 40 °C while others are among the thermophiles (optimal growth temperature of 55 – 80 °C) or even psychrophiles (growth at or below 20 °C) (Drake et al., 2008). Although the name acetogen might suggests the formation of acetate as the defining property for all acetogens, this is not exclusively true (Drake et al., 2006). Acetogens have been found to produce other products from acetyl-CoA like ethanol, butyrate, butanol (Drake et al., 2006) and even 2,3-butandiol (Köpke et al., 2011), while other bacteria like *Acetobacter aceti* are known to produce acetate but are not part of the acetogen group (Drake et al., 2006).

3.1.1. Acetyl-CoA Pathway

As mentioned before in Chapter 3.1, acetogens are able to use CO_2 for acetyl-CoA synthesis, for assimilation into cell carbon as well as for energy conservation. This ability makes acetogens a very interesting group of microorganisms for applications in the emerging field of circular bioeconomy, using waste products like CO_2 and CO in syngas fermentations for the production of new value products (see Chapter 3.4). Acetogens can utilize CO_2 via the acetyl-CoA pathway, a reductive pathway for the C1 components CO and CO_2. In contrast to other CO_2 fixing pathways such as the Calvin cycle, the reductive tricarboxylic acid cycle or the hydroxypropionate cycle, the acetyl-CoA pathway is a non-circular pathway (Drake et al., 2008). The acetyl-CoA pathway is also called Wood-Ljungdahl pathway (WLP) after the groundbreaking work of Lars G. Ljungdahl and Harland G. Wood which led to discovering its details (Ljungdahl et al., 1966; Ljungdahl and Wood, 1969). Furthermore, due to its simplicity and the catalytic mechanisms for chemical carbon fixation, the WLP is assumed to be of great importance for the evolution of life itself (Wood, 1991).

Table 3-1: Overview of a selection of acetogens which can grow on gases (adapted from Drake et al., 2006 and Takors et al., 2018)

Organism	**Substrates**	**Products**	**Original Reference**
Acetitomaculum ruminis	$H_2 + CO_2$, CO	Acetate	(Greening and Leedle, 1989)
Acetobacterium bakii	$H_2 + CO_2$, CO	Acetate	(Kotsyurbenko et al., 1995)
Acetobacterium malicum	$H_2 + CO_2$	Acetate	(Tanaka and Pfennig, 1988)
Acetobacterium woodii	$H_2 + CO_2$	Acetate	(Balch et al., 1977)
Blautia schinkii	$H_2 + CO_2$	Acetate	(Rieu-Lesme et al., 1996)
Clostridium aceticum	$H_2 + CO_2$, CO	Acetate	(Wieringa, 1936)
Clostridium autoethanogenum[a]	$H_2 + CO_2$, CO	2,3-butandiol, acetate, ethanol	(Abrini et al., 1994)
Clostridium carboxidivorans	$H_2 + CO_2$, CO	Acetate, ethanol, butyrate, butanol	(Liou et al., 2005)
Clostridium drakei	$H_2 + CO_2$, CO	Acetate, ethanol, butyrate	(Küsel et al., 2000; Liou et al., 2005)
Clostridium ljungdahlii	$H_2 + CO_2$, CO	2,3-butandiol, acetate, ethanol	(Tanner et al., 1993)
Clostridium scatologenes	$H_2 + CO_2$, CO	Acetate, ethanol, butyrate	(Liou et al., 2005)
Eubacterium limosum	$H_2 + CO_2$, CO	Acetate, CO_2	(Eggerth, 1935)
Moorella thermoacetica	$H_2 + CO_2$, CO	Acetate	(Fontaine et al., 1942)
Moorella thermoautotrophica	$H_2 + CO_2$, CO	Acetate	(Wiegel et al., 1981)
Sporomusa ovata	$H_2 + CO_2$	Acetate	(Möller et al., 1984)

[a]: species not validly described (Stackebrandt et al., 1999; Humphreys et al., 2015)

The WLP consists of two branches, the methyl branch and the carbonyl branch (see Figure 3-1). In the methyl branch, the initial reaction is a reduction of one molecule of CO_2 to formate via the formate-dehydrogenase and two reduction equivalents (refer to (3.1)). Subsequently, formate is coupled to tetrahydrofolate (THF) under adenosine triphosphate (ATP) consumption. Afterwards, the newly formed formyl-THF is reduced stepwise to methyl-THF using another four reduction equivalents. Then, the methyl group is transferred to a corrinoid iron sulfur protein via the methyl-transferase. In the carbonyl branch of the WLP, a second CO_2 molecule is reduced to a metal-bound carbonyl group via the CO-dehydrogenase. Subsequently, the methyl and carbonyl group are combined with coenzyme A via the acetyl-CoA synthetase to Acetyl-CoA (Müller et al., 2001).

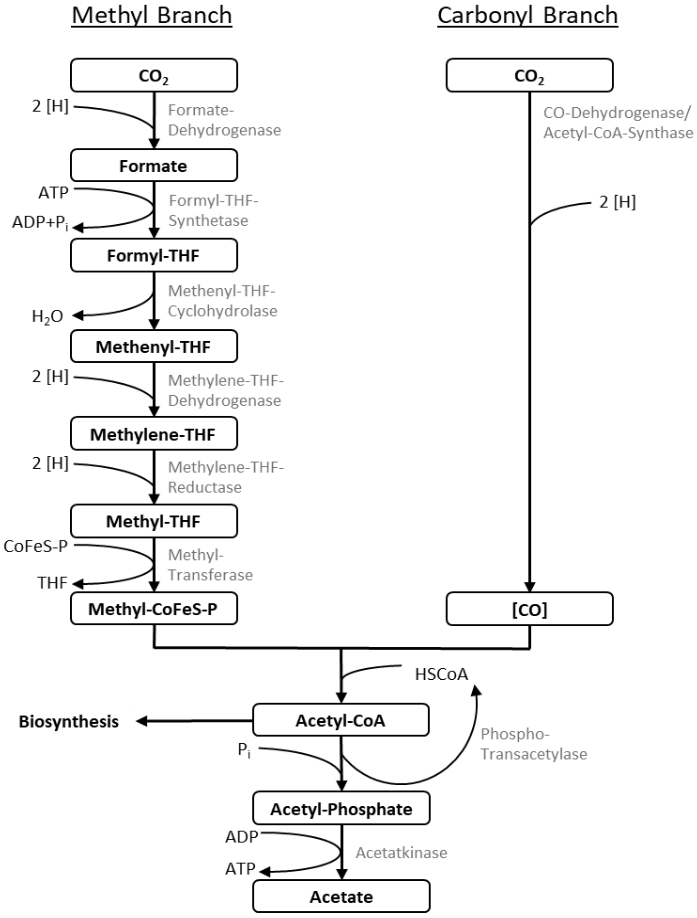

Figure 3-1: The acetyl-CoA “Wood-Ljungdahl” pathway. Abbreviations: [H] = reducing equivalents; ATP = adenosine triphosphate; ADP = adenosine diphosphate; P_i = inorganic phosphate; THF = tetrahydrofolate; CoFeS-P = corrinoid iron sulfur protein; [CO] enzyme-bound CO; HSCoA = coenzyme A (adapted from Müller et al., 2008).

The reduction equivalents for the WLP can be derived from the oxidation of H_2 or from CO via the CO-dehydrogenase, as shown in (3.1) and (3.2) (Drake et al., 2006).

Hydrogenase $$\mathrm{H_2 \rightarrow 2\ H^+ + 2\ e^-} \tag{3.1}$$

CO-dehydrogenase: $$\mathrm{CO + H_2O \rightarrow CO_2 + 2\ H^+ + 2\ e^-} \tag{3.2}$$

The stoichiometry for the formation of acetate from CO_2 and H_2 via the WLP can be described as following:

$$\mathrm{2\ CO_2 + 4\ H_2} + n\ \mathrm{ADP} + n\mathrm{P_i} \rightarrow \mathrm{CH_3COOH + 2\ H_2O} + n\ \mathrm{ATP} \tag{3.3}$$

with an overall free energy change of $\Delta G_0' = -95$ kJ mol^{-1} (Müller et al., 2008). This would allow the theoretical synthesis of 1 – 2 mol of ATP, however, as shown in Figure 3-1, the net ATP gain of the WLP from CO_2 and H_2 is zero. While one mol of ATP is formed during the acetate kinase reaction, 1 mol of ATP is also consumed in the formyl-THF synthetase reaction (Müller et al., 2008). Hence, chemolithotrophic ATP gain can only occur through ion gradient driven phosphorylation and not by substrate-level phosphorylation (Drake et al., 2006).

3.1.1. Energy Conservation in Acetogens

For energy conservation, acetogens can use substrate-level phosphorylation and chemiosmotic mechanisms. However, the substrate-level phosphorylation is only used for energy conservation under heterotrophic growth conditions. Acetogens can grow on a variety of different organic substrates such as carbohydrates, alcohols or carboxylic acids among others (Drake et al., 2006). The utilization of hexoses, e.g., glucose, produces exclusively acetate and is called homoacetogenesis. Glucose is oxidized via the Embden-Meyerhof-Parnas pathway to pyruvate, which is subsequently oxidized to acetyl-CoA and further converted to acetate. This pathway is coupled to the formation of four mol of ATP via substrate-level phosphorylation and 8 reduction equivalents (Müller, 2003), as shown in (3.4).

$$\mathrm{C_6H_{12}O_6 + 4\ ADP + 4\ P_i \rightarrow 2\ CH_3COOH + 2\ CO_2 + 4\ ATP + 8\ [H]} \tag{3.4}$$

The gained reduction equivalents are in turn introduced into the WLP, reducing two mol of CO_2 and producing another mol of acetate, as shown before in (3.3) and Figure 3-1. Therefore, heterotrophic growth on glucose yields in four mol ATP and 3 mol of acetate per mol glucose (Müller, 2003). The relation between glycolysis and the WLP is shown in Figure 3-2. Acetogens are able to conserve more energy by substrate-level phosphorylation than other anaerobes, which could possibly create an advantage for acetogens during competition with other anaerobes under certain *in situ* conditions (Drake et al., 2006).

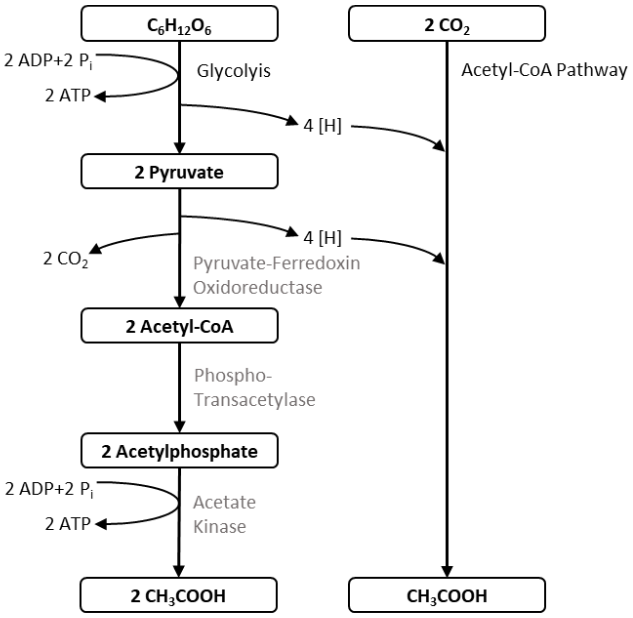

Figure 3-2: The connection between homoacetogenesis and the acetyl-CoA pathway. The two mol of CO_2 used in the acetyl-CoA pathway can be derived from exogenous CO_2 or the CO_2 produced during decarboxylation of pyruvate (adapted from Drake, 1995).

As mentioned already in Chapter 3.1.1, the chemolithoautotrophic net ATP gain in the WLP is zero. However, acetogens produce more dry cell weight per mol of glucose than is theoretically possible through substrate-level phosphorylation (Drake et al., 2006). Furthermore, the ability to grow on just H_2 and CO_2 indicates the capability of acetogens of conserving energy by electron transport phosphorylation or chemiosmotic mechanisms (Drake et al., 2006). The exact mechanisms for energy conservation in acetogens have been a mystery for some time. In the past, acetogens have been divided into two groups regarding bioenergetics: the ones containing cytochromes and quinones and being dependent on H^+ and the others without cytochromes and quinones while being dependent on Na^+ for energy conservation (Poehlein et al., 2012). Only recently, this classification was revised due to the discovery of two novel respiratory electron transport complexes: the Rnf complex (*Rhodobacter* nitrogen fixation), a complex that catalyzes ferredoxin:NAD^+-oxidoreductase activity (Müller et al., 2008), and the Ech complex (energy converting hydrogenase) (Schoelmerich and Müller, 2020). Furthermore, every acetogen that has been analyzed or sequenced until late 2021 have had either Rnf or Ech, never both (Rosenbaum and Müller, 2021). Therefore, acetogens are currently energetically classified as Rnf acetogens or Ech acetogens (Schuchmann and Müller, 2014). The current model for energy conservation in Rnf and Ech acetogens is depicted in Figure 3-3. Both types of electron transport complexes are reversibly coupled to the ion potential across the cell membrane. The Rnf complex pumps Na^+ or

H^+ out of the cell when the electron flow is exergonic, meaning reduced ferredoxin acts as electron donor while NAD^+ acts as electron acceptor (Tremblay et al., 2012; Hess et al., 2013). The Ech complex functions in a similar way, only that it uses H^+ as electron acceptor, thus producing H_2 gas as end product during the respiration (Schoelmerich and Müller, 2019). An ATP synthase translocates Na^+ or H^+ back into the cell, producing ATP from ADP and P_i (Reidlinger and Müller, 1994; Das and Ljungdahl, 1997). An electron-bifurcating, NAD^+ and ferredoxin reducing hydrogenase supplies the electron transport chains with reduced ferredoxin (Rosenbaum and Müller, 2021).

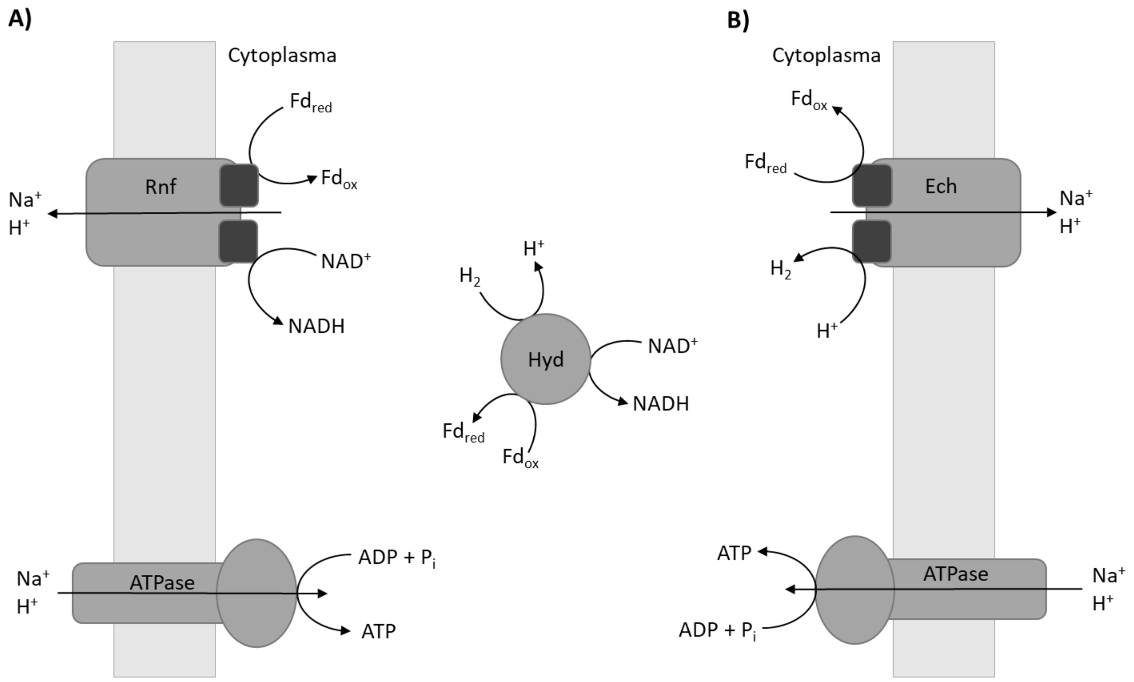

Figure 3-3: Current model for energy conservation by chemiosmotic mechanisms in acetogens. (A) Energy conservation in acetogens with Rnf complex; (B) energy conservation in acetogens with Ech complex. Abbreviations: $Fd_{red/ox}$ = ferredoxin in reduced and oxidized form; Rnf = ferredoxin:NAD^+-oxidoreductase; NAD^+/NADH = nicotinamide adenine dinucleotide; ATPase = ATP synthase; Hyd = hydrogenase; Ech = energy converting hydrogenase (adapted from Rosenbaum and Müller, 2021).

Additionally to Ech and Rnf complexes responsible for energy conservation, some acetogens like *Sporomusa* (Kamlage et al., 1993), *M. thermoacetica* (Gottwald et al., 1975) or *Clostridium aceticum* (Poehlein et al., 2015) also carry the respiratory components quinones and cytochromes. Although cytochrome-dependent respiratory chains were suggested almost 50 years ago, their function in these acetogens has not yet been fully discovered and is still part of ongoing hypothesis and debates (Rosenbaum and Müller, 2021). Only recently, Kremp et al., 2022 were able to show evidence of a cytochrome-containing hydrogenase as electron donor and a methylene-THF reductase as terminal electron acceptor as being part of the respiratory chain in *Sporomusa ovata*. Beside the Ech and Rnf energy conservation processes described above, this would show a third way for chemiosmotic energy conservation in acetogens. Furthermore, these findings prove that there is still much to be discovered until we will fully understand the entirety of the energy conservation process in acetogens.

3.1.2. Oxygen Tolerance and Mechanisms Against Oxidative Stress

Acetogens are classified as strict anaerobes given that many species have been isolated in anaerobic environments and many enzymes of the WLP are very sensitive to oxygen (O_2) (Drake et al., 2006). However, acetogens are also found in aerated soils and other habitats with fluctuating redox conditions such as the rooting zones of sea grass or the intestines of termites (Drake et al., 2008). Therefore, acetogens have developed mechanisms to cope with oxidative stress. One mechanism is the direct removal of O_2 and its byproducts like peroxides through enzymatic reduction. These enzymes are, among others, peroxidase, NADH-oxidase, rubrerythrin, catalase and cytochrome *bd* oxidase (Das et al., 2001; Karnholz et al., 2002; Das et al., 2005). Furthermore, acetogens can shift the reductant flow from the WLP to other terminal electron-accepting processes which are less sensitive to O_2, e.g., switching to a combined lactate-ethanol fermentation (Drake et al., 2008). A third mechanism of coping with oxidative stress is forming symbiotic relationships with aerotolerant bacteria. While the non-acetogen consumes the O_2 and thus protects the acetogen, the latter can in addition use fermentation products like formate or H_2 for acetogenesis. Although these co-culture interactions have been documented so far only under laboratory conditions, it might still represent a basis for oxygen protective mechanisms of acetogens in their natural habitat (Drake et al., 2008). A variety of studies have been conducted on the O_2-tolerance level of different acetogens. While *Clostridium glycolicum* RD-1 was found to tolerate O_2 up 6 % (Küsel et al., 2001), others like *A. woodii*, *M. thermoacetica* or *Clostridium magnum* can tolerate O_2 only in concentrations up to 1 % (Karnholz et al., 2002).

3.1.3. *Acetobacterium woodii*

Acetobacterium woodii DSM 1030 was first isolated from a marine estuary in 1977 by Balch et al. and was named in honor of Harland G. Wood. It is a gram-positive, oval-shaped rod with a size of 1 – 2 µm, which frequently occurs in pairs (see Figure 3-4). Like other acetogens it is classified as a strict anaerobe with the capacity for using H_2 and CO_2 via the acetyl-CoA pathway for the production of its main product, acetate (Balch et al., 1977). *A. woodii* grows optimally at a temperature of 30 °C and a pH of 6.8, however it was reported of being viable at a pH of 5 for several weeks (Balch et al., 1977). *A. woodii* cells are actively motile using one or two subterminal flagella (as shown in Figure 3-4). This acetogen can utilize all four one-carbon compounds CO, CO_2, formate and methanol (Balch et al., 1977; Bertsch and Müller, 2015; Kremp et al., 2018; Moon et al., 2021) as well as other substrates such as glucose, fructose, lactate or glycerol (Balch et al., 1977; Bache and Pfennig, 1981; Tanner et al., 1981; Weghoff et al., 2015). *A. woodii* can also utilize caffeate as electron acceptor (Tschech and Pfennig, 1984) and possesses the ability for mixotrophic growth, the simultaneous utilization of organic and gaseous substrates (Braun and Gottschalk, 1981; Tschech and Pfennig, 1984). Given that *A. woodii* has been studied extensively in the past (Balch et al., 1977; Diekert and Ritter, 1982; Poehlein et al., 2012; Kantzow et al., 2015; Beck et al., 2020), i.e., the Rnf complex was first discovered in *A. woodii* (Müller et al., 2008), it is considered to be a model organism for the study of acetogens. Furthermore, *A. woodii* has been genetically accessible for almost 30 years (Strätz et al., 1994), and recombinant strains for the production of C3 compounds like acetone (Hoffmeister et al., 2016) and lactate (Mook et al., 2022) have been constructed since.

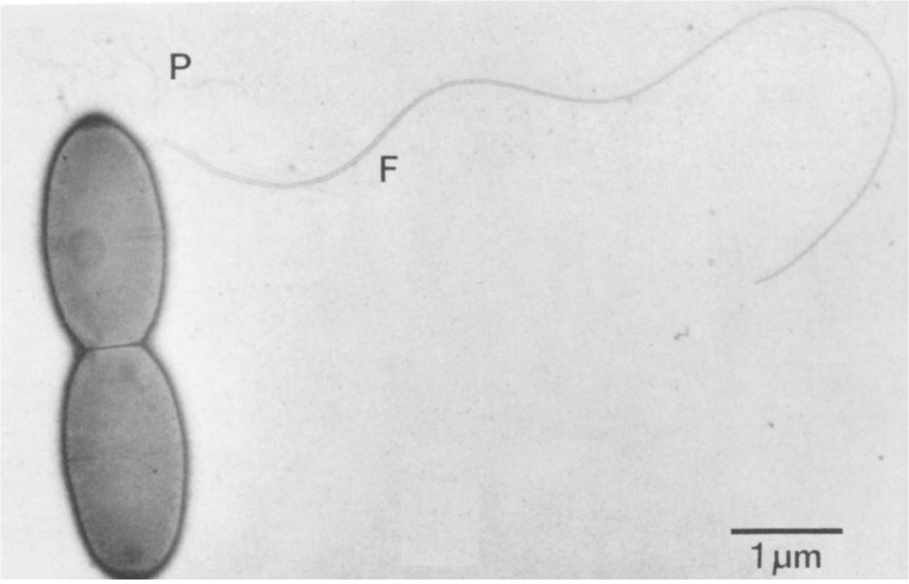

Figure 3-4: Electron microscopic image of *A. woodii*. (F) single, subterminal flagellum; (P) pili-like structures (Balch et al., 1977).

A. woodii can utilize lactate as substrate via a lactate dehydrogenase (LDH) coupled to the electro-transferring flavoprotein subunits EtfA and EtfB (Weghoff et al., 2015). This complex catalyzes the oxidation of lactate to pyruvate while oxidating reduced ferredoxin and simultaneously converting NAD^+ into NADH, as shown in Figure 3-5. Thus, the endergonic electron flow from lactate to NAD^+ is driven by the exergonic electron flow (Fd_{red} to NAD^+) (Weghoff et al., 2015). This lactate uptake mechanisms impedes the accumulation of lactate by the *A. woodii* wild type strain. However, given the genetic accessibility of *A. woodii*, recombinant strains were developed which possess the ability of lactate accumulation. For this, the genes encoding the native LDH/Etf complex were knocked out and a gene encoding a D-lactate dehydrogenase originating from *Leuconostoc mesenteroides* was expressed (Beck et al., 2020). The newly expressed D-lactate dehydrogenase is furthermore controlled either by the promoter P_{tet} via anhydrotetracycline induction (for the strain *A. woodii* P_{tet}_*ldhD*$_{CI}$) or by the promoter P_{bgaL} via lactose induction (for the strain *A. woodii* [P_{bgaL}_*ldhD*_NFP]) (Mook et al., 2022).

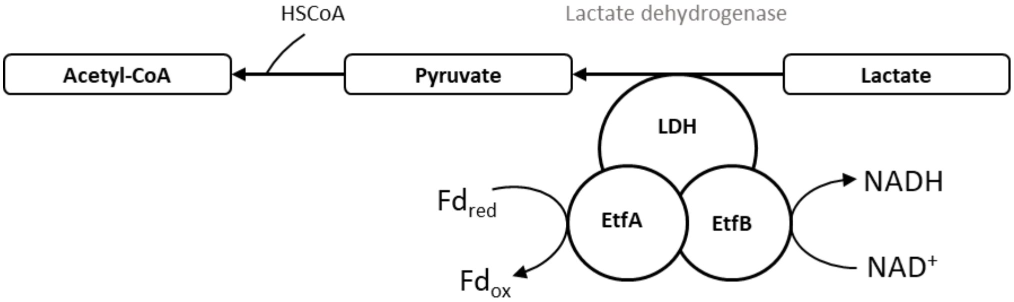

Figure 3-5: Native lactate uptake mechanism in *A. woodii* mediated by the electron-confurcating LDH/Etf complex (adapted from Weghoff et al., 2015). Abbreviations: LDH = lactate dehydrogenase; Etf = electron-transferring flavoprotein.

3.1.4. *Clostridium drakei*

One of the more recently discovered acetogens is *Clostridium drakei* DSM 12750*,* which was isolated from the sediment of an acidic coal mine pond and was first described as *Clostridium scatologenes* SL1 (Küsel et al., 2000). A few years later, 16S rRNA analysis indicated a very close relationship to both *C. scatologenes* and *C. carboxidivorans*, however also proved *C. drakei* being its distinct species (Liou et al., 2005). It was therefore reclassified and renamed in honor of Harold L. Drake (Liou et al., 2005). Its draft genome sequence was published in 2014 (Jeong et al., 2014). *C. drakei* is a terminal spore forming, gram-negative obligate anaerobe with a 3 – 4 µm long rod shape (see Figure 3-6). It is motile and has an optimal growth temperature between 30 and 37 °C and an optimum pH of 5.5 to 7.5 (Küsel et al., 2000; Liou et al., 2005). *C. drakei* can grow autotrophically on H_2 and CO_2 and chemiorganotrophically on a variety of substrates such as ribose, fructose, glucose, glycerol, ethanol, propanol, butanol, lactate, glutamate and other amino acids. Its main metabolic products are acetic acid, butyrate, ethanol, butanol and caproic acid (Liou et al., 2005; Gössner et al., 2008).

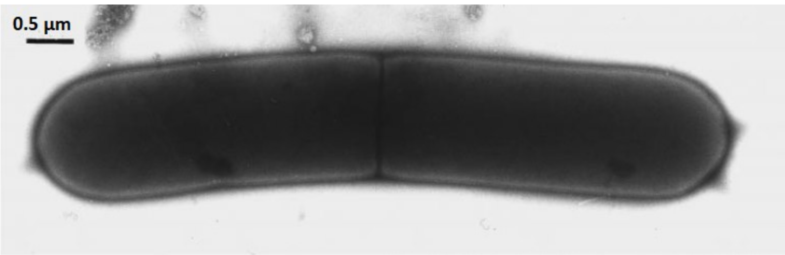

Figure 3-6: Electron microscopic image of C. *drakei* during cell division (Küsel et al., 2000).

Being an acetogen, *C. drakei* can utilize CO_2 via the WLP as sole carbon source (Küsel et al., 2000; Liou et al., 2005). Furthermore, it was reported to possess the ability of using the glycine synthase pathway in functional cooperation with the WLP to enhance CO_2 consumption and cell growth (Song et al., 2020). Especially interesting is however its ability of producing short and medium-chain carboxylic acids through chain elongation via reverse β-oxidation (Wirth and Dürre, 2021). As shown in Figure 3-7, *C. drakei* can utilize both L- and D-lactate, converting one into the other via a lactate racemase. Afterwards, the D-lactate dehydrogenase catalyzes the formation of pyruvate and furthermore acetyl-CoA is formed. From here, acetate can be produced via the phosphotransacetylase and the acetate kinase, yielding in one mol ATP per mol acetate. Furthermore, *C. drakei* possesses the *hcs* (hexanoyl-CoA synthesis) gene cluster which expresses the enzymes butyryl-CoA dehydrogenase (Bcd), crotonase (Crt), 3-hydroxybutyryl-CoA dehydrogenase (Hbd) and thiolase (Thl). These enzymes catalyze the formation of butyryl-CoA and subsequently of hexanoyl-CoA via reverse β-oxidation, consuming acetyl-CoA, NADH and Fd_{ox} per chain elongation cycle. The end products of each chain elongation cycle are butyrate catalyzed by the phosphotransbutyrylase and the butyrate kinase as well as caproate catalyzed by the phosphotransferase and the fatty acid kinase (Wirth and Dürre, 2021).

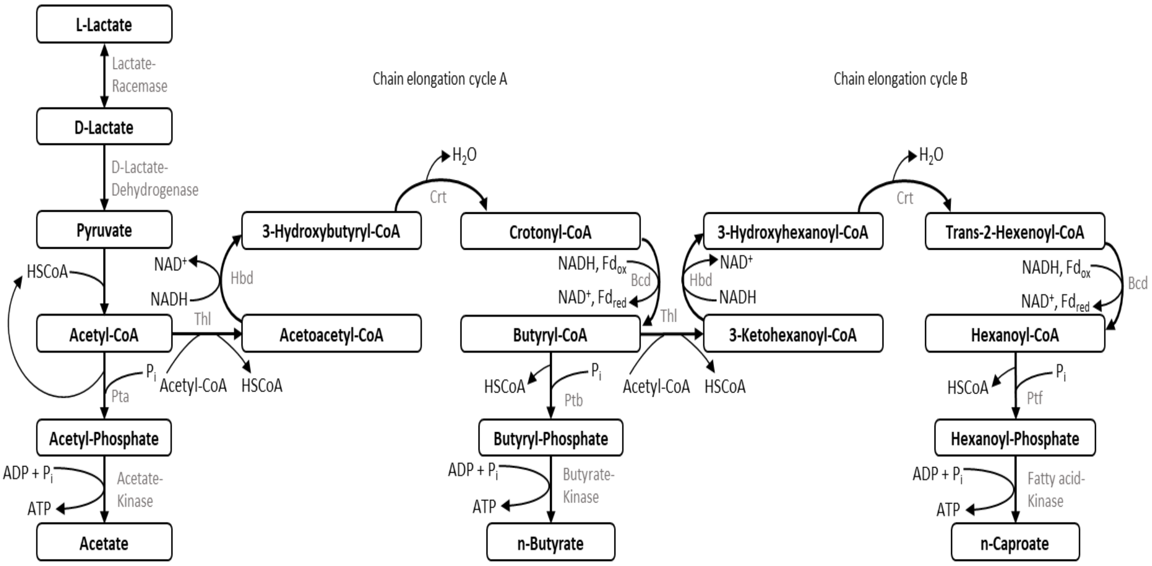

Figure 3-7: Model pathway for short and medium-chain carboxylic acid formation from lactate in *C. drakei*. Chain elongation by reverse β-oxidation using the proteins of the *hcs* cluster (Bcd, Crt, Hbd and Bcd including electron-transferring flavoproteins A and B) is depicted in two chain elongation cycles A and B. Abbreviations: Bcd = butyryl-CoA dehydrogenase; Crt = crotonase; Hbd = 3-hydroxybutyryl-CoA dehydrogenase; Thl = thiolase; Pta = phosphotransacetylase, Ptb = phosphotransbutyrylase, Ptf = phosphotransferase. (Adapted from Kucek et al., 2016a and Wirth and Dürre, 2021).

3.2. Caproic acid

Caproic acid, also called hexanoic acid, is a medium-chain carboxylic acid with six carbon atoms and the chemical formula $CH_3(CH_2)_4COOH$. Its name is derived from the Latin word *capra* for goat, which refers to its pungent, fatty or cheesy odor (Bagby et al., 2000). Caproic acid is a high value product with an annual worldwide demand of about 12,500 tons (PW Consulting Agency, 2021). Applications of this acid are versatile: in the pharmaceutical industry as possible antimicrobial agent (Huang et al., 2011), in the food industry as animal feed for poultry or pigs (van Immerseel et al., 2004; Zentek et al., 2011) as well as flavor additive (Serhan et al., 2016), in the cosmetic industry for fragrances (Liu et al., 2020), and in the chemical industry as lubricating agent as well as for rubber and dye production (Jeon et al., 2013). Furthermore, caproic acid is a precursor for potential biofuels (Harvey and Meylemans, 2014). Main sources for the production of caproic acid are fossil fuels (Wasewar and Shende, 2011) and natural oils from plants such as palm or coconut (Chen et al., 2017). However, it can also be produced via anaerobic fermentation from various substrates, including waste products (Agler et al., 2011; Ge et al., 2015). As described in Chapter 3.1.4, caproic acid is the product of chain elongation via reverse β-oxidation. Besides lactate, ethanol can also be used by chain elongating bacteria to produce caproic acid (Cavalcante et al., 2017). Some examples of caproic acid producing bacteria are *Clostridium kluyveri*, *Megasphaera elsdenii* (Jeon et al., 2013), *C. autoethanogenum* and *C. drakei* (Wirth and Dürre, 2021). Besides its production in pure cultures, there have also been various reports on caproic acid production in mixed cultures, which show some advantages but also some draw backs in comparison to pure culture fermentations (Agler et al., 2011; Spirito et al., 2014; Kucek et al., 2016a).

3.2.1. *In situ* Product Removal

Some metabolic products of microorganisms can become toxic to the microorganism itself once a specific concentration has accumulated in the culture medium. The most famous example therefor is the growth inhibition of *Saccharomyces cerevisiae* through its produced ethanol (Stanley et al., 2010). Other inhibitory metabolic products are various organic acids such as acetic acid (Wang and Wang, 1984) or caproic acid (Huang et al., 2011; Choi et al., 2013). The inhibitory effect is based on the decreasing pH caused by these acids and the resulting collapse of ion gradients like ΔpH (Russell, 1992). At low pH environments, the conjugate-neutral form of organic acids can diffuse into the cytoplasm where it dissociates at the higher internal pH which then increases the concentrations of protons and acid radicals. The collapse of the ΔpH causes a depletion of ATP supply given that the ΔpH is one of the major energy sources for cellular transport functions, and thus causes cell starvation and cell population growth stagnation (Zaldivar and Ingram, 1999). To prevent this toxic effect of organic acids on cell growth and to increase product concentrations, it is necessary to separate the acid from its producer shortly after its secretion into the fermentation medium via so called *in situ* product recovery methods. *In situ* product recovery techniques for caproic acid separation are various, ranging from liquid-liquid extractions (Choi et al., 2013; Jeon et al., 2013; Ge et al., 2015), pertraction (Kucek et al., 2016b; Gildemyn et al., 2017) as well as electrodialysis or electrolytic extraction (Xu et al., 2015; Khor et al., 2017; Selder et al., 2020).

3.3. Bioprocess Engineering Principles

In general, biotechnological cultivations can be classified by their mode of operation: batch, fed-batch or continuous cultivation. Given that only batch fermentations were conducted for this study, this chapter will focus on the fundamentals of bacterial batch fermentations. During this cultivation type, all necessary media and substrate components are provided for the microorganisms at the beginning of the cultivation. An additional feed or exit stream of cultivation medium does not exist, only pH correction media such as bases and acids can be added to the fermenter if needed. Furthermore, specific gases (depending on the demand of the microorganism) enter and leave the vessel during a process. A batch fermentation is therefore, based on the liquid medium, a closed system. (Chmiel et al., 2018)

Microbial growth under substrate limited conditions, as present in a batch fermentation, can be described in six phases as shown in Figure 3-8. During the lag phase (I), the microorganism adapts to the cultivation conditions, the specific cell growth rate μ is zero. In the first transitional phase (II), the cells start duplicating and μ increases until reaching its maximum value μ_{max} during the exponential growth phase (III). When all substrate is consumed or growth is inhibited by toxic byproducts, the growth rate declines in the second transitional phase (IV) leading into the stationary phase where the cells switch to maintenance metabolism (V). Here, the growth rate equals the death rate of the cells. Once the death rate of the cells is greater than the growth rate, the cell population starts to decline and the death phase begins (VI). (Chmiel et al., 2018)

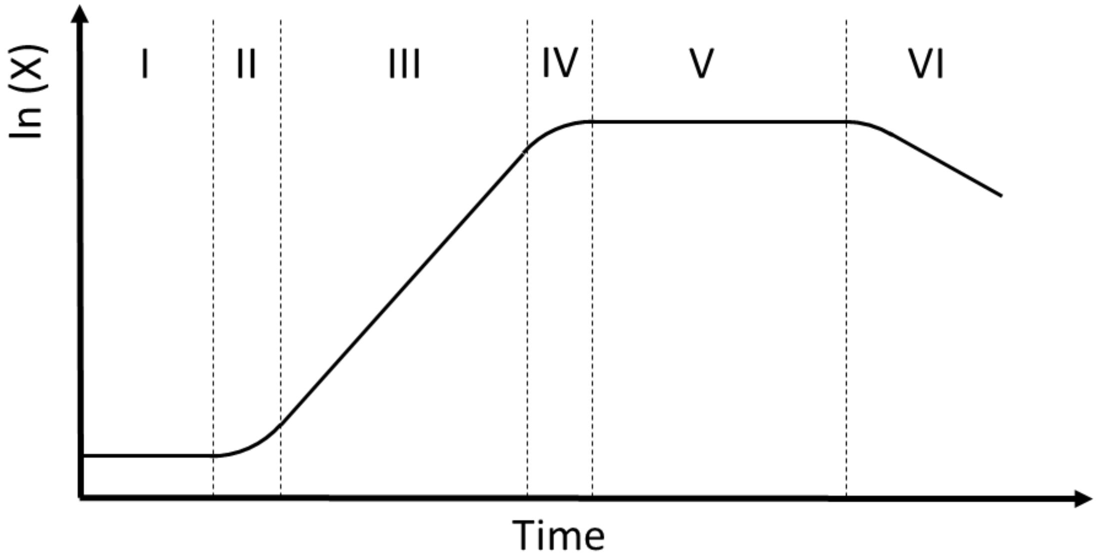

Figure 3-8: Simplified growth curve of microorganisms in a batch cultivation. (I) lag phase; (II) first transitional phase; (III) exponential growth phase; (IV) second transitional phase; (V) stationary phase; (VI) death phase. X = concentration of biomass (adapted from Chmiel et al., 2018).

Standard bacterial batch fermentations are conducted in continuous stirred tank reactors (CSTR). For a mathematical process description of the cells in a CSTR, an unstructured and unsegregated model is used, meaning that all cells are regarded as one component with the same properties. Furthermore, the CSTR is regarded as ideal. It is assumed that the reaction volume inside the volume is of one phase and homogeneously mixed, gradients of reaction components are not present and temperature as well as pressure inside the vessel are constant. With these assumptions, all reaction velocities are independent of the location. In addition, the volume change by addition of pH correction media is usually neglected. (Chmiel et al., 2018) The general mass balance of a bioconversion process for a component *i* can then be described as shown in (3.5).

$$\frac{d(c_i V)}{dt} = \dot{V}_{in} \cdot c_{i,in} - \dot{V}_{out} \cdot c_{i,out} + r_i \cdot V \tag{3.5}$$

where c_i is the concentration of a component i, $\dot{V}$ is the in and outgoing volume flow, r_i is the volumetric reaction rate of the component i, and V is the liquid volume inside the vessel. Given that in a batch fermentation, no liquid enters or leaves the reactor, the volume is considered to be constant and (3.5) can be simplified to

$$\frac{dc_i}{dt} = r_i \tag{3.6}$$

To describe cell growth, substrate consumption and product formation, some process parameters must be defined. The volumetric rate of biomass production r_x can be described via the change in biomass concentration X over time t (see (3.7))

$$\frac{dX}{dt} = r_X = \mu \cdot X \tag{3.7}$$

with the specific growth rate μ. This can be rearranged to Equation (3.8).

$$\mu = \frac{1}{X} \cdot \frac{dX}{dt} \tag{3.8}$$

Assuming that during the exponential growth phase, the growth rate reaches its maximum value and is furthermore constant, Equation (3.8) can be integrated and results in

$$X = X_0 \cdot e^{\mu_{max} \cdot t} \tag{3.9}$$

which can then be transformed into Equation (3.10) to determine the maximum growth rate from process data.

$$\mu = \frac{ln\left(\frac{X_{t_i}}{X_{t_{i-1}}}\right)}{t_i - t_{i-1}} \tag{3.10}$$

Cell growth under substrate limited conditions can be described with the so-called Monod-kinetics, published in 1949 (Monod, 1949). The assumptions for this simple model are that all process parameters are constant and that all nutrients except for the limiting substrate are available in excess. Furthermore, this model is only valid for the exponential, second transitional and stationary growth phases (phases II – V, see Figure 3-8). The Monod equation is described as:

$$\mu(c_S) = \mu_{max} \cdot \frac{c_S}{c_S + K_S} \tag{3.11}$$

where c_s is the concentration of the limiting substrate and K_S is the substrate saturation constant and equals the substrate concentration at the point of $\mu_{max}/2$. (Monod, 1949)

The biomass specific substrate consumption rate q_s and the biomass specific product formation rate q_p can described on the lines of Equation (3.7) as following:

$$\frac{dc_S}{dt} = -q_S \cdot X \tag{3.12}$$

$$\frac{dc_P}{dt} = q_P \cdot X \tag{3.13}$$

with the substrate and product concentrations c_s and c_p.

The link between the substrate concentration and the product concentration can be expressed by the yield coefficient of biomass from substrate $Y_{X/S}$ described in Equation (3.14)

$$Y_{X/S} = \frac{dX}{dc_S} = \frac{\mu}{-q_S} \tag{3.14}$$

Equation (3.14) can also be used to express the relationship between substrate consumption and product formation in the product yield coefficient $Y_{P/S}$, described in Equation (3.15)

$$Y_{P/S} = \frac{dc_P}{dc_S} \tag{3.15}$$

Another important process parameter which is used to compare different biotechnological processes is the volumetric productivity P_{vol}, also called space-time-yield (Chmiel et al., 2018). This parameter can relate to biomass or product concentration. Equation (3.16) shows the volumetric productivity referring to product concentration.

$$P_{vol} = \frac{c_P}{t} \tag{3.16}$$

The carbon balance for a biotechnological process can calculated considering the molar number of atoms and the molar mass of all components in the culture medium at the beginning and the end of a process (Dunn, 2003). According to Utesch et al., 2019, Equation (3.17) can be used for carbon recovery (R_C) calculations

$$R_C = \frac{\sum_i^n n_i \cdot C_i^*}{\sum_j^n n_j \cdot C_j^*} \tag{3.17}$$

with the total generated amount of product compound n_i, the amount of substrate concentration n_j, and the number of carbon atoms of the respective compounds C_i^* and C_j^*.

The determination of gas uptake by microorganisms is fundamental for carbon balancing if these microorganisms use the gas as main substrate. If the pressure p and temperature T of the gas is assumed as constant, gas uptake can be calculated with

$$n_{Gas} = \sum\nolimits_0^t (\dot{V}_{in} - \dot{V}_{out}) \cdot \frac{p}{R \cdot T} \tag{3.18}$$

3.4. Gas Fermentations

The term syngas (synthesis gas) describes a gas mixture of mainly CO and H_2, often also including CO_2, methane and low levels of other gases (Hiller et al., 2003). Syngas is mainly produced from fossil sources such as natural gas, coal or crude oil, yet it can also be produced from renewable sources such as biomass (e.g., lignocellulose from wood or agricultural and urban wastes) (Hiller et al., 2003). Interestingly, syngas can also be obtained from waste gas streams from the industry such as steel mills or petrol refining plants (Asimakopoulos et al., 2018). The production of syngas from biomass is done by gasification, which is conducted at high temperatures (600 – 1,000 °C) and goes through various reaction steps, one of which is the so-called water gas shift where CO and water are converted into CO_2 and H_2 (Abubackar et al., 2011; Griffin and Schultz, 2012). Depending on the type of biomass, the reaction condition and the reactor type used, the produced syngas can vary in its composition and can have different impurities such as H_2S and NH_3 (Takors et al., 2018). Syngas is used for the industrial production of various chemical compounds, e.g., ammonia via the Haber-Bosch process, methanol and other alcohols or different hydrocarbons via the Fischer-Tropsch process. These processes not only operate at temperatures of 200 – 500 °C and pressures from 20 – 300 bar, but they also require expensive metal catalysts (e.g., Fe_2O_3) which drive the operating costs up. Furthermore, these processes require a cleaning and pre-treatment step for the syngas, given that the used catalysts are sensitive to gas impurities which can lead to catalyst poisoning (Griffin and Schultz, 2012). Moreover, a fixed H_2/CO ratio is needed for the conversion of the desired products, resulting often in the addition of H_2 to the syngas (Rostrup-Nielsen, 2000).

Fermentation processes using syngas as feed source have been studied intensively in the past, given that they overcome many of the limitations of the chemical processes mentioned before. The operating conditions are usually mild, with temperatures of 30 – 60 °C, pressures of 1 – 2 bar and often a neutral pH. Furthermore, the microorganisms which function as biocatalysts are cheap and more flexible than their inorganic counterpart as they do not need a fixed H_2/CO ratio to function properly. In addition, they show a high selectivity and are not as sensitive to gas impurities as metal catalysts (Mohammadi et al., 2011). Syngas fermentations therefore pose a great potential for a sustainable production of chemicals while reducing greenhouse gas emissions (Bengelsdorf and Dürre, 2017). One of the main products of syngas fermentations which has proven to be feasible at a large-scale application are so called biofuels. The classic fermentation approach of converting sugars from e.g., corn or sugar cane to ethanol by yeasts or other microorganisms has been referred to be the first generation of biofuels (Naik et al., 2010). However, there have been a lot of concerns regarding the food versus fuel debate, whether or not food products such as corn should be used as origin for fuels and therefore reducing the availability of them to be consumed. The production of biofuels via syngas fermentation based on non-food feedstocks such as agricultural wastes or wood residues was declared as second-generation biofuels and does not compete over land use with agricultural crops for food production (Naik et al., 2010). To produce ethanol from biomass, the biomass is usually subjected to a pretreatment such as drying, size reduction, pelletization or pulverization first (Isaksson et al., 2013). Subsequently, the residues are introduced into a gasifier. Typical gasifier configurations are fixed, moving or fluidized bed while the latter are the most common given that they can be easily scaled to large applications (Liew et al., 2016). As mentioned before, syngas produced via gasification usually contains contaminations which need to be removed. Particulates can be removed through cyclones or filters, while other components need catalysts or other separations techniques (Liew et al., 2016). Some residues like HCN are critical, given that they can cause enzyme inhibition and would hinder a successful fermentation (Shima and Ataka, 2011). Finally, the syngas is compressed and passed into a suitable bioreactor where microorganisms convert it to ethanol (see Figure 3-9 for process scheme) (Devarapalli and Atiyeh, 2015). Such a process is already implemented successfully at industrial scale by LanzaTech (Skokie, IL, USA) at various sites, using waste gases from steel mills and syngas from biomass gasification as feedstocks for the production of ethanol (Daniell et al., 2012; Liew et al., 2016). Furthermore, LanzaTech has shown also that the production of acetone and isopropanol with syngas at pilot scale is also possible (Liew et al., 2022), which demonstrates that syngas fermentation is a promising technology for a variety of carbon-neutral applications and products.

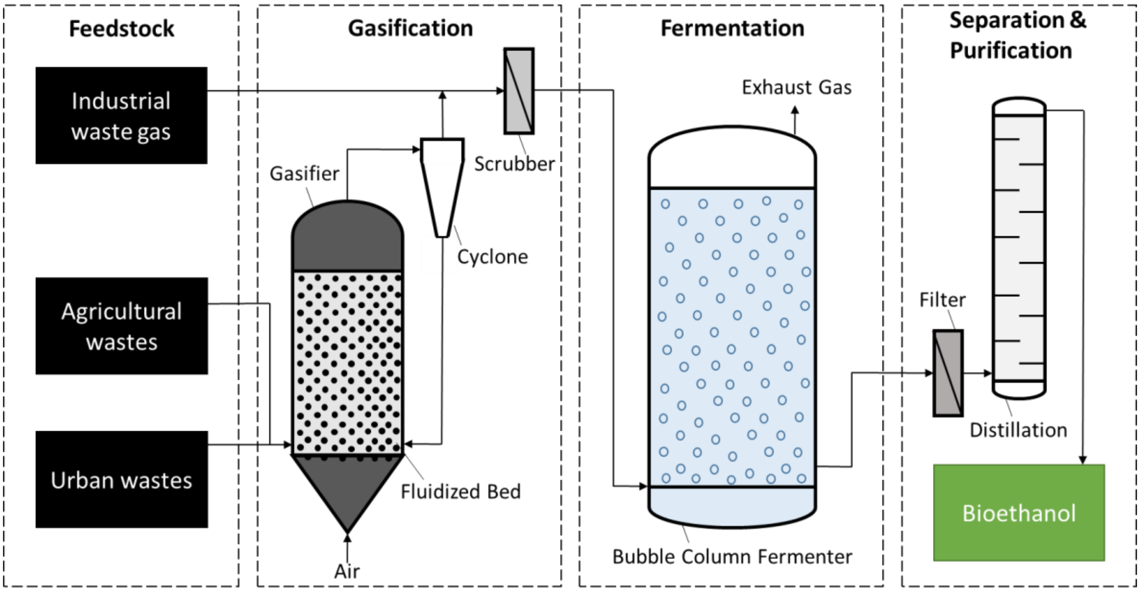

Figure 3-9: Simplified gas fermentation process scheme for biomass to bioethanol production (adapted from Devarapalli and Atiyeh, 2015).

Another gas fermentation process which has already been realized at pilot industrial scale is the so called Rheticus joint project from Siemens Energy AG (München, Germany) and Evonik Industries AG (Essen, Germany). This process uses water and CO_2 as a feedstock and reduces them in an electrolyzer to syngas containing CO_2, CO and H_2. This syngas is then used for hexanol and butanol production in a co-cultivation (refer to Chapter 3.5) with *Clostridium autoethanogenum* and *C. kluyveri*. The electrolyzer is furthermore powered by regenerative energy e.g., from solar panels. A scheme of the process is shown in Figure 3-10.

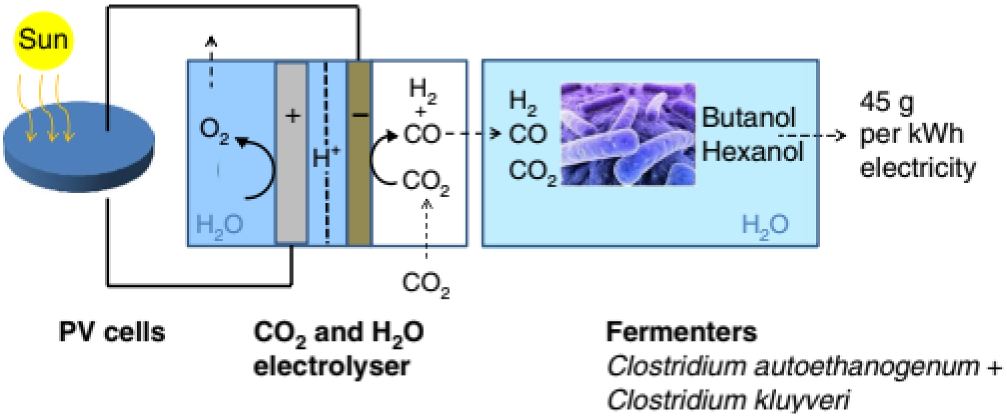

Figure 3-10: Process scheme of the production of butanol and hexanol from CO_2 and H_2O using regenerative energies (Haas et al., 2018).

3.4.1. Gas Mass Transfer in Aqueous Media

Any fermentation process which uses gas as a reaction compound (e.g., anaerobic gas fermentations or aerobic fermentations) are multiphase systems, consisting of a gas and a liquid phase. For a reaction to take place in the bioreactor, the chemical compound in the gas phase must become available to the microorganism in the liquid phase (Villadsen et al., 2011). The gas-liquid mass transfer is therefore key for any fermentation involving gas as a reaction compound. Given that gas solubility for most gases is relatively low, the gas-liquid mass transfer is the major limitation in gas fermentations (Villadsen et al., 2011). This is even more critical for syngas fermentations, as CO is 60 w% and H_2 4 w% less soluble in water compared to oxygen and furthermore, more moles of syngas per carbon equivalent have to be transferred compared to an aerobic fermentation (Bredwell and Worden, 1998). Thus, the rate of the reaction for the microorganisms is usually limited by the gas-liquid mass transfer rate.

Mass transfer in general occurs in two basic processes, molecular diffusion and convective transport (Villadsen et al., 2011). The mass transfer of a chemical compound such as H_2 from a gas bubble phase to the interior of a cell occurs in several steps and can be described as following (see Figure 3-11):

1. Diffusion of H_2 from the gas phase to the gas-liquid interface
2. Transport across the gas-liquid interface
3. Diffusion of H_2 through a relatively laminar liquid film around the gas bubble
4. Transport of dissolved H_2 through the usually well mixed liquid phase
5. Diffusion of H_2 through a relatively laminar liquid film around the cell
6. Transport across the cell membrane
7. Transport to the intracellular reaction site

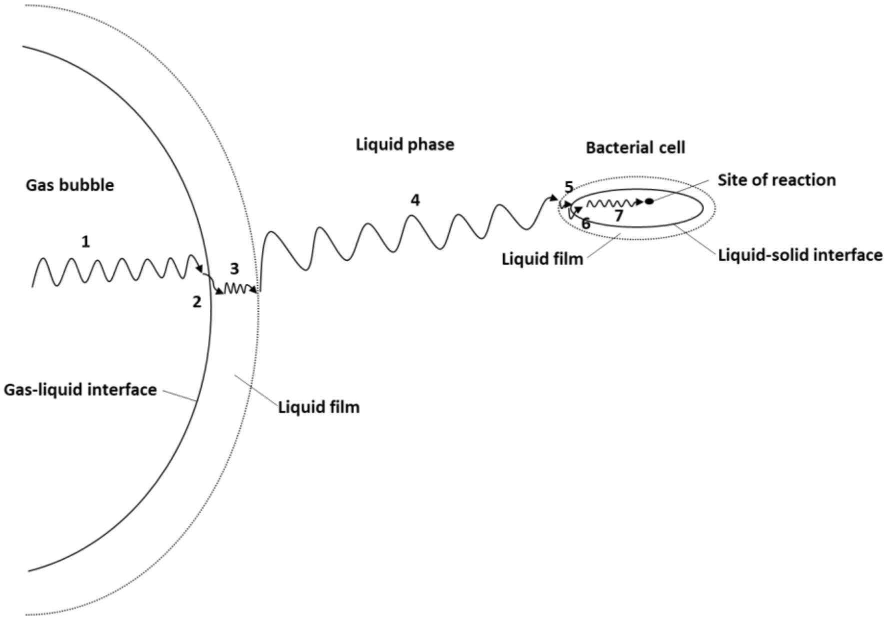

Figure 3-11: Transfer of gas molecules from a gas bubble through bulk liquid to a cell. (1) Diffusion from the gas phase to the gas-liquid interface; (2) Transport across the gas-liquid interface; (3) Diffusion through the laminar liquid film around the gas bubble; (4) Transport of dissolved gas through the bulk liquid phase; (5) Diffusion through the laminar liquid film around the cell; (6) Transport across the cell membrane; (7) Transport to the intracellular reaction site (adapted from Doran, 2013).

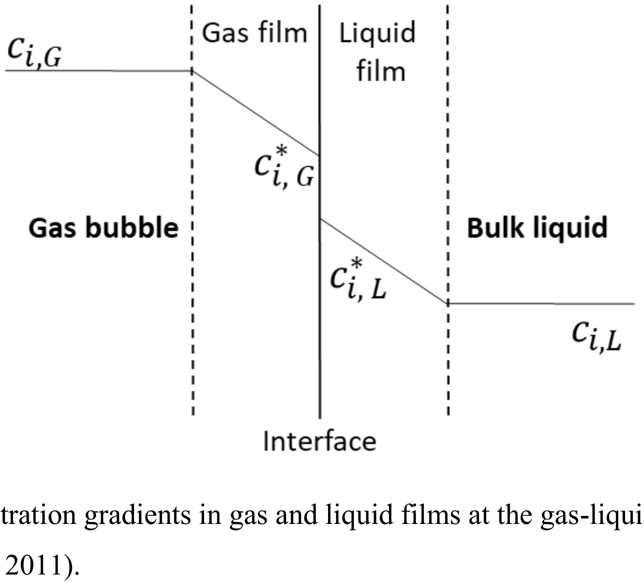

Figure 3-12: Concentration gradients in gas and liquid films at the gas-liquid interface (adpated from Villadsen et al., 2011).

Among a variety of models to describe mass transport phenomena, the so-called two-film theory is the one used the most in bioprocessing (Chmiel et al., 2018). This theory states, that wherever there is a contact between two phases, a mass transfer boundary layer will form. In the case of gas-liquid contact, a liquid layer will form around the interface (see Figure 3-12). The driving force for mass transfer through an interface is the concentration difference across the film layer. The transfer rate *N* of a component *i* through each of the two films can therefore be expressed as the product of a mass transfer coefficient k and the concentration difference across the film. The rate for mass transfer across the gas boundary layer is therefore

$$N_{i,G} = k_G a \cdot \left(c_{i,G} - c_{i,G}^{*}\right) \tag{3.19}$$

and the rate for mass transfer across the liquid boundary layer is

$$N_{i,L} = k_L a \cdot \left(c_{i,L}^{*} - c_{i,L}\right) \tag{3.20}$$

where k_G is the mass transfer coefficient in the gas phase, k_L is the mass transfer coefficient in the liquid phase, c_G describes the concentration in the gas phase, c_G^{*} describes the concentration in the gas film at the interface, c_L describes the concentration in the bulk liquid and c_L^{*} describes the concentration in the liquid film at the interface. The coefficient a is the specific interfacial area of gas bubbles and can be described as

$$a = \frac{A_I}{V} \tag{3.21}$$

with A_I being the area of the interface between the liquid and the gas phase and V being the liquid volume inside a reactor. However, it is difficult to determine the coefficients a and k_L separately from each other in a bioreactor with gas bubble movement. Therefore, both terms are usually used together as the volumetric mass transfer coefficient k_La which can be determined with simple experimental methods (Villadsen et al., 2011).

The concentrations of dissolved gas in the liquid phase (see Equation (3.22)) can be described with Henry's law (Henry, 1803) using the partial pressure p and the Henry solubility constant H_s^{cp} of a gas *i*:

$$c_{i,L} = p_i \cdot H_{s,i}^{cp} \tag{3.22}$$

The Henry solubility constants for different gases are listed in Table 3-2. According to Dalton's law (Dalton, 1802) and under the assumption of ideal gases, the partial pressure of a gas can be calculated with the fraction of the gas in the total gas stream χ_i and the total pressure p:

$$p_i = p \cdot \chi_i \tag{3.23}$$

Table 3-2: List of Henry's law solubility constants for different gases (gas in water at 25 °C) (Sander, 2015)

Gas	**CO**	**CO_2**	**H_2**	**N_2**	**O_2**
H_s^{cp} **[mol L^{-1} atm^{-1}]**	9.5 x 10^{-4}	3.4 x 10^{-2}	9.5 x 10^{-4}	6.1 x 10^{-4}	1.3 x 10^{-3}

The gas-liquid mass transfer is influenced by a variety of physical, chemical and process parameters. As shown in Equation (3.20), the mass transfer is dependent on the mass transfer coefficient k_L, the specific interfacial area of the gas bubbles a and the concentration difference $\left(c_{i,L}^{*} - c_{i,L}\right)$. The concentration difference as the driving force for mass transfer is influenced by the system pressure, the partial pressure of the gas and the temperature of the liquid. As shown in Equation (3.23), increasing the total pressure or the fraction of the desired gas in the gas stream will increase the partial pressure of the gas, which in turn increases the dissolved gas concentration (see Equation (3.22)). Furthermore, the Henry solubility constant is temperature dependent which leads to decreasing solubility of gases with higher temperatures (Wilhelm et al., 1977). However, given that a microorganism's temperature optimum for cell growth is within a narrow temperature range, it is usually not practical changing the temperature to enhance gas-liquid mass transfer in a process. The specific interfacial area of the gas bubbles has a major influence on the mass transfer across the phase boundary layer, which can be increased by smaller bubble sizes and increasing the number of gas bubbles introduced into the reactor. One widespread approach to reach smaller bubble sizes is increasing the power-to-volume ratio $P\ V^{-1}$. In a CSTR this is realized by increasing the stirrer rate of the agitator which causes a higher bubble break-up, thus increasing the interfacial area and enhancing mass transfer. In large scale applications however, this can lead to high operating costs due to excessive power consumption (Bredwell et al., 1999). Another approach for smaller bubble sizes is the introduction of microbubbles, which are surfactant stabilized bubbles with diameters of around 50 µm (Bredwell and Worden, 1998). Increasing the gassing rate will also enhance the gas-liquid mass transfer given that more gas is introduced into the system at the same time. However, the effect is considerably smaller than by increasing the power input (Doran, 2013).

3.4.2. Reactor Types for Gas Fermentation

Enhancing the gas-liquid mass transfer rates is the major challenge for syngas fermentations. There are several reactor types available for syngas fermentations and each has their own set of advantages and disadvantages. The dominant reactor type in published small scale applications is the CSTR (Daniell et al., 2012; Kantzow et al., 2015; Groher and Weuster-Botz, 2016; Hoffmeister et al., 2016; Bäumler et al., 2021). Its versatile application range make it the ideal reactor type for research and process development. As mentioned in Chapter 3.4.1, increasing the power-to-volume ratio $P\ V^{-1}$ is a widespread approach to reach a higher gas to liquid mass transfer due to increased bubble break up. The power input P in a CSTR can be described as following:

$$P_{CSTR} = Ne \cdot \rho_L \cdot N^3 \cdot d^5 \tag{3.24}$$

where Ne is the Newton number, ρ_L the density of the liquid, N the stirrer speed and d the diameter of the impeller. As (3.24) shows, stirrer speed and impeller diameter have the major influence on the power input. The impeller type and the Reynolds flow regime influence the Newton number (Kraume, 2003). In an investigation of 11 different impeller schemes, the dual Rushton-type impeller set up has proven to be the scheme with the highest k_La (Ungerman and Heindel, 2007) and therefore suitable for shear non-sensitive microbial fermentation. Furthermore, installations like baffles in the reactor will also increase the liquid-gas mass transfer by preventing funnel forming and propagating gas bubble breakage. As mentioned before (refer to Chapter 3.4.1), integrating a microbubble sparger (Bredwell and Worden, 1998) and increasing the partial pressures of the used gases also increases the mass transfer into the liquid phase, which has been proven for various applications and can significantly increase product yield (Kantzow and Weuster-Botz, 2016; Oswald et al., 2018). The major disadvantage of CSTR is the high-power consumption at large scale, a result of the high stirrer speeds necessary to reach sufficient $P\ V^{-1}$ ratios. This is also the reason for the dual Rushton-type impeller set up of having the lowest $k_La\ P^{-1}$ ratio despite showing excellent k_La values (Ungerman and Heindel, 2007). Increasing the partial pressure and including a microbubble sparger does not drive energy costs at large scale but requires extra investments in additional equipment.

Bubble column reactors (BCR) are the most common used alternative to the CSTR in syngas fermentations, especially in large scale applications (Abubackar et al., 2011). Crucial for BCR design is the diameter to length ratio and the gas sparger type (Asimakopoulos et al., 2018). Given that the BCR has no stirrer, the mixing of the fermentation broth is driven solely by the gas flow and the incremental density differences (Doran, 2013). BCR with an additional configuration for gas lift are usually referred to as air or gas lift reactors. These gas lift configurations can be realized with an internal or external loop for gas movement (see Figure 3-13).

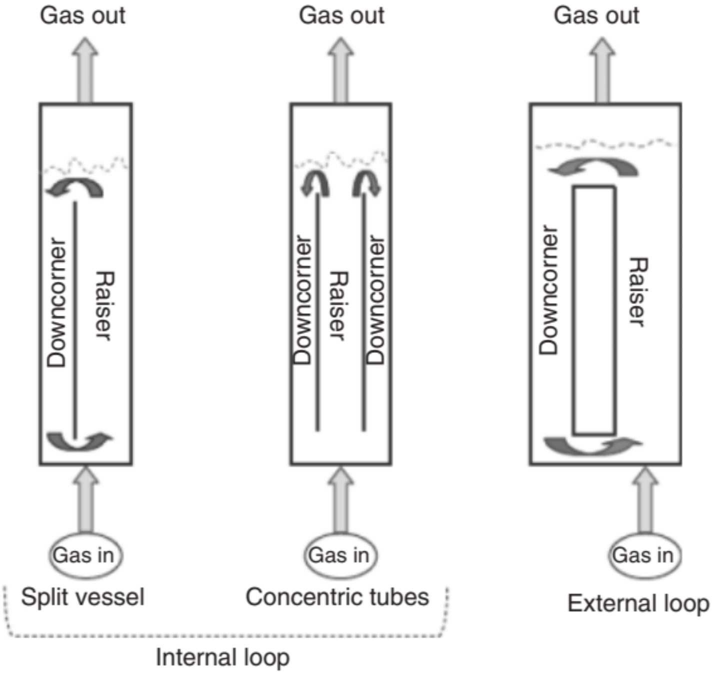

Figure 3-13: Different gas lift reactor configurations (Merchuk and Garcia Camacho, 2010)

The power input of a BCR is caused by the isothermal expansion of the gas introduced at the bottom of the reactor and can therefore be described as following:

$$P_{BCR} = \frac{\dot{V}_{gas} \cdot \rho_{gas}}{M_{gas}} \cdot R \cdot T \cdot \ln\left(\frac{1 + \rho_L \cdot g \cdot h}{p_U}\right) \tag{3.25}$$

where $\dot{V}_{gas}$ is the inlet gas flow rate, ρ_{gas} the density of the gas, M_{gas} the molecular weight of the gas, ρ_U the head space pressure in the vessel, ρ_L the liquid density, R the ideal gas constant, T the temperature, g the gravitational acceleration and h the liquid height above the sparger in the reactor (Takors et al., 2018). Thus, the critical parameters for increasing the mass transfer are the inlet gas flow rate and the height of the reactor above the sparger. Increasing liquid heights inevitably leads to increased partial pressures of the introduced gases at the bottom of the reactor, which increases mass transfer, but may also cause H_2- or CO-inhibition, depending on the used microorganism (Skidmore et al., 2013; Diender et al., 2016). Furthermore, due to the decline of the total pressure with increasing liquid height, axial gradients of gas partial pressures, of biomass and product concentration as well as pH are inevitable (Takors et al., 2018).

A reactor design with high reported mass transfer rates is the hollow fiber membrane reactor. In this set up, the microorganisms are immobilized on the surface of hollow fiber membrane modules. The culture broth is pumped through these modules to supply the microorganism with nutrients and remove toxic byproducts while the gas phase is transported through the inside of each fiber (Abubackar et al., 2011). The membranes are made of synthetic polymers such as polyethylene, polypropylene or polyvinylidene fluoride. Hollow fiber membrane reactors provide a high specific surface area and given that the gas is transferred to the microorganism via diffusion (no bubbles are formed) the gas-liquid mass transfer is increased significantly (Asimakopoulos et al., 2018). Studies have shown a significantly higher k_La for hollow fiber membrane reactor set ups in comparison with CSTR processes (Shen et al., 2014). Furthermore, due to their construction, these reactors can be operated at higher pressures for an increased mass transfer rate, considering the maximum operating pressure of the fibers (Abubackar et al., 2011). Major drawbacks for the hollow fiber membrane reactor are potential performance losses and higher operational costs due to membrane fouling and pore-wetting (Abubackar et al., 2011).

Another promising alternative to CSTR and BCR for syngas fermentations are trickle bed reactors. Here, the microorganisms are immobilized on the surface of carrier materials which form a fixed bed in the reactor. The fermentation medium is dispersed slowly from above the fixed bed, trickling over the carrier and forming a thin liquid film on them. The gas is supplied in counter current to the liquid phase, streaming from bottom to the top of the reactor (Takors et al., 2018). The advantage of the trickle bed reactor is the low thickness of the liquid- and biofilm on the carrier material, leading to high mass transfer rates. Furthermore, this reactor type consumes less energy compared to other reactor types, given that only the transport of the liquid and the gas phase require energy in larger amounts. However, this reactor type also faces axial gradients of pH and product concentrations along its height. Moreover, one major challenge for large scale applications is that the working volume (i.e., liquid phase and biomass volume) of this reactor is small in comparison with other set ups (Takors et al., 2018).

3.5. Co-Cultures

Most industrial fermentation processes are conducted in pure cultures, meaning the cultivation of only one microorganism species. Monocultures are especially important in the field of biopharmaceutics given its high demand on reproducibility, traceability and purity. However, in the last years, cultivations of two microorganisms simultaneously have gained more interest. Co-cultivations provide advantages such as the evasion of potential process limitation caused by the accumulation of byproducts, the metabolic burden of gene overexpression or thermodynamic limitations (Sabra et al., 2010; Mittermeier et al., 2023). This is accomplished through the division of labor (Roell et al., 2019) and the usage of different feed sources (Sabra et al., 2013; Wu et al., 2016). Furthermore, co-cultivations usually reduce the number of process steps, by integrating two or more cultivations in one process (Mittermeier et al., 2023). However, the complexity of co-cultivation processes is the main draw back in comparison to monocultures. Being of artificial nature, a process design which shows big potentials on paper might show incompatibilities of the species during cultivation, causing competitive or antagonistic behavior and thus loss of process performance (Mittermeier et al., 2023). It is therefore key, to fully understand the interactions of both species in order to develop a feasible co-culture process. These interaction mechanisms can be classified into six types: mutualism, commensalism, parasitism, competition, amensalism and neutralism (Mittermeier et al., 2023). Mutualism describes a mechanism where both species benefit from each other, e.g., by metabolite exchanging or functional differentiation (Che and Men, 2019). Commensalism refers to an interaction where only one specie benefits from the other without having any effect on the partner (Ma et al., 2019). Both mentioned interaction mechanisms describe cooperative relationships, while parasitism, competition, amensalism describe a negative interaction. In a parasitic interaction, one specie benefits from the other while also having a negative effect on the other (Faust and Raes, 2012). Competition describes a state, where both species compete with each other, e.g., for substrates, and thus negatively affecting each other. In amensalism, only one partner has a negative effect on the other and in neutralism, no interaction takes place (Mittermeier et al., 2023). For the application in biotechnological processes, usually only the positive interaction mechanisms are of interest. Examples for these types of interactions are: using one microorganism to provide substrate for the other, combining up- and downstream in one process, preventing microbial inhibition, or cultivating two species with completely different optimal growth conditions like anaerobic and aerobic microorganism together (Mittermeier et al., 2023). The array of species used in co-cultivation processes is vast. It ranges from bacterial consortia of equal genera, e.g., co-culture of *C. autoethanogenum* and *C. kluyveri* for the production of medium-chain fatty acids (Diender et al., 2016) or mixed bacterial consortia like the one described in this study, to fungal consortia with yeast or filamentous fungi (Ahamed and Vermette, 2008; Farias and Maugeri Filho, 2019). In addition, several studies have been reported on mixed bacterial-fungal consortia (Ho et al., 2012; Wang et al., 2019).

3.6. Electrochemical Basics

The basic electrochemical system is the electrochemical cell (see Figure 3-14), consisting of two so-called half-cells, each with different metallic electrodes in an electrolyte solution. Both half-cells are separated from each other, e.g., by an ion-selective membrane, a salt bridge or other. However, the separator enables ions to move from one half-cell to the other. When an electrical current is applied to both electrodes, an oxidation reaction takes place on the electrode of one of the half-cells, while a reduction reaction happens on the other. In other words, electrons are donated from one electrode to the ions of the electrolyte and are then taken up from the electrolyte to the electrode of the other half-cell which causes a flow of electrical current I from one electrode to the other. In this way, electricity can be used to drive non-spontaneous redox reactions and the system is called electrolytic cell. When spontaneous redox reactions happen in the cell, electrical energy is generated, and the cell is referred to as galvanic cell. (Bagotsky, 2006; Zoski, 2007)

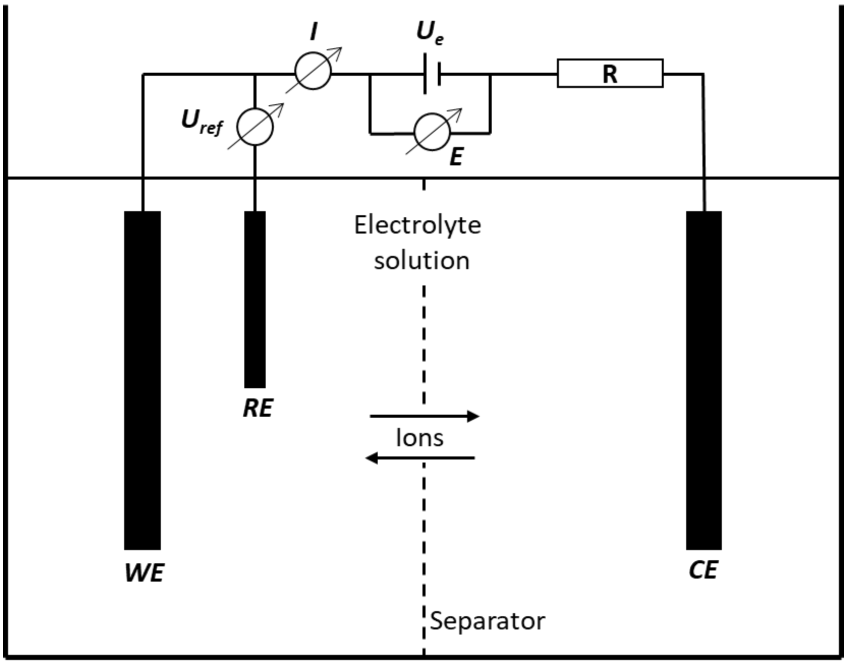

Figure 3-14: Schematic depiction of an electrochemical cell. Abbreviations: WE = working electrode; RE = reference electrode; CE = counter electrode; U_{ref} = voltage between WE and RE; I = circuit current; U_e = applied cell voltage; E = cell voltage; R = overall circuit resistance.

The electrical potential of an electrochemical cell can be calculated from the potential of both electrodes. Each electrode potential is defined relative to the standard hydrogen electrode (SHE) which, by convention, adds up to 0 V. The SHE is used as a form of comparison for all other electrode potentials and is based on a platinum electrode in an ideal solution of 1 M H^+ at 25 °C and 1 atm. To describe the relationship between the electrode potential E and the concentrations of the ions of a redox pair, the Nernst-equation (see Equation (3.26)) can be used:

$$E = E^0 + \frac{RT}{z \cdot F} \cdot \ln\left(\frac{c_{ox}}{c_{red}}\right) \tag{3.26}$$

where E^0 is the standard cell potential, R is the universal gas constant (8.314 J K^{-1} mol^{-1}), T is the temperature, z the number of electrons transferred in the redox reaction, F is the Faraday constant (9.65 x 10^4 C mol^{-1}), and c_{ox} / c_{red} are the oxidized and reduced species respectively (Zoski, 2007). Electrodes can be defined as working (WE) and counter electrode (CE), with the WE being the electrode in the half-cell where the reaction of interest takes place. During experiments, the cell potential is measured as the difference between the potential of the WE half-cell and the reference electrode, usually the before mentioned SHE (Zoski, 2007). In practice, reference electrodes like the Ag/AgCl, 3 M KCl electrode are used (E vs. SHE = 203 mV), which in turn are referenced to the SHE, as it is difficult to operate directly with the SHE (Zoski, 2007).

The electrical voltage *U* of an electrical system correlates with the electrical resistance R_{elec} and the electrical current *I* and is described in Ohm's law (See Equation (3.27)).

$$I = \frac{U}{R_{elec}} \tag{3.27}$$

The amount of substance generated during an electrochemical reaction *n* and its correlation to the total charge *Q* passed through a cell can be described with Faraday's law (Faraday, 1834) (see Equation (3.28)

$$Q = n \cdot z \cdot F \tag{3.28}$$

The relationship between the electrical charge, time and the electrical current is described in Equation (3.29).

$$I = \frac{\Delta Q}{\Delta t} \tag{3.29}$$

In order to compare electrochemical processes using different sizes of electrodes, the rate of the electrochemical reaction $r_{e/s}$ has to be normalized to the area of the electrode (Zoski, 2007). For this, the electrical current density j is used. The reaction which takes place on the electrode-solution interface is of a heterogeneous nature and can be described with Equation (3.30).

$$r_{e/s} = \frac{I}{nFA} = \frac{j}{nF} \tag{3.30}$$

with the current density described as the electrical current per surface area of the electrode (see Equation (3.31)).

$$j = \frac{I}{A} \tag{3.31}$$

3.6.1. Hydrogen Generation via Electrolysis

Hydrogen can be generated by applying an electrical current to two electrodes which are submerged in an aqueous electrolyte. The electrical current causes the water molecules to split up into hydrogen and oxygen, as shown in Equation (3.34).

$$\text{cathode reaction: } 2\ \mathrm{H^+} + 2\ \mathrm{e^-} \rightarrow \mathrm{H_2} \tag{3.32}$$

$$\text{anode reaction: } 2\ \mathrm{H_2O} \rightarrow \mathrm{O_2} + 2\ \mathrm{H^+} + 4\ \mathrm{e^-} \tag{3.33}$$

$$\text{total reaction: } 2\ \mathrm{H_2O} \rightarrow \mathrm{O_2} + 2\ \mathrm{H_2} \tag{3.34}$$

Given that the electrolysis reaction takes place at two different electrodes, the reaction can be described with Equation (3.32) for the cathode side and with Equation (3.33) for the anode side. This reaction requires a minimum theoretical amount of energy of 237 kJ mol^{-1} at an ideal voltage of 1.23 V (Hamann and Vielstich, 2005). However, various electrical resistances of the system lead to a necessary overpotential for the electrolysis to take place. These resistances are usually due to the gas bubbles covering the electrode surface, the ion transfer resistance in the electrolyte, resistances in the system circuits and due to the half-cell separator (Zeng and Zhang, 2010).

Equation (3.35) can be used to calculate the theoretical amount of generated hydrogen n_{H2}, applying the electrical charge Q, the electrons per molecule H_2 z_{H2} and the Faraday's constant F:

$$n_{H_2} = \frac{Q}{z_{H_2} \cdot F} \tag{3.35}$$

Due to the electrical resistances mentioned above, the actual amount of generated H_2 will always be below its theoretical value. The discrepancy of theoretical to actual value can be calculated with experimental data of generated H_2 and Equation (3.36), which is called Faradic or Coulombic efficiency (Zeng and Zhang, 2010).

$$\eta_F = \frac{z_{H_2} \cdot F \cdot n_{H_2}}{\Delta Q} \tag{3.36}$$

Industrial electrolysis is usually conducted with alkaline solutions, at high temperatures or using a proton exchange membrane (PEM). Alkaline electrolyzer are the most common, and operate in a KOH solution at about 80 °C. They can reach Faradic efficiencies of about 70 % (Zeng and Zhang, 2010). PEM electrolyzers operate at similar temperatures but the electrolyte of this system is the membrane itself, making it more efficient due to short response times. PEM fuel cells reach Faradic efficiencies up to 82 % (Zeng and Zhang, 2010). These operating parameters however are not suited for the application in biotechnology, involving living organisms growing at an optimal pH of 7 and temperatures of 30 – 40°C.

3.6.2. Redox Potential

The oxidation / reduction potential (ORP), or simply redox potential, describes the predisposition of chemical compounds to be reduced or oxidized and is measured in V. This means, that a chemical compound dissolved in an aqueous solution will tend to either gain or lose electrons when another compound is introduced into the medium. A solution with a higher ORP value will likely oxidize the introduced compound (gain electrons) and a solution with a low ORP value will likely reduce the introduced compound (lose electrons to the compound). In practice, the measurement of ORP can only be done by measuring the potential difference between an electrode which is in direct contact with the aqueous solution (sensor) and a reference electrode connected to the solution via a salt bridge. The reference electrode is defined by the standard hydrogen electrode and therefore, the discrepancy of E vs. SHE of the solution can be determined. The potential can be determined by applying the previously discussed Nernst-Equation (3.26). (Zoski, 2007) A low ORP is a very important growth condition for anaerobic organisms as the standard redox potential of many metabolic processes is low, e.g., the standard redox potential of the CO_2/acetate half-cell reaction in the acetyl-CoA pathway is -290 mV (Drake et al., 2008). This low ORP requirement can also be explained, by the high tendency of oxygen to accept electrons, thus a solution with a high O_2 content has a higher ORP. During fermentation of anaerobic species, redox active substances can be metabolized or produced by the microorganism, which leads to a change in ORP (Hunting and Kampfraath, 2013), e.g., acetogens can metabolize small amounts of dissolved oxygen in the medium (Boga and Brune, 2003), thus reducing the ORP of the fermentation medium. In general, a reduction of ORP at the beginning of an anaerobic cultivation has been reported, and furthermore, cell growth will only start when a sufficiently low ORP has been reached (Jacob, 1970).

3.6.3. Cyclic Voltammetry

Cyclic voltammetry is an analytical method in electrochemistry, to characterize electrodes and redox processes that take place at its surface (Hamann and Vielstich, 2005). Cyclic voltammetry can provide insights about the potential of redox reactions, the oxidation state of redox species, the rate of electron transfer or possible chemical processes associated with the electron transfer, amongst others (Bard, 2008). The measurement involves a linearly increasing and decreasing WE potential (vs. RE) cycle in between to potentials E_S^I and E_S^{II}, called switch potentials. The switch potentials are usually defined within the electrochemical stability range of the electrolyte, i.e., the anodic potential being below the potential where O_2 generation begins and the cathodic potential being below the potential of H_2 generation (Schmidt, 2003). The alteration of the electrical potential over time $\frac{dE}{dt}$, can be referred to as scan rate ν_{SR}. These potential cycles are repeated various times (Hamann and Vielstich, 2005). A typical cyclic voltammogram is shown in Figure 3-15 together with the diagram of WE potential vs. time.

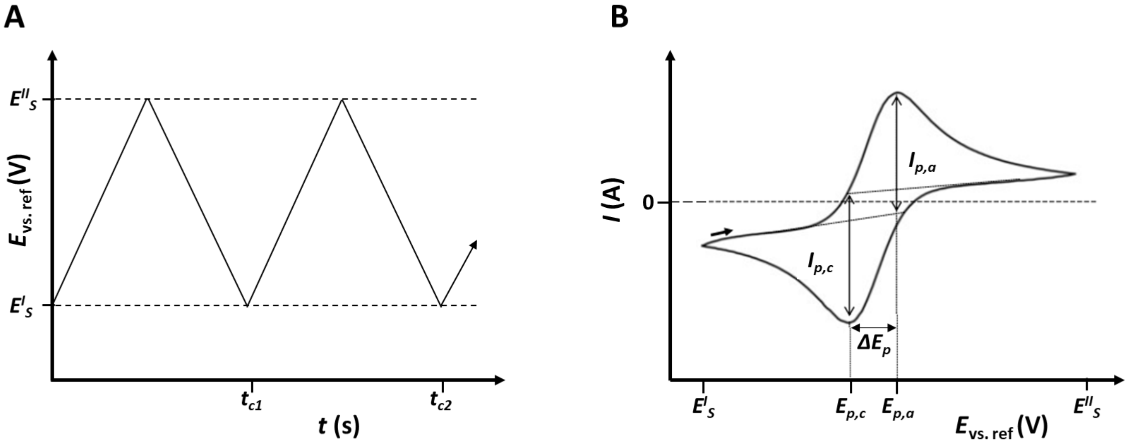

Figure 3-15: (A) working electrode potential over time. (B) typical cyclic voltammogram. Abbreviations: $\boldsymbol{E_S^I}$ and $\boldsymbol{E_S^{II}}$ = switch potentials; t_c = time of one cyclic voltammetry cycle; $I_{p,a}$ = anodic peak current; $I_{p,c}$ = cathodic peak current; $E_{p,a}$ = anodic peak potential; $E_{p,c}$ = cathodic peak potential; ΔE_p = potential difference between anodic and cathodic peak potential (adapted from Utesch, 2019).

The WE acts as anode during the interval where positive currents are flowing and as cathode, when negative currents are present. Electrochemically active compounds in the solution are indicated in the cyclic voltammogram as peaks. These can be present during the anodic or cathodic phase (or both), and can be described with the peak current $I_{p,a}$ / $I_{p,c}$ and peak potentials $E_{p,a}$ / $E_{p,c}$. These peaks indicate the optimal potential at which the compound is oxidized or reduced. If both the anodic and cathodic peak are identical, the system can be regarded as reversible (Bard, 2008). The peak current of a reversible system can be calculated with the Randles-Ševčik equation (3.37).

$$I_p = 0.466 \cdot z_i \cdot F \cdot A_e \cdot c_i \cdot \sqrt{\frac{z_i \cdot F \cdot v_{SR} \cdot D_i}{R \cdot T}} \tag{3.37}$$

This equation demonstrates that the peak current is dependent on the universal gas constant R, the Faraday constant F, the electrode surface area A_e, the temperature T of the system, the scan rate of the cyclic voltammetry v_{SR}, as well as the concentration, the diffusion coefficient and the number of transferred electrons of the chemical compound c_i, D_i, z_i.

3.7. Electrobiotechnology

The combination of biotechnology and electrochemistry is called electrobiotechnology. In 1911, M.C. Potter proved that the degradation of organic matter during a *S. cerevisiae* fermentation could produce electricity (Potter, 1911). The range of applications of combining microbial or enzymatic processes with electrochemistry has grown ever since. One relevant application field is the generation of electricity via so called microbial or enzymatic fuel cells (MFC/EFC). The purpose of MFC/EFCs is converting the chemical energy of substances during a biotechnological process into electrical energy (Harnisch and Holtmann, 2019). In a MFC, bacteria degrade organic matter for the production of ATP. The electrons involved in the electron transport chain for the production of ATP end up at a terminal electron acceptor, which is usually a chemical compound such as oxygen, nitrate or sulfate. However, some bacteria can transfer electrons outside the cell to a metal oxide, which in the case of a MFC would be an electrode, thus producing electrical power (Logan, 2008). EFCs operate in a similar way: here oxidoreductase enzymes catalyze the conversion of chemical to electrical energy (Rasmussen et al., 2016). The substances used as substrates in these fuel cells can come from waste waters or organic and inorganic matter from sediments (Harnisch and Holtmann, 2019). Some MFC applications have already moved on from lab scale and seem to be just a few steps away from commercial application (Hiegemann et al., 2016). Another widespread application in the field of electrobiotechnology is the cleaning of water and soil. It has been reported that X-ray contrast agents, nitrobenzene and nitrate were successfully removed from waste and ground water with microbial electrochemical technologies (Harnisch and Holtmann, 2019). Further applications include water recycling (Cao et al., 2009), sensors for analytics (Turner, 2013) and the synthesis of desired products with the aid of electricity, called bioelectrosynthesis (Harnisch and Holtmann, 2019). The term electro-fermentation, which has been used widely in past publications usually refers to similar processes. As Moscoviz et al., 2016 defined: “electro-fermentation (EF) is a novel process that consists of electrochemically controlling microbial fermentative metabolism with electrodes. The electrodes can act as either electron sinks or sources that allow unbalanced fermentation. They can also modify the medium by changing the redox balance.” This definition of electro-fermentation includes all systems, where electricity is not necessarily the primary energy source or the product of interest but is just a mean to increase productivity or selectivity for the desired product (Fruehauf et al., 2020).

In theory, electricity can influence a biological system by transferring electrodes. Electron transfer phenomena between bacteria and electrodes can be classified into two categories (see Figure 3-16): direct (DET) and indirect (IET) electron transfer (Harnisch et al., 2015; Choi and Sang, 2016; Gong et al., 2020). DET describes the transfer via membrane proteins such as cytochromes or via pili. Electron transfer via membrane proteins was reported in a MFC with *Shewanella oneidensis*, which converted lactate to acetate (Di Min et al., 2017), while electron transfer via pili was observed in *Geobacter sulfurreducens* using acetate and producing CO_2 (Reguera et al., 2005). IET describes electron transfer with the aid of mediators, which can include self-excreted electron mediators, artificial mediators or primary metabolites. *Shewanella* sp. can secret flavin mononucleotides and riboflavin, which can be used to transfer electrons to metal oxides or anodes (Lin et al., 2018). An example of IET with artificial mediators is the improved lipid production in *Rhodosporidium toruloides* using the redox mediator Neutral Red (Arbter et al., 2019). Furthermore, examples for IET with primary metabolites are manifold, ranging from H_2 (Villano et al., 2010) to formate (Li et al., 2012).

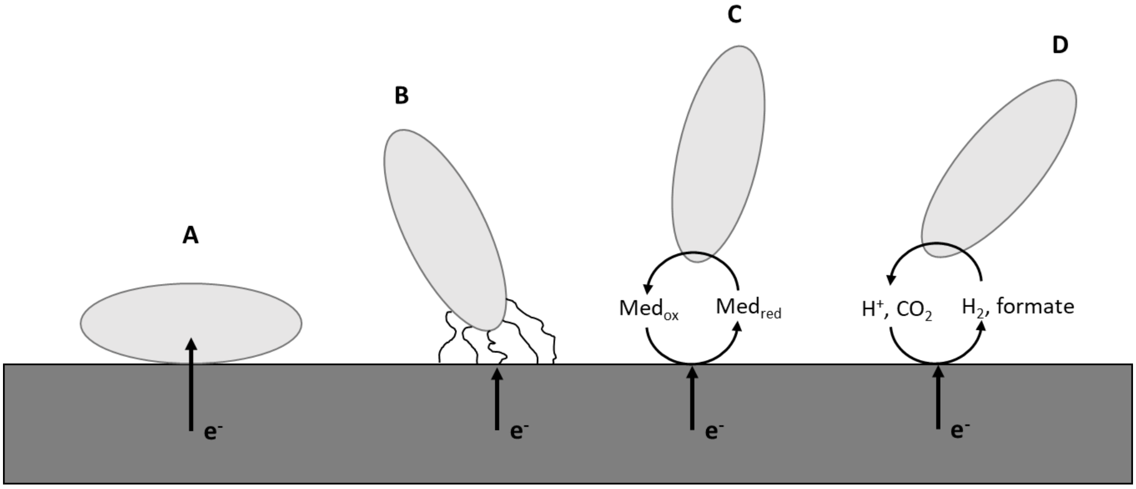

Figure 3-16: Cathodic electron transfer mechanisms for microorganisms. (A) direct electron transfer via membrane proteins; (B) direct electron transfer via pili / nanowires; (C) indirect electron transfer via redox mediators; (D) indirect electron transfer via byproducts / metabolites (adapted from Choi and Sang, 2016).

3.7.1. Bioelectrochemical Systems

Bioelectrosynthesis or electro-fermentations take place in so called bioelectrochemical systems (BES). This term describes all systems which contain at least two electrodes and an electrolyte, but also where at least one reaction is catalyzed by enzymes or microorganisms (Krieg et al., 2014; Schröder et al., 2015; Moscoviz et al., 2016). As mentioned earlier (refer to Chapter 3.6), the electrode where the reaction of interest occurs is referred to as WE, while the second electrode is named CE. In most BES, both electrodes are divided from each other by a separator, hence creating a CE and WE chamber. The separator’s task is to maintain redox gradients; thus, it has to be conductive for the ions of the electrolyte, and has to prevent crossover reactions (Krieg et al., 2014). Several materials for separators are used in current BES with the most common being polymer electrolyte membranes such as Nafion® (PEM). The biggest disadvantage of PEMs is their high price, which makes them hardly suitable for large scale applications. Lower priced separators can be ultrafiltration membranes or ceramic separators (Krieg et al., 2014). Electrode materials in BES also vary greatly, depending on the requirements of a process. Not only the redox processes taking place at the electrolyte have to be considered when choosing a suitable electrode material, but also the interactions of the microbes with the electrodes (Krieg et al., 2014). The variety of materials for electrodes ranges from gas diffusion electrodes (Liu and Logan, 2004) to carbon materials such as carbon fabrics (Kipf et al., 2013) to stainless steel (Soussan et al., 2013).

BES are generally classified into two categories: single- and two-chamber reactors (Krieg et al., 2019). However, the number of subcategories is vast, and some BES do not fit in either category. Figure 3-17 shows three general reactor set ups for BES.

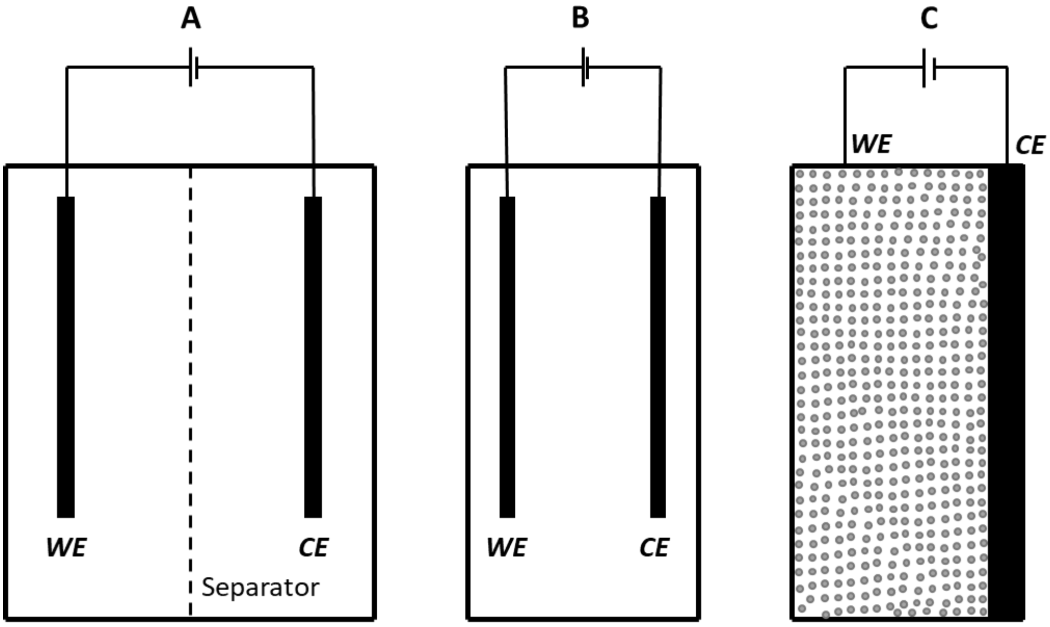

Figure 3-17: Simplified reactor set ups for BES. (A) two-chamber BES with separator; (B) single-chamber BES without separator; (C) fluidized bed BES where the particles function as WE (adapted from Krieg et al., 2014).

Most subcategories of BES are named after their geometrical design. There are, among others, cube-type reactors, both as single- and two-chamber set up, which have a simple set up and are suitable for lab and pilot scale applications (Ditzig et al., 2007; Rader and Logan, 2010; Cusick et al., 2011), cylindrical reactors (Bo et al., 2014), bottle-type reactors which are especially suitable for screening purposes (Kobayashi et al., 2013), column type (Guo et al., 2010) or rotating disk reactors (Cheng et al., 2011). One of the most commonly used two-chamber BES is the so-called H-Cell reactor which consists of two chambers, mostly bottles, connected by a tubular bridge which is closed half-way via an ion selective membrane (Logan et al., 2006; Krieg et al., 2019). This reactor type has an easy and inexpensive set up, making it an ideal system for lab scale studies, such as acetic acid or butyrate production from CO_2 (Nevin et al., 2010; Young Jeon et al., 2012). However, disadvantages of this system are the poorly mixed zones inside the bridge between the two chambers, a large unused volume for the CE chamber, high energy losses and low current densities due to the large distance between the two electrodes and a design which is hardly scalable to industry scale (Rozendal et al., 2006; Harnisch and Schröder, 2009; Sun et al., 2014). Most of the aforementioned reactor systems were applied in lab scale, where BES might already outperform conventional bioreactors, depending on the application. However, the lack of economically feasible large-scale concepts for the majority of BES is probably the biggest issue and prevents up to date successful commercial applications (Harnisch and Holtmann, 2019).

Due to the great variety of BES concepts, process comparison between studies and reactors are difficult. Therefore, the publication of reactor design and process parameters has been encouraged in the past (Krieg et al., 2014; Krieg et al., 2019). These parameters include the aforementioned productivity (3.16), Faradic efficiency (3.36), current density (3.31), product (3.15) and biomass yield (3.14) and growth rate (3.8) as well as those listed in Table 3-3.

Table 3-3: Important parameters for the characterization of BES. Abbreviations: ρ = liquid density; N = stirrer speed; d = stirrer diameter; η = dynamic viscosity; P = power input; V_L = liquid volume; A_e = surface area of an electrode; V_R = reactor volume.

Parameter	**Equation**	**#**
Reynolds number	$Re = \frac{\rho \cdot N \cdot d^2}{\eta}$	(3.38)
Newton number	$Ne = \frac{P}{\rho \cdot N^3 \cdot d^5}$	(3.39)
Specific volumetric power input	$\frac{P}{V_L}$	(3.40)
Surface to volume ratio	$SVA = \frac{A_e}{V_R}$	(3.41)

3.7.2. All-in-One electrode

As mentioned before in Chapter 3.7.1, the commonly used H-Cell system has a variety of disadvantages like high energy losses, low current densities, half of the reactor volume (CE chamber) cannot be used in the process and the reactor is unsuited for large scale application. To solve some of these issues, the AiO electrode shown in Figure 3-18 was developed by Utesch and Zeng (2018). It has a cylindrical rod shape and can be integrated in any standard bioreactor due to its standardized screw thread (PG 21). The AiO electrode can be sterilized via heat *in situ*, due to the scaffold made up of polyether ether ketone (PEEK), a material with a high temperature resistance. The WE is made up of platinized titanium mesh (coating density $\rho = 50$ g m^{-2}, coating thickness 2.5 µm) and faces outward to ensure contact with the fermentation medium where it produces the desired gas, H_2 in the case of this study. Therefore, the entire bioreactor functions as the WE chamber. Inside the working electrode grid is a ceramic separator which separates the WE from the CE chamber. The inside of the ceramic separator forms the CE chamber, with a platinum coated titanium rod functioning as CE. The ceramic separator ensures that H_2 and O_2 generated during electrolysis stay separated and prevents diffusion of bacterial cells into the CE. The CE chamber is left open at the top, so generated O_2 can leave the reactor unhindered. The surface area of the WE adds up to 74.8 cm^2 while the surface area of the CE is 13.8 cm^2. Given that WE and CE chamber differ greatly in size, electrochemical processes can take place without strongly affecting ion transfer or pH change (Utesch and Zeng, 2018). This design not only allows an effective *in situ* H_2 generation, but it has also been utilized in various BES applications, such as the control and optimization of electricity-aided production of 1,3-propandiol and lipids (Arbter et al., 2019; Utesch et al., 2019; Arbter et al., 2021; Arbter et al., 2022; Zhang et al., 2023).

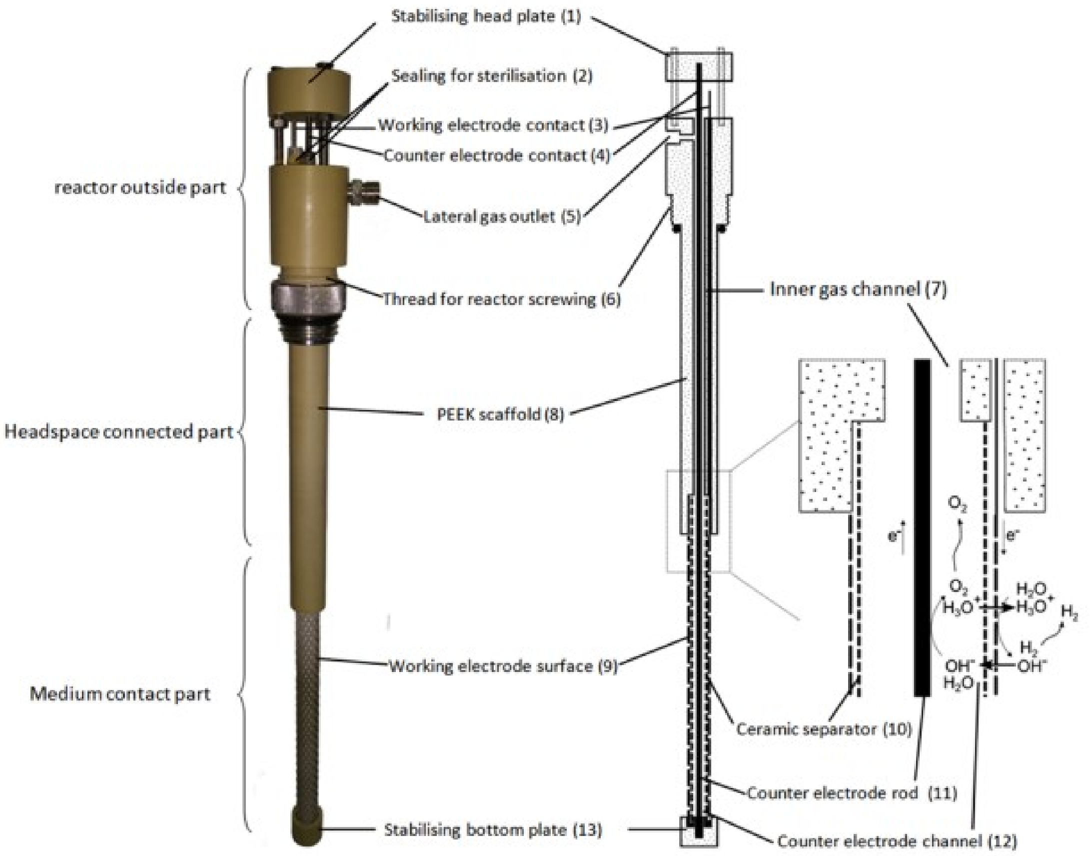

Figure 3-18: Blueprint and working principle of the All-in-One electrode (from Utesch and Zeng, 2018)

4 Materials and Methods

4.1. Microorganisms

All bacterial strains used in this study are listed in Table 4-1. All recombinant *A. woodii* strains were provided by the working group of Frank R. Bengelsdorf of the Institute of Microbiology and Biotechnology of the Ulm University. The construction of *A. woodii* [P_{bgaL}_*ldhD*_NFP] as well as their features are described by Mook et al., 2022. *A. woodii* P_{tet}_*ldhD*$_{\text{CI}}$ was constructed and described by Beck, 2020. The *C. drakei* and *A. woodii* wild type strains were obtained from the German Collection of Microorganisms (DSMZ 12750 and 1030 respectively).

Table 4-1: Overview of bacterial strains used in this study.

Strain	**Genotype**	**Source**
A. woodii WT	*Acetobacterium woodii WB1*	DSMZ 12750
A. woodii P_{tet}_*ldhD*$_{\text{CI}}$	*Acetobacterium woodii ΔlctBCD ΔpyrE*::*pyrE*-P_{tet}-*ldhD*	(Beck, 2020)
A. woodii [P_{bgaL}_*ldhD*_NFP]	*Acetobacterium woodii ΔlctBCD ΔpyrE* [p83_P_{bgaL}_NFP]	(Mook et al., 2022)
C. drakei	*Clostridium drakei SL1*	DSMZ 1030

4.2. Cryo-Culture Preparation

The strains listed in Table 4-1 were delivered as a lyophilized culture in a glass ampoule. The ampoule was opened under sterile and anaerobic conditions by carefully gassing the ampoule with CO_2. The lyophilized culture was then dissolved in 3 mL of anaerobic and sterile pre-culture medium (see Table 4-2). Then the complete volume of cell broth was used to inoculate a 100 mL anaerobic bottle filled with 50 mL of anaerobic and sterile pre-culture medium. The bottle was incubated at 30 ° for about 120 h. Subsequently, 2 mL of this cell broth were transferred to a second bottle with fresh pre-culture medium. In an anaerobic chamber, 35 mL of the cell culture were filled into an anaerobic bottle containing 15 mL degassed DMSO (20 % *v/v*). The cell broth and the DMSO were mixed by shaking. Then 1.8 mL of cell-DMSO broth were filled into 2 mL cryo-tube. These vials were stored at -80 °C for further cell cultures. Subsequent preparation of cryo-cultures was prepared the same way except the cell broth for long-term storage was taken from a pre-culture which was incubated at 30 °C until it had reached an OD_{600} of 1 - 2.

4.3. Fermentation Media

All media used in this study are described in Table 4-2 - Table 4-11.

Table 4-2: Composition of the pre-culture medium (Hoffmeister et al., 2016)

Substance	**Concentration [g L^{-1}]**
NH_4Cl	0.20
KH_2PO_4	1.76
K_2HPO_4	8.44
Yeast extract	6.00
Uracil	0.02
Cysteine-HCl x H_2O	0.30
$NaHCO_3$	10.00
	Concentration [mL L^{-1}]
Resazurin solution (0.1 %)	1.00
Trace elements solution (see Table 4-4)	2.00
Selenite-tungsten solution (see Table 4-6)	1.00
Na_2S solution (15 g L^{-1})	20.00
Fructose solution (500 g L^{-1})	20.00
Vitamin solution (see Table 4-5)	2.00
$MgSO_4$ x 7 H_2O solution (165 g L^{-1})	2.00

For the preparation of the pre-culture medium, all chemicals except cysteine and $NaHCO_3$ as well as the Na_2S, fructose, vitamin and $MgSO_4$ solutions were dissolved in deionized (DI) water. The solution was then degassed at 90 °C for 30 min. with 100 % N_2. Afterwards, cysteine and $NaHCO_3$ were added. The medium was filled in previously degassed anaerobic bottles under a N_2 atmosphere. The bottles were closed airtight and then sterilized at 121 °C for 20 minutes. Before inoculation, the Na_2S, fructose, vitamin and $MgSO_4$ solutions were added under sterile conditions to each bottle.

For the pre-cultivation of *C. drakei*, a sodium-DL-Lactate solution (233 g L^{-1}) was added to the medium in 50:50 or 75:50 (*v/v*) ratios with fructose.

Table 4-3: Composition of the main fermentation medium

Substance	**Concentration [g L^{-1}]**
$(NH_4)_2SO_4$	0.70
KH_2PO_4	1.76
K_2HPO_4	8.44
Yeast extract	3.00
Uracil	0.02
Cysteine-HCl x H_2O	0.30
$NaHCO_3$	10.00
	Concentration [mL L^{-1}]
Trace elements solution (see Table 4-4)	2.00
Selenite-tungsten solution (see Table 4-6)	1.00
Na_2S solution (15 g L^{-1})	1.00
Vitamin solution (see Table 4-5)	2.00
$MgSO_4$ x 7 H_2O solution (165 g L^{-1})	2.00

For the main fermentation medium, NH_4Cl was replaced with $(NH_4)_2SO_4$, given that the release of Cl_2 gas caused by the electrode from the medium should be prevented due to safety reasons. For the preparation, all chemicals except cysteine and $NaHCO_3$ as well as the Na_2S, fructose, vitamin and $MgSO_4$ solutions were dissolved in DI-water, filled into the bioreactor and were then sterilized at 121 °C for 20 min. *in situ*. After sterilization, the hot medium was gassed with N_2 for 10 min. to remove any traces of oxygen. Subsequently, cysteine and $NaHCO_3$ as well as the Na_2S, vitamin and $MgSO_4$ solutions were added. The resazurin solution was added to the fermentation medium for the first experiments, however, due to a growth inhibiting effect, it was left out during later experiments (refer to Chapter 5.2.6)

For *C. drakei* cultivations, sodium-DL-Lactate was added in different concentrations to the medium.

Table 4-4: Composition of the trace elements solution (Tschech and Pfennig, 1984)

Substance	**Concentration [g L^{-1}]**
Nitrilotriacetic acid	12.8
$MnCl_2$ x 2 H_2O	0.1
$FeCl_2$ x 4 H_2O	2.0
$CoCl_2$ x 6 H_2O	0.2
	Concentration [mg L^{-1}]
$ZnCl_2$	70.0
$CuCl_2$ x 2 H_2O	2.0
H_3BO_3	6.0
Na_2MoO_4 x 2 H_2O	36.0
$NiCl_2$ x 6 H_2O	24.0

For the preparation of the trace elements solution, nitrilotriacetic acid was first dissolved in 200 mL of DI-water. Then, the pH was adjusted to 6.5 with 1 M of KOH. Afterwards, the other chemicals were added and dissolved. Finally, the pH of the solution was adjusted to 7.0 and sterilized at 121 °C for 20 minutes.

Table 4-5: Composition of the vitamin solution (Wolin et al., 1963)

Substance	**Concentration [mg L^{-1}]**
Biotin	25.0
Folic acid	25.0
Pyridoxine-HCl	50.0
Thiamine-HCl	50.0
Riboflavin	50.0
Nicotinic acid	50.0
D-Ca-pantothenate	50.0
Cyanocobalamine	25.0
α-Aminobenzoic acid	50.0
Lipoic acid	25.0

For the preparation of the vitamin solution, all chemicals were dissolved in DI-water and then sterilized via filtration (0.2 µm cut-off).

Table 4-6: Composition of the selenite-tungsten solution (Tschech and Pfennig, 1984).

Substance	**Concentration [g L^{-1}]**
NaOH	0.5
	Concentration [mg L^{-1}]
Na_2SeO_3 x 5 H_2O	3.0
Na_2WO_4 x 2 H_2O	4.0

For the preparation of the selenite-tungsten solution, NaOH was dissolved in DI-water first. Subsequently, the other chemicals were added and the solution was sterilized in an autoclave at 121 °C for 20 minutes.

Table 4-7: Modified Tanner medium for *C. drakei* cultivation (Tanner, 2007)

Substance	**Concentration [g L^{-1}]**
NaCl	2.00
NH_4Cl	2.50
KCl	0.25
KH_2PO_4	0.25
$CaCl_2$ x 2 H_2O	0.10
Yeast Extract	3.00
MOPS	20.00
Cysteine-HCl x H_2O	0.30
	Concentration [mL L^{-1}]
Resazurin solution (0.1 %)	1.00
Trace elements solution 2 (see Table 4-8)	10.00
Vitamin solution 2 (see Table 4-9)	10.00
$MgSO_4$ x 7 H_2O solution (165 g L^{-1})	3.00
Fructose solution (500 g L^{-1})	20.00

The modified Tanner medium was prepared as the pre-culture medium listed in Table 4-2.

Table 4-8: Trace elements solution 2 for modified Tanner medium (Tanner, 2007)

Substance	**Concentration [g L^{-1}]**
Nitrilotriacetic acid	2.0
$MnSO_4$ x H_2O	1.0
$(NH_4)_2Fe(SO_4)_2$ x 6 H_2O	0.8
$CoCl_2$ x 6 H_2O	0.2
	Concentration [mg L^{-1}]
$ZnSO_4$ x 7 H_2O	1.0
$CuCl_2$ x 2 H_2O	20.0
Na_2SeO_3 x 5 H_2O	20.0
Na_2MoO_4 x 2 H_2O	20.0
$NiCl_2$ x 6 H_2O	20.0
Na_2WO_4 x 2 H_2O	20.0

The trace elements solution 2 (Tanner medium) was prepared as the trace elements solution listed in Table 4-4.

Table 4-9: Vitamin solution 2 for modified Tanner medium (Tanner, 2007)

Substance	**Concentration [mg L^{-1}]**
Biotin	2.0
Folic acid	2.0
Pyridoxine-HCl	10.0
Thiamine-HCl	5.0
Riboflavin	5.0
Nicotinic acid	5.0
D-Ca-pantothenate	5.0
Cyanocobalamine	5.0
α-Aminobenzoic acid	5.0
Lipoic acid	5.0
2-Mercaptoethansulfonate	2.0

The vitamin solution 2 (Tanner medium) was prepared as the vitamin solution listed in Table 4-5.

Table 4-10: 104b. PY + X Medium (DSMZ, Germany)

Substance	Concentration [g L^{-1}]
Trypticase peptone	5.0
Peptone from meat (Pepsin-digested)	5.0
Yeast Extract	10.0
L-Cysteine-HCl × H_2O	0.5
D-Glucose	5.0
	Concentration [mL L^{-1}]
Resazurin solution (0.1 %)	0.5
Salt solution (see Table 4-11)	40.0

The 104b. PY + X Medium (DSMZ, Germany) was prepared as the pre-culture medium listed in Table 4-2.

Table 4-11: Salt solution for 104b. PY + X Medium (DSMZ, Germany)

Substance	Concentration [g L^{-1}]
$CaCl_2 \times 2\ H_2O$	0.25
$MgSO_4 \times 7\ H_2O$	0.50
K_2HPO_4	1.00
KH_2PO_4	1.00
$NaHCO_3$	10.00
NaCl	2.00

The salt solution for 104b. PY + X Medium (DSMZ, Germany) was prepared as the trace elements solution listed in Table 4-4.

The $MgSO_4$, fructose, lactate and resazurin stock solutions were sterilized in an autoclave (121 °C, 20 min.) while the Na_2S stock solution was sterilized via filtration (0.2 µm cut-off).

4.4. Serum Bottle Pre-Culture Fermentation

The pre-cultures for all *A. woodii* strains were cultivated heterotrophically at 30 °C in a non-shaken incubator in 100 and 200 mL anaerobic serum bottles filled with 50 and 100 mL of the previously described pre-culture medium (refer to Table 4-2), respectively. Pre-cultures for *C. drakei* were first conducted in the DMSZ medium 104b (see Table 4-10) and then, the strain was adapted to the Tanner medium (see Table 4-7). Subsequently, *C. drakei* was adapted to the standard pre-culture medium (refer to Table 4-2). The medium was supplemented with lactate in different lactate/fructose ratios (50:50 and 75:25 (*v/v*)). The pre-cultures for both strains were incubated for 33 - 38 h. The end of a pre-culture fermentation was determined by taken a 2 mL sample of cell broth under sterile conditions and measuring the OD_{600} (see chapter 4.6).

For *C. drakei* growth inhibition tests, anaerobic pre-culture bottles filled with 50 mL of standard pre-culture medium (refer to Table 4-2) were supplemented with caproic acid concentrations in between 1.2 and 16.5 g L^{-1}. Then, the bottles were inoculated with 3 mL of *C. drakei* cell broth and monitored for 40 h. All fermentations were conducted in duplicates. Additionally, two cultures were conducted without the addition of caproic acid for control purposes.

4.5. Stirred-Tank BES Batch Fermentations

All batch fermentations were conducted in a 2.0 L stirred-tank bioreactor (KSF2000; Bioengineering AG, Wald, Switzerland) with a working volume of 1.3 - 1.4 L. Before each fermentation the medium was sterilized *in situ* at 121 °C for 20 min. Afterwards, the cultivation medium was degassed with N_2 to ensure anaerobic conditions. An ORP sensor (Pt4805-DPAS-SC-K8S/225; Mettler Toledo GmbH, Gießen, Germany) was installed to ensure an ORP value lower than -200 mV prior to inoculation. The pH of the culture was measured via pH sensor (405-DPAS-SC-K8S/225; Mettler Toledo, GmbH, Gießen, Germany) and controlled at pH 7.0 ± 0.2 by the addition of a 5 M KOH solution. The culture medium was agitated with three Rushton disk turbines at different stirrer speeds in between 200 – 1,300 rpm. For power input calculations, a Newton number of 13.5 was assumed for the system (3 Rusthon type disk turbines each with Ne = 4.5). The temperature was controlled at 30 °C. CO_2 gas flow was set to 0.01 vvm for *A. woodii* and to 0.003 vvm for *C. drakei* cultivations and the fermentation medium was saturated with CO_2 before inoculation. Gas flows were set via mass flow meters (EL-FLOW; Bronkhorst High-Tech B.V., Ruurlo, Netherlands). For inoculation, the transfer volume from pre-culture to bioreactor was calculated to reach a theoretical starting OD_{600} in the bioreactor of 0.1 – 0.2. The production of lactate was induced with the addition of 1 mM lactose for *A. woodii* [P_{bgaL}_*ldhD*_NFP] and with the addition of 0.1 g L^{-1} anhydrotetracycline for *A. woodii* P_{tet}_*ldhD*$_{CI}$ cultivations.

For the lactate dependent process control, lactate concentrations in the medium were determined with the TRACE C2 control (TRACE Analytics GmbH, Braunschweig, Germany) and a dialysis probe with a membrane for low lactate concentrations. Sampling rate of the TRACE C2 was set to one sample per hour. The automated current adjustment for H_2 generation by the AiO electrode was regulated by a LabVIEW script containing a PID algorithm. The process variable lactate concentration (g L^{-1}) was transmitted with 4-20 mA via an analog digital converter (USB-6001; National Instruments Corp., Austin, TX, USA) to the host computer. The control variable was the electrical current (A) applied to the AiO electrode by a power supply (2231A-30-3; Keithley, Solon, OH, USA) via RS232 communication. The setpoint was the desired lactate concentration. The D value of the controller was set to 0 while proportional gain was set to 0.01 and the integral time to 2 min with a sampling time of 10 ms.

For co-culture fermentations, *A. woodii* [P_{bgaL}_*ldhD*_NFP] was inoculated first and grown until stationary phase to ensure sufficient production of lactate. Then, 90 mL of a *C. drakei* culture (OD_{600} = 0.96 ± 0.03) from a pre-culture bottle were added to the bioreactor.

Samples of the cell broth were taken at different intervals during each fermentation via sampling port at the bottom of the reactor.

4.5.1. AiO-Electrode Operations

For the BES fermentations, H_2 was supplied by the AiO-electrode via *in situ* electrolysis. The electrode material was platinized titan with a platin coating thickness of $d = 2.5$ µm and a coating density of $\rho = 50$ g m^{-2} (METAKEM GmbH, Usingen, Germany). The working electrode was a metal mesh cylinder with total surface area of 74.8 cm^2 while the counter electrode was metal rod with a surface area of 13.8 cm^2. The working electrode of the new AiO design was a double mesh cylinder with a total surface area of 205.7 cm^2. The electrodes were separated by a ceramic separator and the O_2 which was generated during electrolysis in the anode chamber left the reactor through an exhaust duct (refer to Utesch, 2019 and chapter 3.7.2 for details). The AiO-electrode was controlled chronopotentiometrically by a potentiostat (Interface 1000; Gamry Instruments, Warminster, PA, USA) or a power source (2231A-30-3; Keithley, Solon, OH, USA) and was operated without reference electrode to maintain a constant electrical current of 400 - 600 mA.

For cyclic voltammetry (CV) analysis of the AiO-electrode, control and data acquisition was performed with the software Gamry Framework V 7.07 (Gamry Instruments, Warminster, PA, USA). CV analysis were run with reference electrode (Ag/AgCl RE-1B; ALS Co. Ltd, Tokyo, Japan) at a temperature of 30 °C, a stirrer rate of 200 rpm and a N_2 gassing rate of 5 L h^{-1}. The CV scan was performed in between -0.9 and 1.5 V (*E* vs Ag/AgCl) with a scan rate of 50 mV s^{-1} and a step size of 10 mV. In total, 4 cycles were performed.

4.5.2. Stirred-Tank Gas Fermentations

Conventional gas fermentations were conducted out in a 2.0 L stirred-tank bioreactor (Labfors; Infors AG, Bottmingen, Switzerland) with a working volume of 1 L in the laboratory of Prof. Dr. Weuster-Botz at the Chair of Biochemical Engineering, TUM School of Engineering and Design. Before each batch fermentation the medium and the bioreactor were sterilized at 121 °C for 20 min in an autoclave. Afterwards, the cultivation medium was degassed with a gas mixture of H_2/CO_2 (70/30 %) for 4 h prior to inoculation to ensure anaerobic conditions and to saturate the medium with the respective gasses. The flow rates of the gas mixture were adjusted to 0.5 vvm and 0.025 vvm, respectively. The pH of the culture was measured via pH sensor and controlled at pH 7.0 ± 0.1 by the addition of a 3 M NaOH solution. The culture was agitated with two Rushton turbines at 1,000 rpm ($P\ V^{-1} = 6.8\ \mathrm{W\ L^{-1}}$) and the temperature was controlled at 30 °C.

4.6. Analytics

The off gas was monitored constantly with a mass flow meter (EL-FLOW prestige; Bronkhorst High-Tech B.V., Ruurlo, Netherlands) and a mass spectrometer (Omnistar GDS 300; Pfeiffer Vacuum GmbH, Asslar, Germany). The optical cell density of the culture was measured offline with a spectral photometer (V3000PC; VWR international GmbH, Darmstadt, Germany and Genesys 150; Thermo Fischer Scientific, Waltham, MA, USA) at 600 nm (OD_{600}). The samples were diluted with filtered DI-water if necessary to reach an absorption value in between 0.1 and 0.6. OD-measurements were blanked against filtered DI-water and performed in technical triplicates. Organic acid concentrations were determined via high performance liquid chromatography (HPLC) system (Smartline; Knauer Wissenschaftliche Geräte GmbH, Berlin, Germany) equipped with an UV- and RI-detector (UV Detector 2500 and RI Detector 2300; Knauer Wissenschaftliche Geräte GmbH) and an Aminex HPX-87H column (Biorad Laboratories Inc., Berkley, USA). The measurements were run at 30 °C with 0.1 % trifluoroacetic acid as eluent and a constant flow rate of 0.6 mL min^{-1}. Samples were centrifuged (Heraeus Fresco 17; Thermo Fisher Scientific) at 13,000 rpm for 5 min. and the supernatant was filtered (0.22 µm cut-off) before being loaded into the HPLC system for measuring. Internal standards for propionate, formate, succinate, lactate, acetate and butyrate (UV) were used for the analysis while caproate and fructose (RI) standards were added as external standards to each measurement if necessary. The software ChromGate V3.3.1 (Knauer Wissenschaftliche Geräte GmbH) was used for HPLC control and for the evaluation of the chromatograms. Dry cell weight (DCW) was determined gravimetrically for each strain for the calculation of a correlation factor (OD_{600} – CDW). For this purpose, 1 mL of cell broth was filled in a previously dried 1.5 mL Eppendorf tube (24 h at 80 °C), centrifuged (13,000 rpm, 5 min.) and the supernatant discarded. Subsequently, the cell pellet was dried over night at 80 °C and afterwards the weight Eppendorf tube was determined. The correlation factor of 0.51 g L^-1 was estimated by linear regression by plotting the determined DCW versus the OD_{600} of a fermentation. The analysis of metals (Na, K, Mg, Fe, Cu, Co, Zn, Ni, Mn, and Se) in the culture medium with an operating AiO-electrode was conducted with inductively coupled plasma optical emission spectrophotometry (ICP-OES) in the central lab (Zentrallabor) of the Hamburg University of Technology.

For the experiments conducted in the laboratory at the TUM School of Engineering and Design, organic acids, inlet and exhaust-gas as well as optical cell density were carried out according to (Bäumler et al., 2021).

4.6.1. Calculations of Process Performance Parameters

The volumetric productivity was calculated using Equation (3.16) and the time value when the maximum product concentration was reached for the first time. The calculation of the product formation rates q_{Lac} and q_{Cap} as well as the lactate consumption rate $-q_{Lac}$ rates was done via linear regression. The maximum growth rate was calculated with Equation (3.10). The biomass and product yields from substrate, $Y_{X/S}$ and $Y_{P/S}$, were calculated with the Equations (3.14) and (3.15), respectively. Carbon balancing was done using the Equation (3.17).

5 Results and Discussion

5.1. Characterization of AiO Electrode in Fermentation Medium

Since previous applications with the AiO electrode used different cultivation media (Arbter et al., 2019; Utesch et al., 2019), the electrode was characterized in the cultivation medium described in Chapter 4.3 before fermentation experiments were conducted. Although for the AiO electrode set up as described in Chapter 3.7.2 the polarity of the cathode (in this case the WE) is negative and thus the applied currents and voltages are also negative, the absolute values of currents and voltages were used for better illustration purposes. For the characterization, the hydrogen evolution rate in the BES set up for a constant current of 600 mA was first determined (j = 8.0 mA cm^{-2}; P = 2.5 W). The results are shown in Figure 5-1. During the first 2 h of the experiment, the hydrogen evolution rate increased constantly and reached 4.5 mmol h^{-1}. After 3 h, the H_2 evolution rate reached a value of 6.0 mmol h^{-1} and showed a more constant output. The maximum H_2 evolution rate added up to 9.0 mmol h^{-1}, while the average output over the whole experiment added up to 7.3 mmol h^{-1}. After 15 h, the current was increased to 700 mA for another 23 h (data not shown). The average H_2 evolution rate added up to 8.9 mmol h^{-1}. With the total of 295.67 mmol of generated H_2 during the entire experiment, a Faradaic efficiency of 70 % was determined with Equation (3.36) for the AiO electrode in the cultivation medium. The electrode potential (see Figure 5-1) increased rapidly during the first minutes to a maximum of 8.5 V. Afterwards, the potential decreased again and after 2 h, the potential reached its average value of 4.7 V. The AiO generates fine bubbles during its operation, turning the cultivation medium completely turbid (see Figure 5-2). These fine bubbles are one of the reasons, for the high H_2 mass transfer efficiency of the AiO electrode, as determined by Utesch, 2019. For further characterization, CV was conducted as described in Chapter 4.5.1. The CV is shown in Figure 11-1 in the appendix.

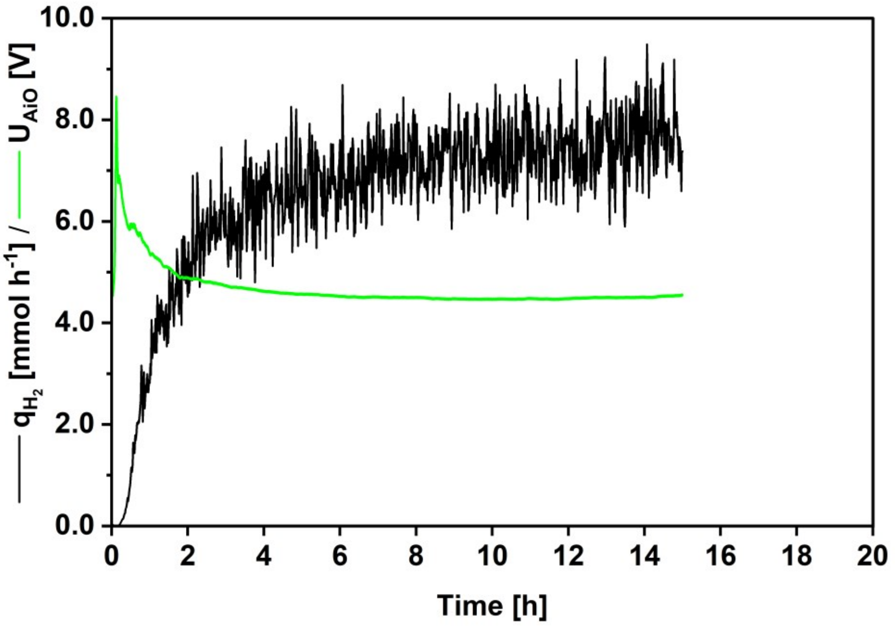

Figure 5-1: Hydrogen evolution rate of the AiO electrode in the BES set up, measured in the exhaust gas of a stirred-tank bioreactor (black line, mmol h^{-1}); voltage of the AiO at constant operating current of 600 mA (green line, V). Parameters: $T = 30$ °C; pH = 7.0; $P\ V^{-1} = 4.7$ W L^{-1}; $\dot{V}_{CO_2} = 0.01$ vvm; $V_0 = 1.4$ L; $I_{AiO} = 600$ mA; $U_{av} = 4.7$ V.

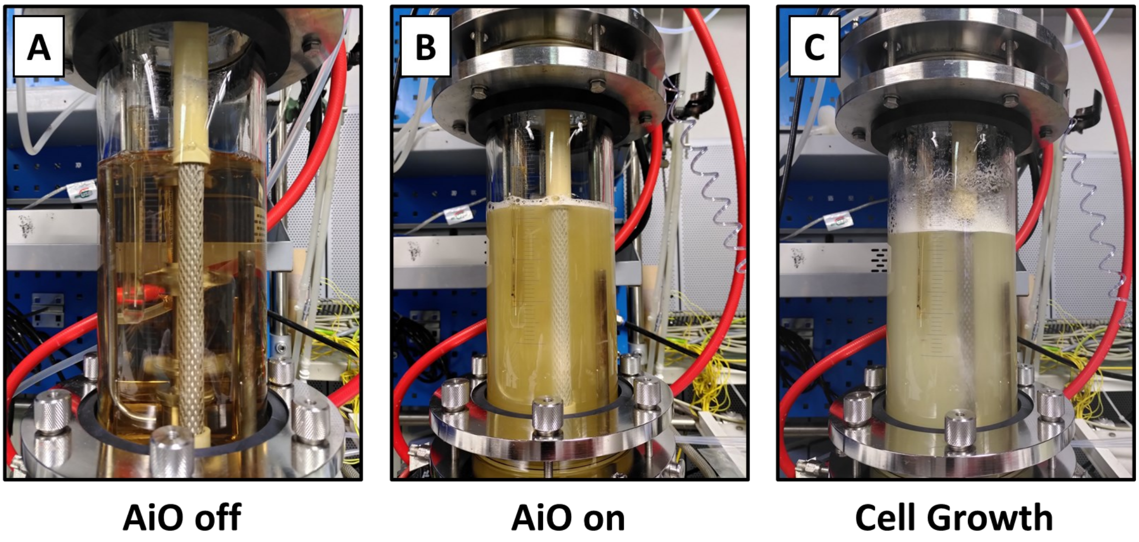

Figure 5-2: AiO electrode operation in a stirred tank bioreactor. (A) unstirred bioreactor without electrode activity. (B) stirred bioreactor with operating AiO electrode at 600 mA – the turbidity of the medium is due to H_2 formation. (C) bioreactor during a fermentation of *A. woodii* P$_{tet}$_*ldhD*$_{CI}$ with working AiO electrode.

As shown by Utesch and Zeng (2018), higher electrical currents produce a higher H_2 evolution rate, but also higher necessary voltages. The current set point of 600 mA was therefore chosen to be the standard setting for fermentations, as higher voltages can cause cell growth inhibition (see Chapter 5.2.7). The average H_2 evolution rate was proven suitable for cell growth and lactate production and is 1.2-fold higher than previously published (Utesch and Zeng, 2018). The Faradaic efficiency of 70 % however was 1.2-fold lower than reported (Utesch, 2019) which is assumed to be due to the use of different cultivation media. Industrial electrolyzers reach Faradaic efficiencies of 70 to 82 % (Zeng and Zhang, 2010). These operating parameters however are not suited for the application with living cells (see Chapter 3.6.1).

5.1.1. Alternative AiO Electrode Designs

As shown in the following Chapter 5.2, the H_2 production rate of the original AiO electrode design was the limiting factor in autotrophic BES fermentations. To supply more H_2, the electrical current would have to be increased, resulting in higher current densities and higher voltages. As high voltages seem to inhibit cell growth (see Chapter 5.2.7), maintaining the current density at 8 mA cm^{-2} by increasing the surface could result in lower voltages but higher currents (see Equation (3.31)). Therefore, new electrodes were designed to reach higher surface areas. The first design is shown in Figure 5-3. The diameter of cathodic metal mesh cylinder was increased by a factor of 1.6 and a second metal mesh cylinder was inserted. This double cylinder design reached a total surface area of 205.7 cm², an increase of 2.8-fold in comparison to the original design. Since potential limiting effects due to the anode surface are possible, the anode rod was equipped with a metal cylinder mesh, increasing its surface by 2.5-fold to 34.9 cm². With this cathode area, a theoretical current of 1.6 A would be possible, leaving the current density constant at 8 mA cm^{-2}. For the second AiO redesign, just the diameter of the cathode cylinder was increased, reaching a new surface area of 130.9 cm² (no blueprint shown).

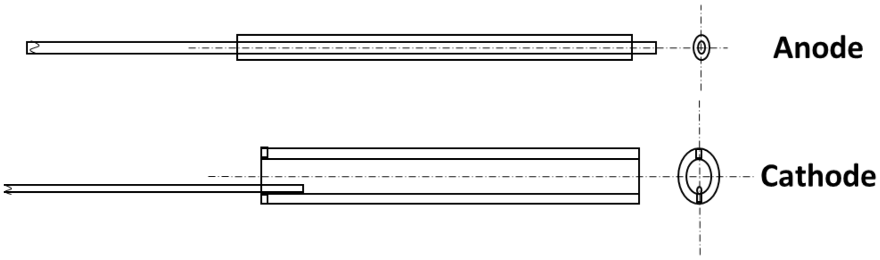

Figure 5-3: Blueprint of the alternative AiO electrode design with double cylinder as cathode and larger anode surface area.

Both electrodes were assessed in fermentation medium in the same conditions as the experiment shown in Figure 5-1. Only the current was increased to 800 mA for the double cylinder cathode (j = 3.9 mA cm^{-2}). For the larger cylinder cathode, the current was left at 600 mA (j = 6.1 mA cm^{-2}). The results are shown in Figure 5-4. Both new electrodes showed a faster response time as the original design, reaching 6 mmol h^{-1} already after 1 h. The H_2 evolution rate of the design with the double cathodic cylinder increased even further, to an average value of 13.7 ± 0.9 mmol h^{-1}, a 1.3-fold increase compared to the original design (operated at 800 mA). However, the average voltage during the experiment added up to 5.2 V, a value at which inhibition effect might already occur. The H_2 evolution rate of the design with the larger cathodic cylinder only reached an average value of 7.9 ± 2.1 mmol h^{-1}, which is a 1.1-fold increase in comparison to the original design. The average voltage during the experiment however added up to 11 V, probably due to the larger distance between cathode and anode than in the original design. Given that both new electrode designs showed high average voltages during their operation, no fermentation experiments with *A. woodii* were conducted as growth inhibition was expected. For future applications however, an increase of cathode surface and reducing faradaic losses (e.g., by using different separator materials to reduce cathodic O_2 reduction) at the same time could result in an AiO design with higher H_2 evolution rates required for successful autotrophic BES fermentations.

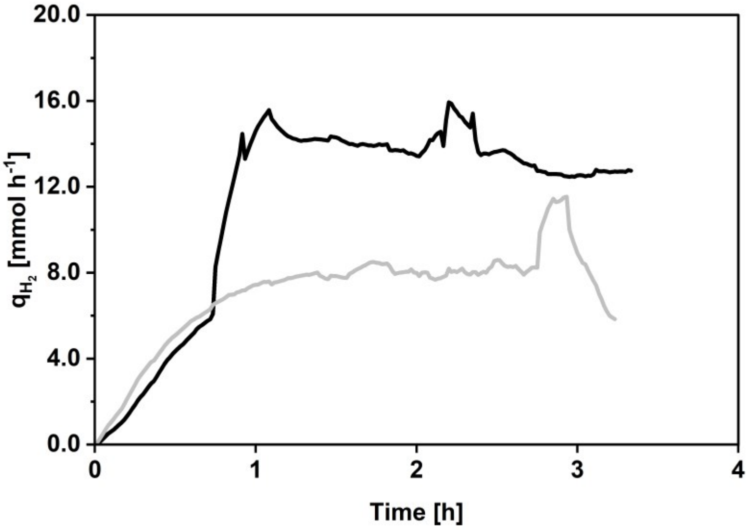

Figure 5-4: Hydrogen evolution rate of alternative AiO electrode designs measured in the exhaust gas of a stirred-tank bioreactor. The black line indicates the H_2 evolution of the double cylinder cathode with enhanced anode design. The grey line indicates the H_2 evolution of the larger cathode cylinder design. Parameters: T = 30 °C; pH = 7.0; $P\ V^{-1}$ = 4.7 W L^{-1}; V_{CO_2} = 0.01 vvm; V_0 = 1.4 L.

5.1.2. Effect of the AiO Electrode on Iron Concentration in the Medium

After each BES fermentation with the AiO electrode, the cathode surface was darker than before (see Figure 5-6). Only the thorough cleaning of the electrode parts with so called piranha etch, a mixture of H_2SO_4 and H_2O_2 (Gostin et al., 2013), was able to remove the electrodeposited components from the surface. Furthermore, an increase in cell voltage was observed with each use of the AiO electrode. Samples of fermentation medium with operating AiO electrode were therefore taken for 35 h to investigate if any of the trace metals were part of the electrodeposition layer. The results are shown in Figure 5-5. The concentrations of sodium, zinc and nickel stayed constant over the course of the experiment while iron concentration decreased 2.8-fold. The analysis of magnesium and potassium were inconclusive, and the concentrations of copper, cobalt, manganese and selenite were below the detection limit of the ICP-OES. These results suggest an iron deposition on the surface of the AiO electrode during operation in the fermentation medium. The influence on iron as redox mediator by the AiO electrode was already published by Utesch et al., 2019, which makes these result cohesive. Other fermentation medium components are likely to be also part of the layer, which is deposited on the electrode surface, however this cannot be verified at this point. Since iron is an essential metal for *A. woodii*, the reduction of iron in the culture medium could have an effect on its growth. However, the remaining concentration measured during this experiment should still be sufficient for regular metabolic functions.

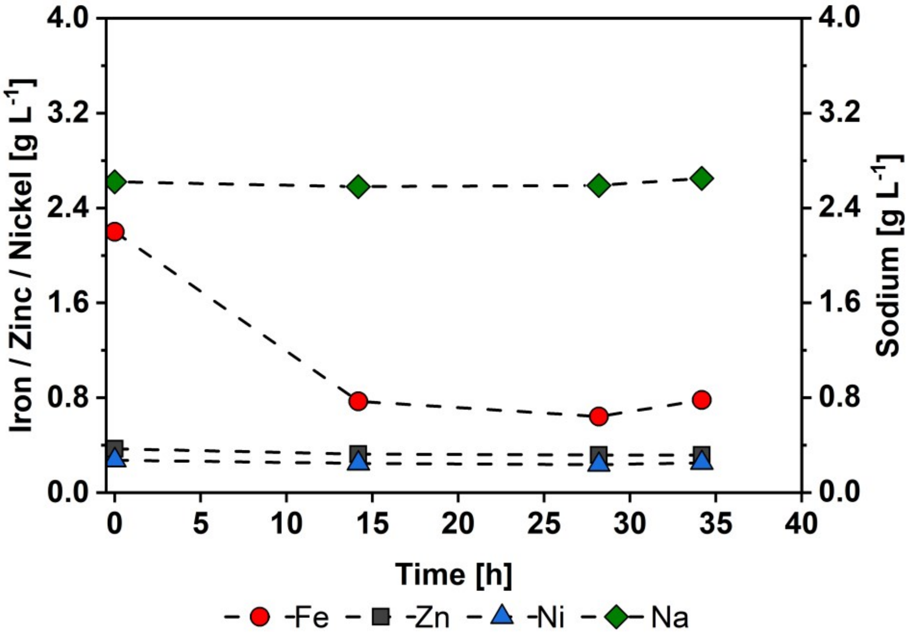

Figure 5-5: Concentration of selected metal compounds in the fermentation medium over time during experiment with working AiO electrode and without cells. Red circles show iron concentrations; black squares show zinc concentrations; blue triangles show nickel concentrations; green diamonds show sodium concentrations. Parameters: T = 30 °C; pH = 7.0; $P\ V^{-1}$ = 0.3 W L^{-1}; V_0 = 1.3 L; I_{AiO} = 600 mA; U_{av} = 5.2 V.

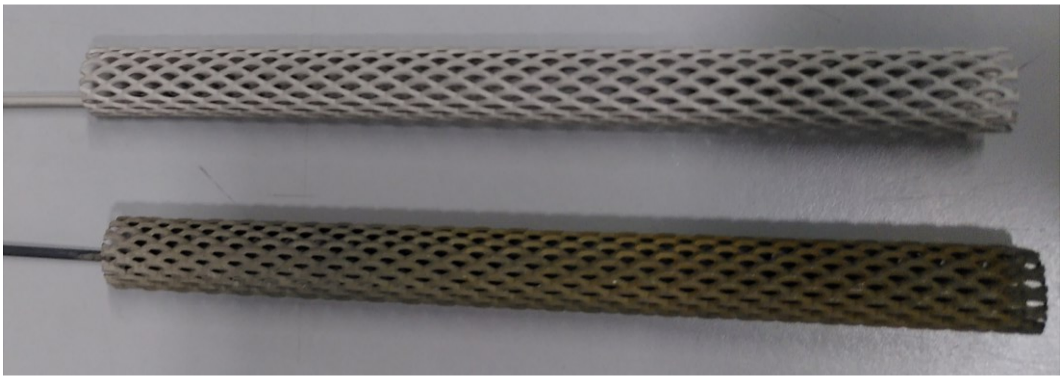

Figure 5-6: Electrodeposition of media components on the surface of the AiO electrode after usage in a BES cultivation.

5.2. *Acetobacterium woodii* Stirred-Tank Batch Fermentations

As mentioned in Chapter 3.1.3, *A. woodii* is capable of growing on various substrates such as hexoses or H_2 / CO_2. This chapter describes the characterization of different *A. woodii* strains growing in pure cultures with different bioreactor set ups. It was necessary to compare growth and product formation between the recombinant lactate producers *A. woodii* P_{tet}_*ldhD*$_{CI}$ and *A. woodii* [P_{bgaL}_*ldhD*_NFP] and the wild type strain, as well as compare important process and metabolic performance parameters between fermentations with fructose as substrate, conventional gas fermentations and fermentations utilizing the AiO electrode (here referred to as BES). Parts of the results presented in this chapter were published in the peer-reviewed journal *Engineering in Life Science* (Herzog et al., 2022).

5.2.1. Autotrophic BES Cultivation of *A. woodii* Wild Type Strain

The results of a fermentation with the *A. woodii* wild type strain using H_2 generated by the AiO electrode are shown in Figure 5-7. For this process, the CO_2 gas flow was turned off after inoculation to ensure high H_2 concentrations in the medium. The CO_2 flow was turned on again after 8 h. The AiO electrode showed a maximum H_2 production rate of 9.9 mmol h^{-1}. The stirrer rate was set to 1,000 rpm and the I_{AiO} to 600 mA. The average voltage of the AiO electrode added up to 4.0 V over the course of the fermentation. The pre-culture lasted 23 h and reached an OD_{600} of 3.8. For inoculation, 37 mL of pre-culture broth were transferred to the bioreactor. Autotrophic cell growth started almost immediately after inoculation; no distinguishable lag phase was observed. During the first 8 h the cells reached the maximum cell growth rate of 0.12 h^{-1}. Afterwards, the cells grew constantly until the end of the fermentation with a 6-fold lower growth rate of 0.02 h^{-1}. The maximum OD_{600} was reached after 72 h at 1.47. During the first 8 h, *A. woodii* WT culture started to produce lactate at a rate of 0.03 g h^{-1}, reaching a maximum concentration of 0.24 g L^{-1}. Subsequently, the cells consumed the afore produced lactate until all was depleted after 24 h of fermentation time. The main product acetate was produced constantly during the fermentation, with a maximum acetate formation rate of 0.14 g L^{-1}, reaching a maximum concentration of 5.7 g L^{-1} at the end of the process. Formate started accumulating in low concentrations after 4.5 h and increased slowly to the maximum of 0.46 g L^{-1} after 22 h of fermentation time. Then, formate concentrations decreased to 0.31 g L^{-1} at 47 h before reaching again 0.46 g L^{-1}. At the beginning of the fermentation, the ORP added up to -220 mV, but decreased drastically to -591 mV in the first 6 h of the process. After the CO_2 gas flow was turned on at 8 h, the ORP increased to -416 mV. Subsequently, the ORP decreased during the following 20 h to -534 mV and stayed at this value until the fermentation was terminated after 74 h. The overall H_2 uptake added up to 442.2 mmol while the CO_2 uptake was 211.9 mmol in total. Carbon balances were closed within the estimation error of 5 %. A summary of the most important performance parameters of this process can be found in Table 5-1.

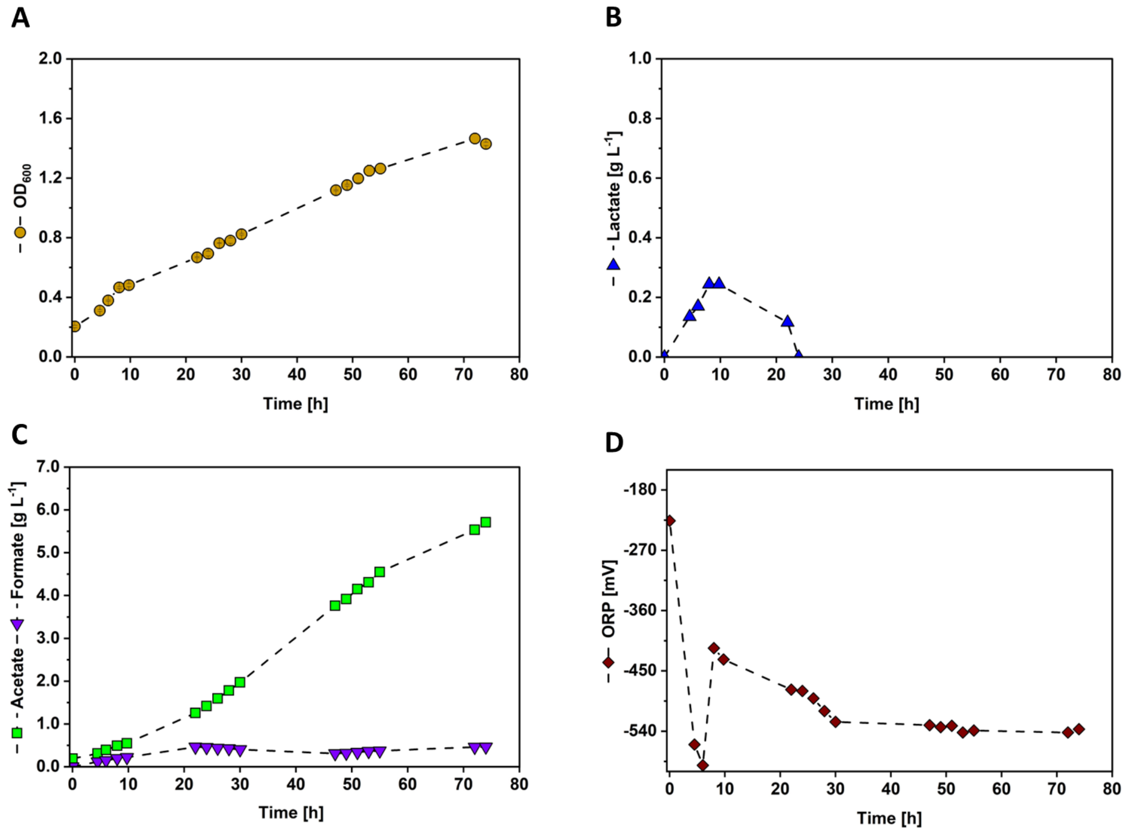

Figure 5-7: Autotrophic stirred-tank batch BES fermentation of *A. woodii* WT. (A) optical cell density (orange circles, OD_{600}); (B) concentration of lactate measured in the cultivation medium (blue triangles, g L^{-1}); (C) concentration of acetate (green squares) and formate (purple triangles upside down) measured in the cultivation medium (g L^{-1}); (D) ORP measured during the cultivation (brown diamonds, mV). Parameters: T = 30 °C; pH = 7.0; $P\ V^{-1}$ = 4.7 W L^{-1}; V_{CO_2} = 0.01 vvm; V_0 = 1.4 L; I_{AiO} = 600 mA; U_{av} = 4.0 V.

This fermentation proved, that autotrophic growth of *A. woodii* WT with the AiO electrode serving as H_2 provider was successful. As Figure 5-7 A furthermore indicates, the *A. woodii* WT culture adapted almost immediately to the autotrophic growth conditions, although the pre-culture fermentation was conducted heterotrophically with fructose. In comparison to published data of autotrophic *A. woodii* WT cultivations, μ_{max} was up to 2.4-fold higher (Groher and Weuster-Botz, 2016; Kantzow and Weuster-Botz, 2016). However, μ_{max} was maintained only for 4 h and then decreased by a factor of 4 to 0.03 h^{-1}. The observed production of lactate by the *A. woodii* WT strain was unusual, given that the production of acetate is energetically preferred and no published data for native lactate production from *A. woodii* exist. The lactate uptake, however, falls in line with current metabolic models: lactate is consumed for NADH and pyruvate generation via the native electron confurcating Ldh/Etf complex, as explained in Chapter 3.1.3. Regarding the main product acetate, process performance of this autotrophic cultivation is lower than in comparable publications. Although the biomass specific acetate formation rate of 23.2 g g^{-1} d^{-1} reached a slightly higher value than published by Groher and Weuster-Botz, 2016 (21.0 g g^{-1} d^{-1}), the total acetate concentration is up to 7.7-fold lower (Demler and Weuster-Botz, 2011) and the volumetric productivity up to 9.7-fold lower (Groher and Weuster-Botz, 2016). However, the AiO electrode generated on average only 7.1 mmol L^{-1} h^{-1} of H_2, which is up to 156-fold less hydrogen than provided in other conventional gas fermentation set ups (Kantzow and Weuster-Botz, 2016). This implies, that the BES fermentation with *A. woodii* WT is H_2 limited.

Table 5-1: Important process performance parameters of all batch processes with *A. woodii* discussed in this chapter.

Strain	**H_2 Supply**	**Special Set up**	**OD_{max}**	**μ_{max}**	**$Y_{X/S}$**	**c_{Lac}**	**q_{Lac}**	**$Y_{P/S}$**	**P_{vol}**	**c_{Ac}**	**c_{Form}**
[-]	[-]	[-]	[-]	[h^{-1}]	[$g\ g^{-1}$]	[$g\ L^{-1}$]	[$g\ h^{-1}$]	[$g\ g^{-1}$]	[$g\ L^{-1}\ d^{-1}$]	[$g\ L^{-1}$]	[$g\ L^{-1}$]
WT	AiO	No Lactate	1.47	0.12	0.11	0.24	-	0.77	1.85	5.70	0.46
P_{tet}_*ldhD*$_{CI}$	AiO	OD_{Ind} 0.5	0.73	0.11	0.10	0.25	0.01	0.07	0.11	1.84	0.33
P_{tet}_*ldhD*$_{CI}$	AiO	OD_{Ind} 0.7	0.86	0.09	0.13	0.40	0.02	0.11	0.13	3.82	0.58
[P_{bgaL}_*ldhD*_NFP]	-	Hetero-trophic	2.11	0.12	0.18	0.68	0.06	0.10	0.43	5.41	2.04
[P_{bgaL}_*ldhD*_NFP]	Gas	0.5 vvm	2.01	0.10	0.03	8.07	0.27	0.21	2.29	16.1	1.2
[P_{bgaL}_*ldhD*_NFP]	Gas	0.025 vvm	2.19	0.11	0.04	3.55	0.18	0.11	2.40	17.2	1.0
[P_{bgaL}_*ldhD*_NFP]	AiO	-	1.27	0.11	0.09	0.51	0.04	0.07	0.20	5.51	0.87

5.2.2. Autotrophic BES Cultivation of *A. woodii* P_{tet}_*ldhD*$_{\mathrm{CI}}$

The strain *A. woodii* P_{tet}_*ldhD*$_{\mathrm{CI}}$ was the first recombinant *A. woodii* strain which is capable of producing lactate autotrophically to be used in BES fermentations for this study. The results of the BES fermentations are shown in Figure 5-8. To investigate the effect of the induction time point, two fermentations with different OD_{Ind} were conducted. The first fermentation was induced at a later time point, at an OD_{Ind} of 0.7 while the second fermentation was induced earlier at an OD_{Ind} of 0.5. As for the BES process with *A. woodii* WT, the CO_2 gas flow was turned off after inoculation to ensure high H_2 concentrations in the medium for both *A. woodii* P_{tet}_*ldhD*$_{\mathrm{CI}}$ cultivations. The CO_2 flow was turned on again after 11 h. The AiO electrode was set to I_{AiO} = 600 mA and the average voltage of the AiO electrode added up to 3.5 V over the course of both fermentations. A maximum H_2 production rate of 5.1 mmol L^{-1} h^{-1} was generated by the AiO electrode. The stirrer rate was set to 1,000 rpm. The pre-culture lasted 30 h and reached an OD_{600} of 3.3 ± 1.5. The inoculation volume was calculated to reach an initial OD_{600} of 0.1 in the bioreactor. In both fermentations, *A. woodii* P_{tet}_*ldhD*$_{\mathrm{CI}}$ started growing shortly after inoculation, reaching a μ_{max} of 0.11 h^{-1} (early induction) and 0.09 h^{-1} (later induction) during the first 11 h of the fermentation. The cultivation being induced at an OD_{Ind} of 0.5 reached a maximum cell density of 0.73 after 33 h. Afterwards, the OD_{600} decreased to 0.68 ± 0.03 and stayed constant until the end of the fermentation. The cultivation which was induced at an OD_{Ind} of 0.7 reached a maximum cell density of 0.86 at 80 h during a second growth phase. Before, the culture had reached stationary phase at an OD_{600} of 0.78 ± 0.02 after 36 h of fermentation time. The lactate production was induced with 0.1 g L^{-1} anhydrotetracycline. After induction, both cultivations started producing lactate with a maximum lactate formation rate of 0.01 g h^{-1} (early induction) and 0.02 g h^{-1} (later induction), respectively. While the cultivation which was induced earlier stopped producing lactate already 21 h after induction at a lactate concentration of 0.25 g L^{-1}, the cultivation which was induced at a later time point produced lactate for 46 h and reached a maximum concentration of 0.4 g L^{-1}. Acetate was produced by both cultivations from the beginning on, however, the cultivation with the OD_{Ind} of 0.5 stopped acetate production at the same time as lactate production ceased. The maximum acetate concentrations added up to 1.8 g L^{-1} (OD_{Ind} = 0.5) and 3.8 g L^{-1} (OD_{Ind} = 0.7), respectively. Formate was produced in low concentrations, reaching a maximum of 0.3 g L^{-1} (OD_{Ind} = 0.5) and 0.6 g L^{-1} (OD_{Ind} = 0.7), respectively after 40 h. Subsequently, part of the formate was consumed by the *A. woodii* P_{tet}_*ldhD*$_{\mathrm{CI}}$ strain again. The pH of both cultures fluctuated around 7.1 ± 0.2, while the ORP decreased rapidly to the minimum values of -549 mV (OD_{Ind} = 0.5) and -631 mV (OD_{Ind} = 0.7), respectively during the first 12 h of the fermentation. Subsequently, the ORP values increased due to the addition of CO_2 to average values of -500 ± 78 mV (OD_{Ind} = 0.5) and -457 ± 85 mV

(OD_{Ind} = 0.7), respectively for the rest of the cultivation. A summary of the most important performance parameters of this process can be found in Table 5-1.

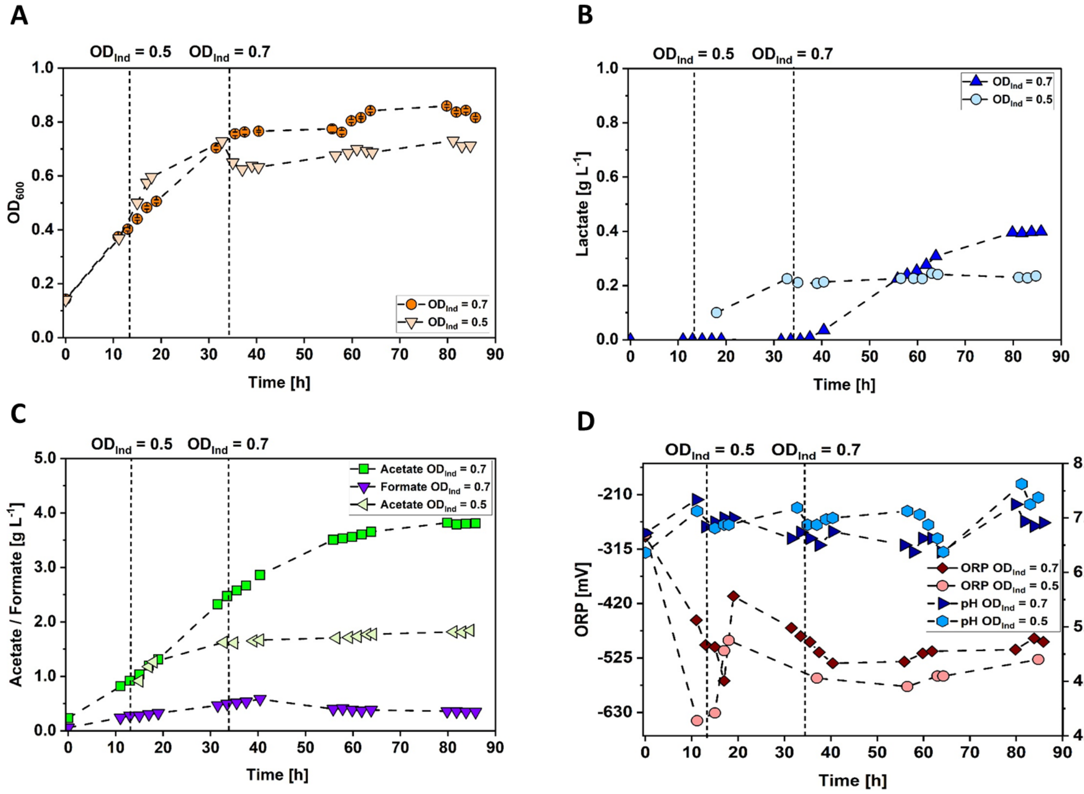

Figure 5-8: Autotrophic stirred-tank batch BES fermentation of *A. woodii* P$_{tet}$_*ldhD*$_{CI}$. Comparison of induction OD_{600} (OD_{Ind}) at 0.5 (lighter colors) and at 0.7 (darker colors). (A) optical cell density (orange circles and triangles, OD_{600}); (B) concentration of lactate (blue triangles and circles, g L^{-1}); (C) concentration of acetate (green squares and triangles) and formate (purple triangles upside down) (g L^{-1}); (D) ORP measured during the cultivation (brown diamonds and pink circles, mV). The vertical dashed lines indicate the time point of induction with 0.1 g L^{-1} anhydrotetracycline. Parameters: T = 30 °C; pH = 7.0; $P\ V^{-1}$ = 4.7 W L^{-1}; V_{CO_2} = 0.01 vvm; V_0 = 1.5 L; I_{AiO} = 600 mA; U_{av} = 3.5 V.

The BES cultivation with the *A. woodii* P$_{tet}$_*ldhD*$_{CI}$ strain proved that lactate production from CO_2 and *in situ* generated H_2 was possible. The maximum growth rate of the cultivation with late induction was only 8 % smaller than in the BES cultivation with the *A. woodii* wild type strain. However, μ_{max} of the fermentation with early induction was 25 % decreased. Maximum OD_{600} of the *A. woodii* P$_{tet}$_*ldhD*$_{CI}$ cultivations were also 1.7 (OD_{Ind} = 0.7) and 2.0-fold (OD_{Ind} = 0.5) lower than in the *A. woodii* wild type cultivation. Maximum acetate concentrations were 1.5 (OD_{Ind} = 0.7) and 3.1-fold (OD_{Ind} = 0.5) lower. This data suggests a lower performance in general of *A. woodii* P_{tet}_*ldhD*$_{CI}$. Although the *A. woodii* P_{tet}_*ldhD*$_{CI}$ strain was able to produce lactate, the maximum concentration was 3.3-fold lower than reported by (Mook et al., 2022) in bottle cultivations. Given that the AiO electrode only produced 5.1 mmol L^{-1} h^{-1} during the fermentation, H_2 limitation is assumed to be the reason for low lactate production and overall low performance. This also falls in line with the performance of the *A. woodii* wild type strain cultivated in the BES. Comparing the two fermentations with different induction OD_{600}, the cultivation with the early induction time point performed worse. OD_{max} was reduced 2.2-fold, maximum lactate concentration 1.6-fold and volumetric productivity 1.2-fold. This suggests strongly that a later induction time point is beneficial for the cultivation of *A. woodii* P_{tet}_*ldhD*$_{CI}$. This could be due to the induction agent anhydrotetracycline. Although this derivative of tetracycline shows lower antibiotic activity than tetracycline (Gossen and Bujard, 1993), it could still negatively affect bacterial growth. Furthermore, by inducing the strain, a forced metabolic shift towards lactate takes place, redirecting redox energies in the already limited system away from biomass production.

5.2.3. Heterotrophic Cultivation of *A. woodii* [P_{bgaL}_*ldhD*_NFP]

A. woodii [P_{bgaL}_*ldhD*_NFP] was cultivated heterotrophically on 3.2 g L^{-1} fructose to obtain reference performance parameters for autotrophic batch fermentations. Furthermore, the AiO electrode was turned on during the last 34 h after fructose was depleted, to investigate if *A. woodii* [P_{bgaL}_*ldhD*_NFP] would adapt to autotrophic growth after having reached stationary phase during heterotrophic growth. The results of this fermentation are depicted in Figure 5-9. The current I_{AiO} was set to 600 mA and the average voltage of the AiO electrode added up to 4.6 V over the course of the fermentation. CO_2 gas flow was set to 0.01 vvm and the stirrer rate to 800 rpm. The pre-culture lasted 35 h and reached an OD_{600} of 1.6. For inoculation, 87 mL of pre-culture broth were transferred to the bioreactor. The *A. woodii* [P_{bgaL}_*ldhD*_NFP] culture started growing at an OD_{600} of 0.15 and after a lag phase of about 8 h, the cells transitioned into the exponential growth phase. The maximum growth rate of 0.12 h^{-1} was reached in between 12 and 20 h of fermentation time. After 20 h, the culture was induced with the addition of 1 mM lactose. By extrapolation of the exponential growth curve, it is assumed that the stationary phase was reached at about 25 h. The maximum OD_{600} value was measured after 33.5 h at 2.1. Subsequently, cell concentration started to decline and reached a final OD_{600} value of 1.8. After inoculation, fructose concentration in the medium started to decline immediately, during the first 12 h with a consumption rate of 0.07 g h^{-1}. Subsequently, the fructose consumption rate increased 3.6-fold to the maximum consumption rate of 0.25 g h^{-1}. After 33.5 h, only 0.1 g L^{-1} of fructose was detected in the medium and this concentration stayed constant until the end of the fermentation. Lactate formation started immediately after induction at 20 h. The maximum lactate formation rate added up to 0.06 g h^{-1} and reached a concentration of 0.6 g L^{-1} after 33.5 h when fructose was depleted. The lactate concentration stayed constant afterwards until reaching 60 h, when the *A. woodii* [P_{bgaL}_*ldhD*_NFP] strain started producing lactate again, increasing the concentration to its maximum value of 0.7 g L^{-1}. Acetate concentration increased significantly with the start of the exponential growth phase, reaching 3.8 g L^{-1} after 33.5 h. After a short stationary phase, the *A. woodii* [P_{bgaL}_*ldhD*_NFP] strain kept on producing acetate until the end of the fermentation, adding up to a final value of 5.4 g L^{-1}. Formate was not detected in the cultivation medium until 18 h into the process. Its concentration increased slowly to 0.6 g L^{-1} in the first 33.5 h. Subsequently, the formate production rate increased 9.8-fold and the maximum formate concentration of 2.2 g L^{-1} was measured after 58 h. The ORP measured at the beginning of the process added up to -362 mV and decreased subsequently to -503 mV after 20 h. After staying constant for the following 13 h, the ORP decreased again rapidly to -584 mV after 40 h. For the rest of the fermentation, the ORP stayed at this level, the minimum value was detected at -594 mV after 58.1 h. The pH value decreased also over the course of the fermentation, despite the addition of KOH for pH correction. From the initial value of 7.1, the pH decreased to a minimum of 6.4 after 33.5 h before increasing again during the last 9 h of the fermentation to 6.6. In addition to fructose consumption, a carbon uptake from CO_2 of 66.5 mmol was estimated for the first 33.5 h of fermentation. During the subsequent 30 h, a total of 110 mmol of CO_2 was taken up by the *A. woodii* [P_{bgaL}_*ldhD*_NFP] strain. Carbon balances were closed with an estimation error of 8 %. A summary of the most important performance parameters of this process can be found in Table 5-1. For the calculation of $Y_{X/S}$, $Y_{P/S}$ and P_{vol}, only the process data up to 33.5 h was used.

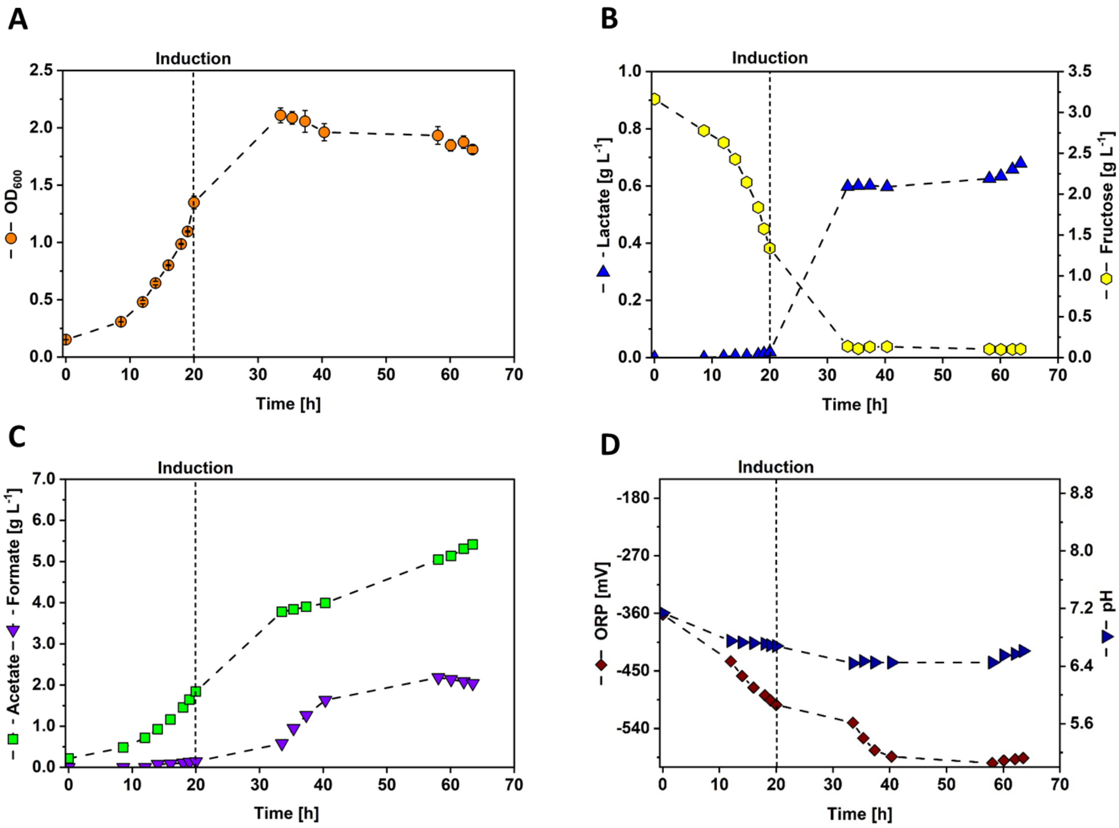

Figure 5-9: Heterotrophic stirred-tank batch fermentation of *A. woodii* [P$_{bgaL}$_*ldhD*_NFP]. (A) optical cell density (orange circles, OD_{600}); (B) concentration of lactate (blue triangles) and fructose (yellow hexagons) measured in the cultivation medium (g L^{-1}); (C) concentration of acetate (green squares) and formate (purple triangles upside down) measured in the cultivation medium (g L^{-1}); (D) ORP (brown diamonds, mV) and pH (dark blue triangles) measured during the cultivation. The dashed vertical line indicates the time point of induction with 1mM lactose. Parameters: T = 30 °C; pH = 7.0; $P\,V^{-1}$ = 2.3 W L^{-1}; V_{CO_2} = 0.01 vvm; V_0 = 1.4 L; I_{AiO} = 600 mA; U_{av} = 4.6 V; $c_{Fruc,0}$ = 3.2 g L^{-1}.

The results shown in Figure 5-9 illustrate that the *A. woodii* [P$_{bgaL}$_*ldhD*_NFP] strain adapted quickly to the conditions in the bioreactor. For evaluation, the experiment was divided into two phases: the first phase being the growth mainly on fructose up to 33.5 h of process time, while the second phase being the last 30 h of the fermentation, where only H_2 and CO_2 were available for the culture. For the first phase, the maximum growth rate of 0.12 h^{-1} is very comparable to the 0.11 h^{-1} of an *A. woodii* WT cultivation with fructose (Heise et al., 1989). The biomass yields from fructose found in literature for *A. woodii* WT vary from 42.5 g mol^{-1} (Tschech and Pfennig, 1984) to 51.5 g mol^{-1} (Neuendorf et al., 2021) and 61.2 g mol^{-1} (Heise et al., 1989), leaving the results for the *A. woodii* [P$_{bgaL}$_*ldhD*_NFP] strain at the lower end with 42.0 g mol^{-1}. Although still comparable, an explanation could be the forced lactate production due to induction, shifting more redox equivalents away from biomass production. The obtained lactate yield from fructose of 0.37 mol mol^{-1} was also comparable to the average yield of 0.38 mol mol^{-1} obtained in bottle fermentations with *A. woodii* P$_{tet}$_*ldhD*$_{CI}$ (Beck, 2020). Interesting but no novelty was that the *A. woodii* [P$_{bgaL}$_*ldhD*_NFP] culture used CO_2 parallel to fructose as carbon source, given that the ability of mixotrophic growth is well known in *A. woodii* (Drake, 1995; Fast et al., 2015). Remarkable in the second phase of the experiment is that the *A. woodii* [P$_{bgaL}$_*ldhD*_NFP] strain started producing formate at high rates immediately when H_2 was available. Figure 5-9 D shows also that the strain became more active again, indicated by the rapid decrease of ORP after this time point. Acetate and especially lactate formation begin not until later, indicating the metabolic focus on formate production. *A. woodii* is known for its ability to use CO_2 and H_2 for formate production (Schuchmann and Müller, 2013; Schwarz et al., 2022), however this experiment shows that *A. woodii* is capable of switching metabolic pathways quite fast. Furthermore, Figure 5-9 B shows that the *A. woodii* [P$_{bgaL}$_*ldhD*_NFP] strain is able to continue lactate production from another substrate after being in a longer lag-phase, which signifies that the metabolic pathway for lactate production is not irreversibly turned off once reaching a stationary phase.

5.2.4. Autotrophic Gas Fermentations with *A. woodii* [P$_{bgaL}$_*ldhD*_NFP]

For performance comparison of the BES with a conventional gas fermentation, *A. woodii* [P$_{bgaL}$_*ldhD*_NFP] was cultivated with two different gassing rates of 0.5 and 0.025 vvm of a H_2/CO_2 gas mixture (70/30 %) in a stirred-tank reactor. The results of both fermentations can be seen in Figure 5-10. Both cultures were inoculated with 70 mL of pre-culture broth with an OD_{600} of 1.45 ± 0.04. Cell growth started in both fermentations after a short lag phase of an estimated 4 h, and the exponential growth phase lasted until 20 h of process time. The maximum growth rate of 0.11 ± 0.01 h^{-1} was reached during the first 15 h in both fermentations. After 20 h, μ decreased in both fermentations, adding up to 0.02 h^{-1} for the process with the higher gassing rate and to 0.01 h^{-1} for the process with the lower gassing rate. A maximum cell density of 2.0 ± 0.2 was reached for the fermentation conducted with 0.5 vvm after 60 h, before cell density decreased to a final value of 1.77 ± 0.04. The process with the lower gassing rate reached a maximum cell density of 2.2 ± 0.1 after 82 h of process time. Lactate production was induced after 15 h with the addition of 1 mM lactose. Shortly after, both *A. woodii* [P$_{bgaL}$_*ldhD*_NFP] cultivations started producing lactate, reaching maximum formation rates of 0.27 g h^{-1} (0.5 vvm) and 0.18 g h^{-1} (0.025 vvm), respectively. While lactate formation stopped after 34 h at a concentration of 3.5 g L^{-1} for the process with 0.025 vvm gassing rate, it continued until the end of the fermentation for the process with 0.5 vvm gassing rate, reaching a maximum of 8.1 g L^{-1}. Both *A. woodii*

[P$_{bgaL}$_*ldhD*_NFP] cultivations produced acetate constantly, adding up to maximum concentrations of 16.1 g L^{-1} (0.5 vvm) and 17.2 g L^{-1} (0.025 vvm), respectively. Up to 20 h of process time, the acetate formation rate added up to 0.5 g h^{-1}, while afterwards it declined 2.5-fold to 0.2 g h^{-1} in both cultivations. Formate production happened in two phases in both cultivations. During the first 12 h, the fermentation with 0.5 vvm sparging rate produced 0.4 g L^{-1} and the process with 0.025 vvm produced 0.3 g L^{-1}. Subsequently, the *A. woodii* [P$_{bgaL}$_*ldhD*_NFP] strain in both cultivations consumed most of the produced formate. Then, after 20 h, formate was accumulated again, reaching the maximum values of 1.2 g L^{-1} (0.5 vvm) and 1.0 g L^{-1} (0.025 vvm), respectively. pH values were constant throughout both cultivations at 6.95. Over the course of the process with 0.5 vvm sparging rate, 1,345.3 mmol of H_2 and 798.0 mmol of CO_2 were taken up by the *A. woodii* [P$_{bgaL}$_*ldhD*_NFP] strain with a maximum H_2 uptake rate of 42 mmol L^{-1} h^{-1} and a maximum CO_2 uptake rate of 23 mmol L^{-1} h^{-1}. The cultivation with 0.025 vvm consumed 1,188.3 mmol H_2 and 665.7 mmol CO_2 during the process, reaching a maximum H_2 uptake rate of 44 mmol L^{-1} h^{-1} and a maximum CO_2 uptake rate of 23 mmol L^{-1} h^{-1}. Carbon balanced were closed within an estimation error of 5 %. A selection of important process performance parameters of both cultivations is listed in Table 5-1.

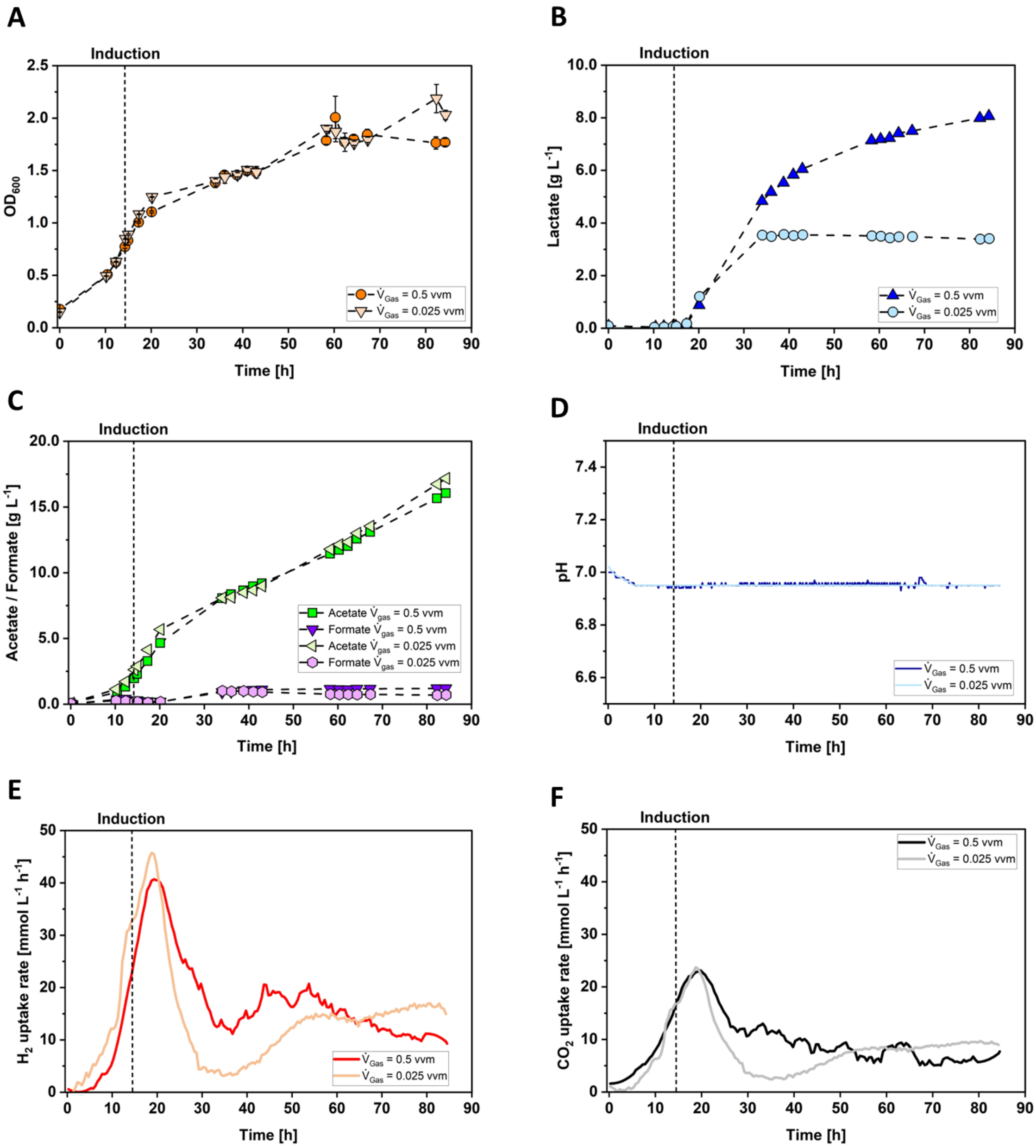

Figure 5-10: Autotrophic stirred-tank batch gas fermentation of *A. woodii* [P_{bgaL}_*ldhD*_NFP]. Comparison of cultivation with a gassing rate of 0.5 vvm (dark colors) and 0.025 vvm (light colors). (A) optical cell density (orange circles and triangles, OD_{600}); (B) concentration of lactate (blue triangles and circles, g L^{-1}); (C) concentration of acetate (green squares and triangles) and formate (purple triangles and circles) (g L^{-1}); (D) pH measured during the cultivation (blue lines); (E) hydrogen uptake rate (red lines, mmol L^{-1} h^{-1}); (F) carbon dioxide uptake rate (black and gray lines, mmol L^{-1} h^{-1}). Parameters: $T = 30$ °C; pH = 7.0; $P\ V^{-1} = 6.8$ W L^{-1}; $V_{CO_2/H_2} = 0.5/0.025$ vvm (H_2:CO_2 70:30); $V_0 = 1.0$ L.

The autotrophic gas fermentations were conducted for comparison with the BES set up. Furthermore, the process with the higher sparging was done to investigate the maximum performance of the *A. woodii* [P_{bgaL}_*ldhD*_NFP] strain when cultivated with a surplus of H_2. While the maximum growth rate of the *A. woodii* [P_{bgaL}_*ldhD*_NFP] strain cultivated in a conventional gas fermentation was not higher than the growth rate of the *A. woodii* WT strain and the *A. woodii* P_{tet}_*ldhD*$_{CI}$ strain cultivated in the BES, the OD_{max} was factor 1.5 to 2.4 higher. The maximum OD_{600} reached compare well to literature results conducted in the same reactor system with similar parameters (Groher and Weuster-Botz, 2016; Hoffmeister et al., 2016). Remarkable is the high lactate concentration of 8.1 g L^{-1} reached in the cultivation with the higher sparging rate. Up to date, this seems to be the highest lactate concentration to be produced from CO_2 in a recombinant *A. woodii* strain to be published (Herzog et al., 2022). As Figure 5-10 B shows, longer fermentation time would have probably resulted in an even higher lactate concentration. In comparison, the fermentation with the lower gassing rate of 0.025 vvm stopped producing lactate after 34 h. It can be assumed that the lower H_2 availability is the reason for this sudden stop of lactate production, given that this was the only difference in between both fermentations. Furthermore, H_2 uptake rate reached its minimum at the same time point, indicating that no more H_2 was being used for lactate production (see Figure 5-10 E). Although the lactate production did not reach as high levels as in the cultivation with the higher sparging rate, the volumetric productivities of 2.3 g L^{-1} d^{-1} (0.5 vvm) and 2.4 g L^{-1} d^{-1} (0.025 vvm) are similar, given that for the calculation of P_{vol}, the time point of product maximum was considered. The product yield from CO_2 for the fermentation conducted at 0.025 vvm is very comparable to $Y_{P/S}$ of the BES fermentation with *A. woodii* P_{tet}_*ldhD*$_{CI}$ induced at an OD_{600} of 0.7 (see Table 5-1), which indicates furthermore a hydrogen limitation for the lower sparged fermentation process, however only referring to lactate production. Acetate production and cell growth do not show any signs of limitation. Both values are very comparable and even 7 – 9 % higher compared to the fermentation with the higher sparging rate. These data thus suggest that the lactate production from CO_2 in *A. woodii* [P_{bgaL}_*ldhD*_NFP] is very sensitive to a lack of H_2. The $Y_{P/S}$ of the cultivation with the higher sparging rate is almost twice as high as the one with the lower sparging rate. This yield coefficient for product from CO_2 can be seen as reference value of what the strain *A. woodii* [P_{bgaL}_*ldhD*_NFP] is capable of, if H_2 is not limited. The low yields for biomass from CO_2 indicate, that most carbon seems to be directed to the production of lactate and acetate. Both cultivations showed a significant reduction of acetate formation rate (2.5-fold) and cell growth rate (6 to 11-fold) after 20 h of fermentation time. This correlates with the time point, where lactate in both cultivations starts accumulating, which shows the redirection of redox energy from the product acetate and biomass toward the lactate metabolism (Weghoff et al., 2015).

Furthermore, this shift in metabolism also correlates with the reduction of both gas uptake rates (refer to Figure 5-10 E and F). However, the reduction of acetate production rate and gas uptake rate was also found by (Groher and Weuster-Botz, 2016), where a gas fermentation of the *A. woodii* WT was conducted and no lactate was produced. This shows that the main acetate metabolism is responsible for the high gas uptake, with lactate continuing to be a side product. The gas uptake rates as shown in Figure 5-10 E and F were 1.5-fold lower than published by Groher and Weuster-Botz, 2016 in an *A. woodii* WT fermentation, however this fermentation was sparged with 80 instead of 70 % of H_2. This suggests that an even higher H_2 availability would also lead to higher gas uptake rates. Interesting is, that although the fermentation with 20 times higher sparging rate produced a 3.3-fold higher amount of lactate, the H_2 uptake rate in both fermentations was almost equal. Furthermore, the ratio of the amount of H_2 put into the system to the amount of H_2 which was taken up by *A. woodii* [P_{bgaL}_*ldhD*_NFP] is reduced with increasing H_2 sparging rate. While the *A. woodii* WT strain cultivated in the BES (see Chapter 5.2.1) took up 60 % of the H_2 produced by the AiO electrode, the *A. woodii* [P_{bgaL}_*ldhD*_NFP] strain cultivated with a gassing rate of 0.025 vvm took up 24 % and the *A. woodii* [P_{bgaL}_*ldhD*_NFP] strain cultivated at 0.5 vvm took up only 2 % of the H_2 which was put into the system during these cultivations. The ratio of produced lactate to used H_2 is also 2.1-fold higher for the fermentation with the sparging rate of 0.025 vvm compared to the one with 0.5 vvm. This could suggest that *A. woodii* uses H_2 more efficiently at lower H_2 availability. In both cultivations, the gas uptake rates increase again after 40 h of fermentation time, after having reached a minimum rate. This could be due to the continued production of biomass, given that the stationary growth phase was not reached until 60 h of process time. Although a H_2 surplus during the fermentation resulted in higher lactate production.

5.2.5. Autotrophic BES Cultivation of *A. woodii* [P_{bgaL}_*ldhD*_NFP]

The results of the cultivation of *A. woodii* [P_{bgaL}_*ldhD*_NFP] in a stirred-tank bioreactor using the AiO electrode for H_2 generation can be seen in Figure 5-11. This cultivation was conducted as the BES fermentation of the *A. woodii* P_{tet}_*ldhD*$_{CI}$ strain but with a lower stirrer rate of 800 rpm. The average voltage of the AiO electrode added up to 3.4 V over the course of the fermentation and the maximum H_2 production rate generated by the AiO electrode added up to 7.1 mmol L^{-1} h^{-1}. After 36 h, the pre-culture had reached an OD_{600} of 1.6 and the bioreactor was subsequently inoculated with 86 mL of the pre-culture broth. Cell growth of the culture set in shortly after induction and reached a maximum growth rate of 0.11 h^{-1} during the 14 h. The maximum OD_{600} of 1.3 was reached after 38 h, before the cell density declined in stationary growth phase to a final 1.1. The culture was induced at an OD_{600} of 0.9 with the addition of 1 mM lactose and lactate production started soon after. The maximum lactate production rate of 0.04 g h^{-1} was reached after 38 h of fermentation time. Subsequently, after 44 h the lactate production stopped at a maximum of 0.5 g L^{-1}. Acetate was produced throughout the fermentation at a rate of 0.2 g h^{-1} adding up to a maximum value of 5.5 g L^{-1} at the end of the process. During the first 12 h, formate was accumulated in low concentrations of 0.3 g L^{-1}. Subsequently, the *A. woodii* [P_{bgaL}*_ldhD*_NFP] strain consumed all formate in the culture medium before producing it again after 40 h. The maximum formate concentration added up to 0.9 g L^{-1} at the end of the fermentation. The initial ORP of -255 mV decreased after inoculation to -352 mV and throughout the process to a minimum of -516 mV at the end of the fermentation. The pH value fluctuated around a value of 6.8 ± 0.2. Over the course of the fermentation, the *A. woodii* [P_{bgaL}*_ldhD*_NFP] strain took up 468.9 mmol of H_2 and 229.0 mmol of CO_2. Carbon balances were closed within an estimation error of 5 %. The most important process performance parameters are listed in Table 5-1.

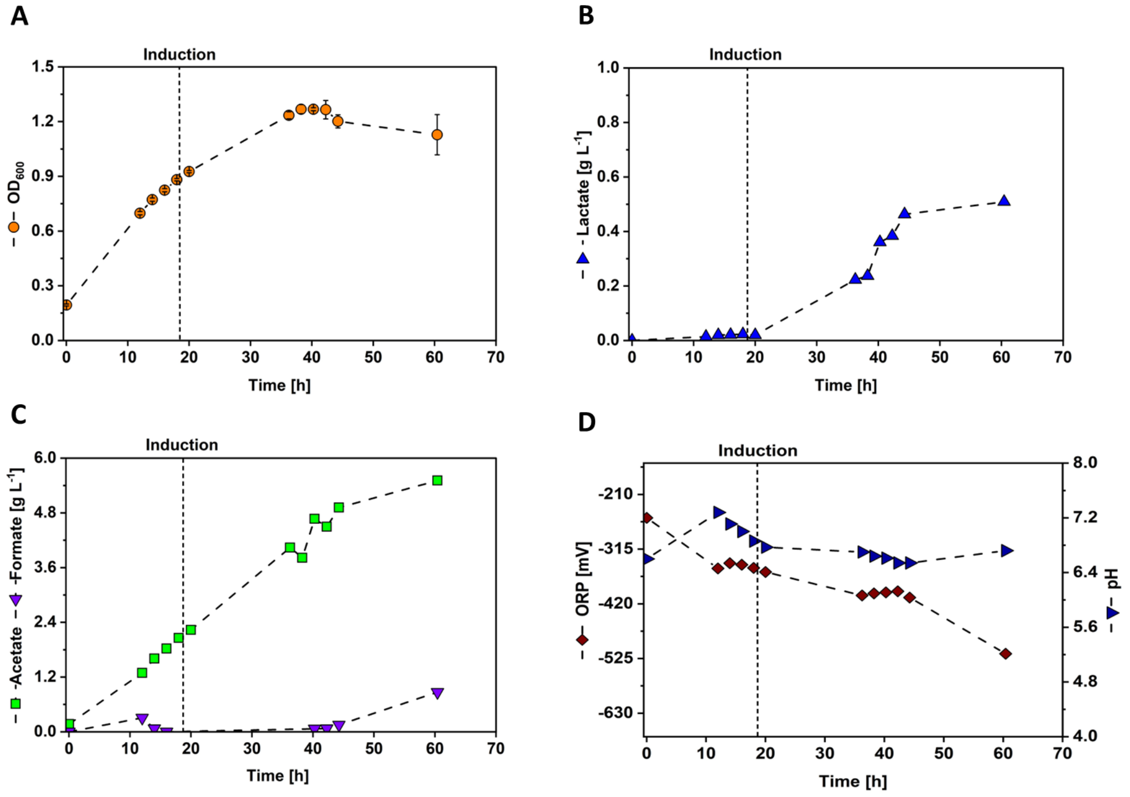

Figure 5-11: Autotrophic stirred-tank batch BES fermentation of *A. woodii* [P_{bgaL}_*ldhD*_NFP]. (A) optical cell density (orange circles, OD_{600}); (B) concentration of lactate (blue triangles, g L^{-1}); (C) concentration of acetate (green squares) and formate (purple triangles upside down) (g L^{-1}); (D) ORP (brown diamonds, mV) and pH (blue triangles) measured during the cultivation. The vertical dashed line indicates the time point of induction with 1 mM lactose. Parameters: $T = 30$ °C; pH = 7.0; $P\,V^{-1} = 2.3$ W L^{-1}; $V_{CO_2} = 0.01$ vvm; $V_0 = 1.4$ L; $I_{AiO} = 600$ mA; $U_{av} = 4.3$ V.

The autotrophic stirred-tank batch BES process of *A. woodii* [P_{bgaL}_*ldhD*_NFP] showed promising results. In comparison, this strain outperformed the *A. woodii* P_{tet}_*ldhD*$_{CI}$ cultivation in the same BES set up. The maximum growth rate was comparable, however the maximum OD_{600} was 1.5-fold, the maximum lactate concentration 1.3-fold, and the volumetric productivity 1.5-fold higher than in the fermentation with the *A. woodii* P_{tet}_*ldhD*$_{CI}$ strain. The maximum lactate production rate was even 2.0-fold higher. These results show that the adaptations made to the *A. woodii* [P_{bgaL}_*ldhD*_NFP] strain by Mook et al., 2022 prove more adapted to the BES process. Furthermore, the *A. woodii* [P_{bgaL}_*ldhD*_NFP] strain is induced with lactose instead of anhydrotetracycline, which has no toxic effect on the strain and could also be a reason for the better performance. However, the H_2 limitation as mentioned in Chapters 5.2.1 and 5.2.2 is also visible in this fermentation, which shows the direct comparison with the gas fermentations of the

A. woodii [P_{bgaL}_*ldhD*_NFP] strain (see Chapter 5.2.4). While the μ_{max} of 0.10 ± 0.01 h^{-1} (n = 6, averaged over all autotrophic *A. woodii* fermentations mentioned up to this point) seems to be the maximum possible growth rate of these *A. woodii* strains under autotrophic conditions, all other process performance parameters are higher in the gas fermentation (compare data in Table 5-1). The OD_{max} is 1.6-fold, volumetric productivity 11.5-fold and maximum lactate concentration 15.8-fold lower in the BES cultivation referring to the gas fermentation with the higher sparging rate. Even compared to the gas fermentation with the lower sparging rate, the maximum lactate concentration is still 6.8-fold lower in the BES system, although the yield of carbon to lactate ($Y_{P/S}$) shows only a 1.6-fold difference. The difference in H_2 availability shows clearly that the reason for this lower performance in BES system is its lower H_2 production rate. While the BES system produced H_2 at a rate of 7.1 mmol L^{-1} h^{-1}, the gas fermentation with the sparging rate of 0.025 vvm provided H_2 at a rate of 60.2 mmol L^{-1} h^{-1} and the gas fermentation with the gassing rate of 0.5 vvm even 971.0 mmol L^{-1} h^{-1} of H_2. This accounts for a difference of 8.5-fold and 136.8-fold in H_2 sparging rate, respectively. This strongly suggests that the maximum possible performance of the *A. woodii* [P_{bgaL}_*ldhD*_NFP] strain cannot be reached in the BES at its current configuration.

5.2.6. Growth Inhibition Effects of Resazurin

Working with autotrophic BES fermentations of *A. woodii* and the culture medium described in Chapter 4.3, a change of color was noticed during fermentations with continuous CO_2 sparging and running AiO electrode. This change of color can be seen in Figure 5-12 and Figure 5-13. The redox indicator resazurin was added to the culture medium of the fermentations shown in Figure 5-12 and Figure 5-13 and after its irreversible change to resorufin, this indicator turns the medium into a bright pink above a specific ORP value (Bueno et al., 2002). Thus, during the analysis of fermentation samples, which was done under aerobic conditions, the medium of the samples usually turned pink. However, with advancing fermentation time, a decoloring effect was noticed, as shown in Figure 5-12 A and B. The culture medium then no longer changed color under aerobic conditions but maintained a greyish tone. In exceptions, the culture medium also turned blue (Figure 5-12 C), green (not shown) and black (Figure 5-12 D). An experiment under sufficiently high ORP conditions for resorufin to turn pink in the bioreactor and without the addition of cells was performed to investigate the time frame of this color change. As shown in Figure 5-13, the color of the medium already started turning to a darker violet after only 2 h of running AiO and CO_2 sparging.

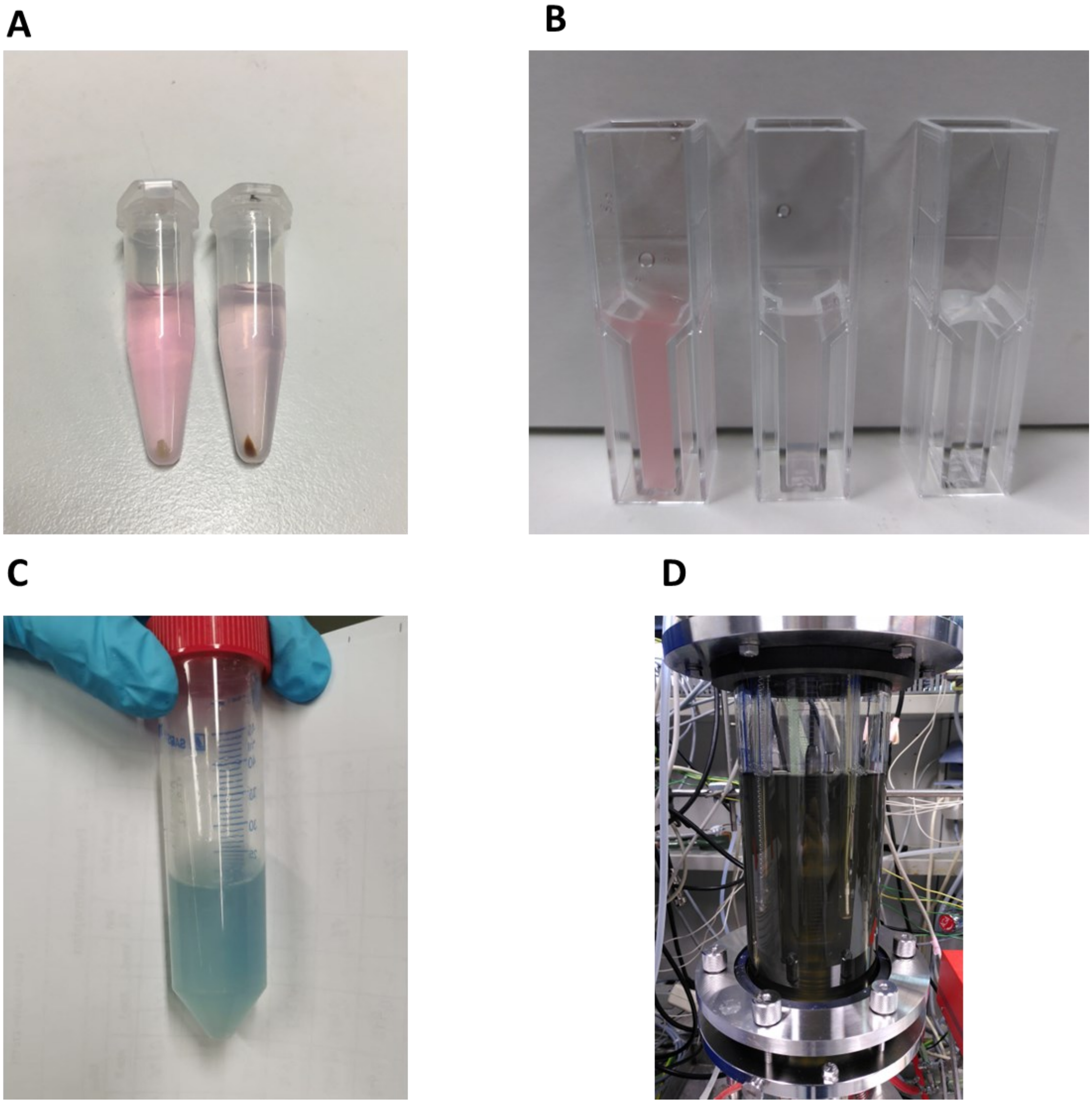

Figure 5-12: Color changes of the cultivation medium with added resazurin during autotrophic stirred-tank batch fermentations of different *A. woodii* strains with the AiO electrode and CO_2 sparging. (A) Centrifuged cell broth samples from a fermentation with *A. woodii* [P_{bgaL}_*ldhD*_NFP]. The left sample was taken at the time point t = 0 h, the right sample at t = 12 h. (B) Cell broth from the same fermentation as (A): left cuvette shows a sample at t = 0, center cuvette shows sample at t = 12 h, right cuvette shows DI-water. (C) Cell broth taken from a fermentation with *A. woodii* [P_{bgaL}_*ldhD*_NFP] after 60 h of fermentation time. (D) Fermentation broth of a fermentation with *A. woodii* [P_{bgaL}_*ldhD*_NFP] after 24 h.

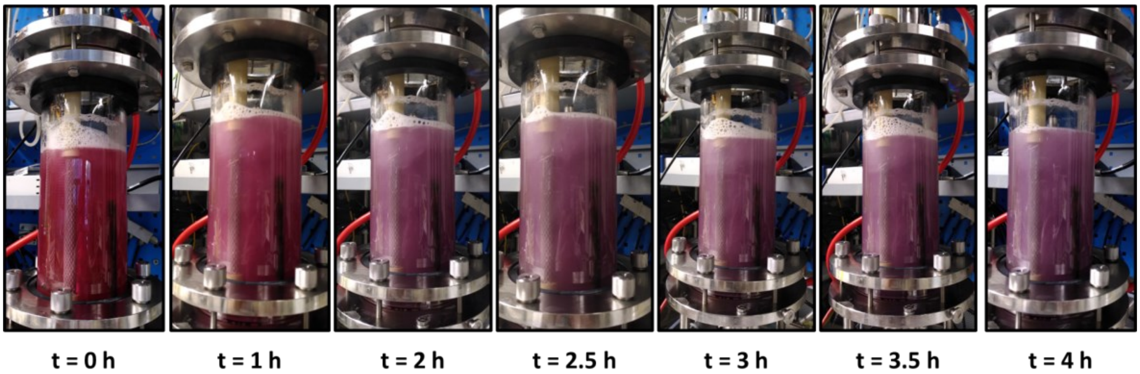

Figure 5-13: Color change of the fermentation medium with added resazurin with active AiO electrode and CO_2 sparging. The pictures show the running BES reactor prior to inoculation with *A. woodii* [P_{bgaL}_*ldhD*_NFP] during a time interval of 4 h.

Unfortunately, this effect was not always reproducible, however it occurred in 40 % of the conducted fermentations with resazurin. Furthermore, the phenomenon is not fully understood. Although resazurin can change its color to purple as seen in Figure 5-13, it does this in its original state before being irreversibly changed to resorufin, which then shows the pink color as seen in Figure 5-12 and Figure 5-13 (Bueno et al., 2002). Furthermore, resazurin can also be used as pH indicator, turning to darker purple colors above a pH of 6.5 (Chen et al., 2015). However, the pH of all experiments where this phenomenon happened was controlled at 7 and no correlation of drastic pH change to color change was observed. Furthermore, as mentioned before, the change from pink (resorufin) to blue/purple (resazurin) should not be possible, due to the irreversible reduction reaction. One correlation with the color change, which was observed though, was cell growth inhibition. Once the color change or decolorization occurred, cell growth of *A. woodii* was inhibited. A direct comparison of cell growth of *A. woodii* [P_{bgaL}_*ldhD*_NFP] in a culture medium with and without resazurin is shown in Figure 5-14. When the decolorization or the color change occurred, it affected cell growth either in complete inhibition (see Figure 5-14, blue triangles) or in an early stop of cell growth at low OD_{600} (see Figure 5-14, red triangles). Toxic effects of resazurin on cell cultures has been reported before, however only after an incubation of 8 days or more (Pace and Burg, 2015), which is not the case in the fermentations reported in this study. However, since the color change was linked to cell inhibition, resazurin was left out in the culture medium for future bioreactor fermentations.

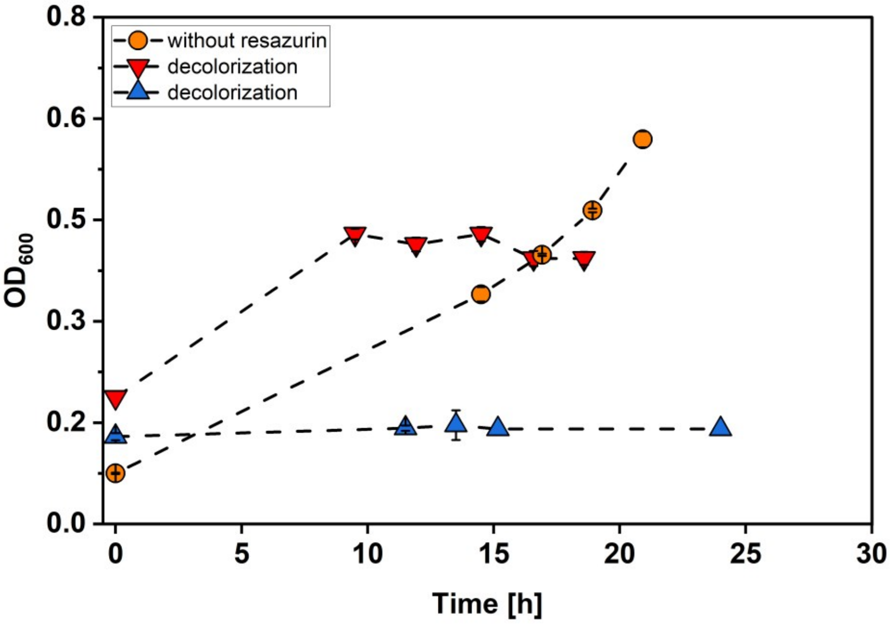

Figure 5-14: Comparison of cell growth in culture medium with and without resazurin. Orange circles: OD_{600} measured in a fermentation of *A. woodii* [P$_{bgaL}$_*ldhD*_NFP] without resazurin; red triangles: OD_{600} measured in a fermentation of *A. woodii* [P$_{bgaL}$_*ldhD*_NFP] with resazurin and with observed decolorization of the typical resorufin pink; blue triangles: OD_{600} measured in a fermentation of *A. woodii* P$_{tet}$_*ldhD*$_{CI}$ with resazurin and with observed decolorization of the typical resorufin pink.

5.2.7. Growth Inhibition Effects of Electrical Voltage

For the operation of the AiO electrode, a constant electrical current was chosen as a set point (see 4.5.1 for details), thus, the potentiostat regulated the necessary voltage to reach the desired current. Over the course of an *A. woodii* fermentation using the AiO electrode, the voltage could therefore vary. As already mentioned in Chapter 5.1, electrodeposition of metals and other media components happened on the surface of the WE with each use. Furthermore, cells and cell debris as well as media components also adsorbed to the porous surface of the ceramic separator during AiO usage. This led to increasing electrical resistances in the AiO electrode with each fermentation, increasing therefore the necessary voltage to reach and hold the desired electrical current set point (see Equation (3.27)). Over the course of this study, many fermentation experiments showed a lack of cell growth and therefore, a meta data study of a major part of the fermentations performed was conducted, to investigate whether high AiO voltages caused this cell growth inhibition. Average AiO voltages ranged from a minimum of 3.7 V to a maximum of 11.4 V. The relationship between average voltage during a fermentation and the cell density increase during the first 20 h can be seen in Figure 5-15 A. For a better presentation, cell density intervals of 0.1 were chosen. Although the standard deviations of the average voltage values in the intervals up to a $\Delta OD_{20\ h}$ of 0.4 are rather high at 1.8 ± 0.2 V, the tendency is clear. Fermentations with higher average voltages tended to grow less in the first 20 h than fermentations with lower voltages. Especially, when comparing the bar of the cell density interval 0.4 – 0.5 (4.2 ± 0.5 V) to the bar of the cell density interval of 0.1 – 0.2 (7.7 ± 2.0 V), this relationship is clear. The same data set was used to evaluate the relationship between the maximum cell growth rate and the average voltage over the course of a fermentation. For this evaluation, electrical voltages were also divided into intervals. Given that most fermentations showed a U_{av} of 4 – 6 V, this range was divided in 0.5 V steps, while the rest was divided in 1 V steps. As shown in Figure 5-15 B, the result is similar. High growth rates were only reached during fermentations with low electrical voltages. Here, the intervals between 5 and 6 V are statistically not significant. However, the comparison of the interval 4.0 – 4.5 V (0.071 ± 0.012 h^{-1}) and the interval 7 – 8 V (0.034 ± 0.004 h^{-1}) suggests strongly that high voltages cause *A. woodii* growth inhibition. The negative effects of high voltages on living cells have been known for quite some time (Mizuno and Hori, 1988). However, the investigation if microbial cells are damaged from lower currents or voltages, has only recently been studied, due to the increased interests in bioelectrochemistry (Luo et al., 2005; Valle et al., 2007; Yang et al., 2010). Electrical voltages can lead to the destruction of cell membrane, thus cell density can decrease and growth can be inhibited (Ding et al., 2016). It is assumed that the negative effects observed during this study only occur during higher voltages due to the low contact time of the cells with the electrode surface. In a sufficiently mixed system, the bacterial cells should not come into contact with the electrode for longer periods of time, thus reducing exposition time to cell membrane damaging voltages. In conclusion, for the BES to function well and for *A. woodii* cells to grow sufficiently, AiO voltages should always be kept below 4.5 V.

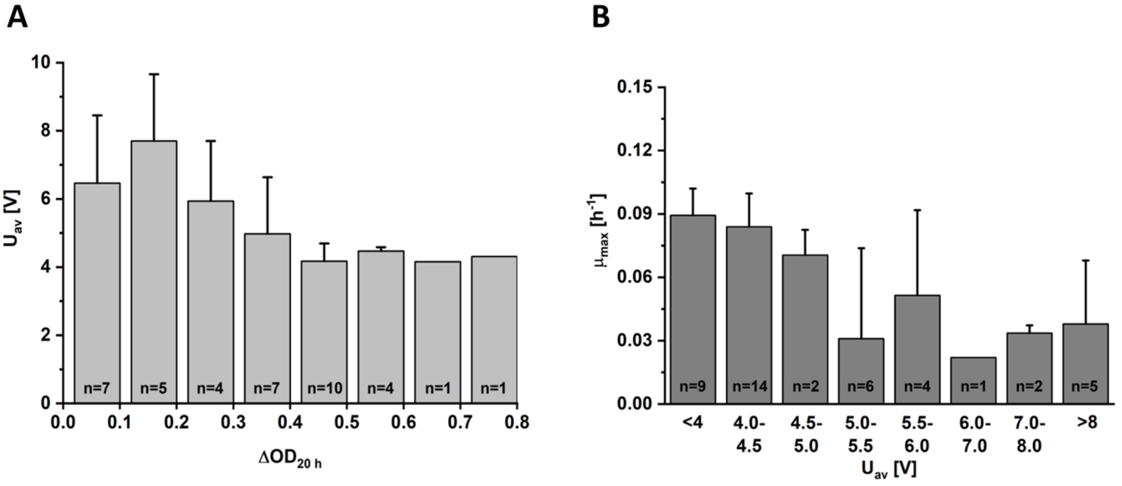

Figure 5-15: Growth inhibition effects of electrical voltage. (A) average AiO voltage (U_{av}, V) vs. cell density increase during the first 20 h of fermentation time ($\Delta OD_{20\,h}$). (B) maximum growth rate (μ_{max}, h^{-1}) vs. average AiO voltage (U_{av}, V). The number of data points used for average value calculation is indicated at the lower end of each bar.

5.3. *Clostridium drakei* Stirred-Tank Batch Fermentations

This chapter describes the characterization of *C. drakei* during fermentations using lactate as primary carbon source. For this, inhibiting concentrations of caproate were determined. Furthermore, *C. drakei* was cultivated in stirred-tank batch fermentations to obtain important process performance parameters. By adaptation of the substrate composition in the pre-culture, the stirred-tank batch fermentations were optimized. At last, the impact of inoculation cell density and the working AiO during the batch fermentation was investigated.

5.3.1. Growth Inhibition Effects of Caproate

As mentioned in Chapter 3.2.1, caproic acid has an inhibiting effect on microorganisms. Although numerous studies of this inhibitory effect exist (Zaldivar and Ingram, 1999; van Immerseel et al., 2004), no data has been published on specific inhibition concentrations of caproic acid for *C. drakei*. Therefore, bottle fermentations of *C. drakei* growing on lactate were conducted with various initial caproate concentrations (see Chapter 4.4 for details). The caproic acid concentrations were chosen in between 0.0 and 16.5 g L^{-1} and the increase in cell density during the first 40 h of the fermentations ($\Delta OD_{40\,h}$) was chosen as relevant parameter for inhibitory levels determination. The bottle fermentations were conducted in duplicates and the results can be seen in Figure 5-16. While the control fermentation with no added caproate added up to a $\Delta OD_{40\,h}$ of 2.65 ± 0.17, the fermentation with an added caproate concentration of 1 g L^{-1} reached a $\Delta OD_{40\,h}$

of 3.02 ± 0.07. This suggests that 1 g L^{-1} of caproate does not have an inhibitory effect on *C. drakei*, and furthermore, that the $\Delta OD_{40\,h}$ range for an uninhibited culture could be higher than the results of the control fermentation. From 2 g L^{-1} and higher however, the inhibitory effect of caproate can be seen clearly. The fermentations with 2 and 3 g L^{-1} caproate reached a $\Delta OD_{40\,h}$ of 0.16 ± 0.14 and 0.35 ± 0.22, respectively. This accounts for a decrease in $\Delta OD_{40\,h}$ of up to 17-fold in comparison with the control fermentation. The fermentations with a caproate concentration higher than 3 g L^{-1} showed even a growth decline during the first 40 h. This data suggests that the inhibitory concentration of caproate for *C. drakei* lies in between 1 and 2 g L^{-1} of caproate. Growth inhibition concentration of caproic acid for *Clostridia* were reported at 3.5 g L^{-1} (Kenealy et al., 1995), however, production of caproic acid by *C. kluyveri* in a pH uncontrolled environment was at 6.8 g L^{-1} (San-Valero et al., 2019). Given that for the here presented experiment, caproic acid was added to the medium before cell growth started, 1.5 g L^{-1} as inhibitory concentration seems to fall in line with recent publications. However, future inhibition experiments should be conducted where caproic acid is added during the exponential growth phase, as it is not produced by *C. drakei* before this point.

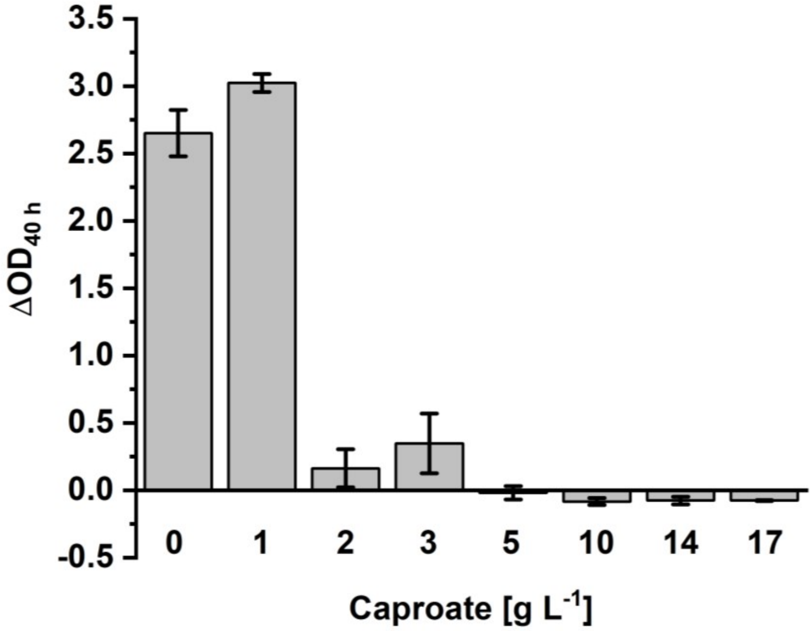

Figure 5-16: Cell growth inhibition by caproic acid during bottle fermentation of *C. drakei*. The increase in cell density in the first 40 h ($\Delta OD_{40\,h}$) is shown as the relevant parameter for inhibitory concentrations of caproate. Each bottle fermentation was conducted as duplicate.

5.3.2. Heterotrophic Stirred-Tank Batch Fermentations of *C. drakei*

For the characterization of cell growth and caproic acid production on lactate, *C. drakei* was cultivated in a stirred-tank bioreactor with low stirrer rates of 210 rpm to exclude possible shear stress effects. 10 g L^{-1} of lactate were added prior to inoculation. The pre-culture lasted 32 h and reached an OD_{600} of 3.6. Subsequently, 80 mL of the pre-culture broth were transferred to the bioreactor. The results of the stirred-tank batch fermentation can be seen in Figure 5-17. The fermentation was reproduced (n = 2), the data set of the second fermentation is shown in Figure 11-2 in the appendix. The cell density of *C. drakei* duplicated in the first 15 h of the fermentation, but then, no further cell growth was observed. The OD_{600} stayed constant at 0.41 ± 0.03 for 16 h before a second growth phase with $\mu_{max} = 0.04$ h^{-1} started. This growth phase lasted for 20 h, reaching an OD_{600} of 0.93 ± 0.08 after 49 h of fermentation time. The subsequent stationary phase at an OD_{600} of 0.96 ± 0.04 lasted 17 h, the maximum OD_{600} value was observed at 1.04. During the last 4 h, cell density declined to a final value of 0.89. Lactate was consumed by *C. drakei* from the beginning of the fermentation. The lactate consumption rate during the initial 21 h added up to 0.06 g L^{-1} h^{-1}, reducing the lactate concentration by 11 % to 9.5 g L^{-1}. Towards the end of the first stationary growth phase, the lactate consumption rate almost doubled to 0.11 g L^{-1} h^{-1} and during the exponential growth phase it reached a maximum value of 0.24 g L^{-1} h^{-1}. After 66 h, the lactate concentration added up to 0.13 ± 0.18 g L^{-1}, however, the data suggest that lactate consumption due to low concentration already stopped at around 58 h of fermentation time. Acetate was produced at a constant rate of 0.06 g L^{-1} h^{-1} and reached a final concentration of 4.53 ± 0.53 g L^{-1}. Butyrate was produced at a similar rate as acetate during the initial 15 h, however, the production rate then increased to 0.15 g L^{-1} h^{-1}, reaching a peak concentration of 1.57 ± 0.65 g L^{-1} after 21 h. Subsequently, butyrate concentration decreased to 1.26 ± 0.27 g L^{-1} before increasing again to a maximum of 3.14 ± 0.08 g L^{-1} after 64 h. The product of interest, caproate, was detected in the medium after 23 h of fermentation. The caproate production rate added up to 0.01 g L^{-1} h^{-1} in the first 31 h and increased afterwards to 0.08 g L^{-1} h^{-1} in between 39 h and an estimated 58 h of fermentation time. The maximum concentration of 1.50 g L^{-1} was measured after 64 h, when the culture had already become stationary. ORP levels decreased from the initial -308 mV to -463 mV after 15 h and then stayed constant at low levels of -481 ± 10 mV for another 34 h. During the last 19 h, ORP had increased to -453 ± 5 mV. pH was constant at 6.76 ± 0.01 throughout the fermentation. Carbon balances were closed within an estimation error of 5 %. The most important process performance parameters are listed in Table 5-2.

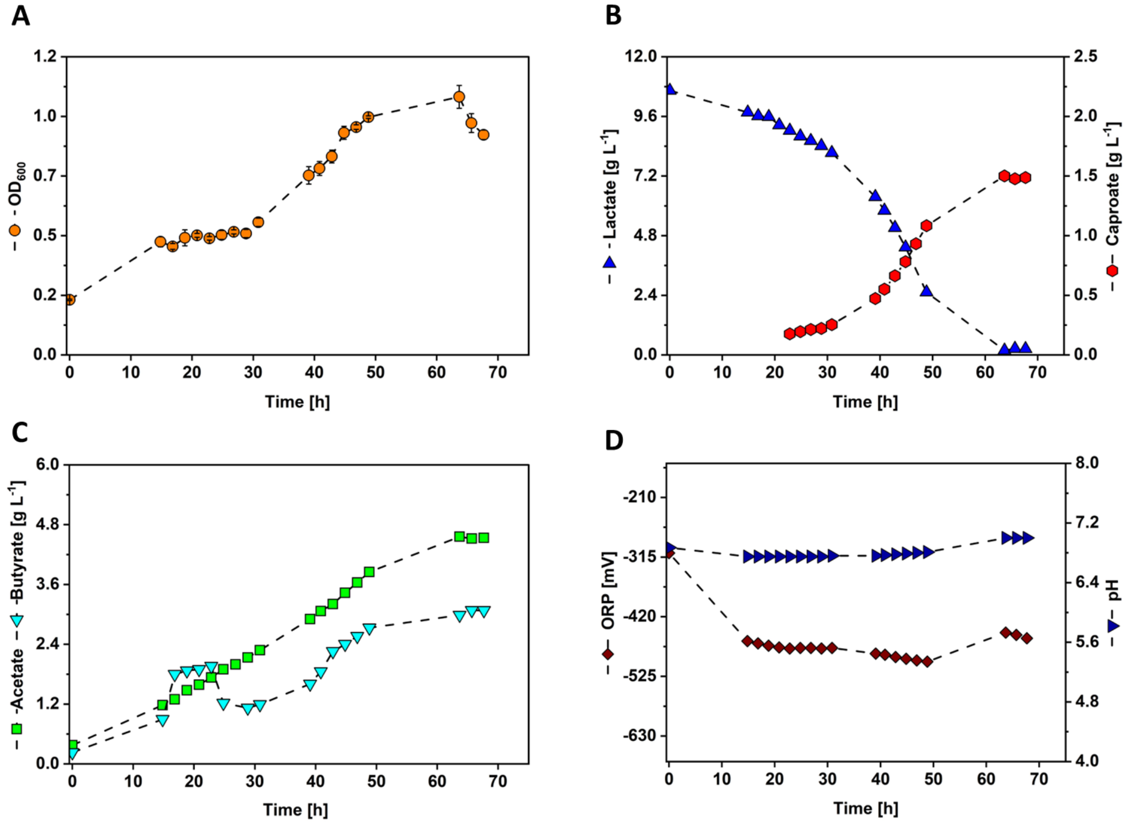

Figure 5-17: Stirred-tank batch fermentation of *C. drakei* with lactate as substrate. (A) optical cell density (orange circles, OD_{600}); (B) concentration of lactate (blue triangles) and caproate (red hexagons, g L^{-1}); (C) concentration of acetate (green squares) and butyrate (cyan triangles, g L^{-1}); (D) ORP (brown diamonds, mV) and pH (blue triangles) measured during the cultivation. Parameters: T = 30 °C; pH = 7.0; $P\ V^{-1}$ = 0.04 W L^{-1}; V_{CO_2} = 0.003 vvm; $V_0 = 1.4$ L; $c_{Lac,0} = 10.6$ g L^{-1}.

It is well known that *C. drakei* possesses the ability to grow on lactate (Liou et al., 2005), however to the authors best knowledge, this study presents the first data of a stirred-tank batch fermentation with *C. drakei* growing in lactate. As Figure 5-17 A shows, cell growth exhibited two phases. Given that during the first phase only 7 % (g g^{-1}) of the lactate was consumed while cell density had already doubled, it is assumed that a second substrate i.e., yeast extract components, was used as main substrate during this first growth phase. This indicates, that *C. drakei* had not yet fully adapted to lactate as main carbon source during the pre-culture fermentation. The high lactate consumption rate of 7.3 ± 1.7 g d^{-1}, however, shows that once adapted, *C. drakei* grows efficiently on lactate. The decrease in cell density during the last 4 h could be explained by cell lysis due to the toxic effects of organic acid, as mentioned in Chapter 3.2.1. Furthermore, the caproate concentration of 1.5 g L^{-1} matches the assumed inhibitory concentration discussed in Chapter 5.3.1 (see Figure 5-16). Comparing Figure 5-17 A with Figure 5-17 B, indicates that caproate is produced mainly during the second growth phase, with 83 % being produced during this stage. Caproate yield from lactate added up to 0.13 g g^{-1} which is 2.3-fold lower than reported by similar processes (Zhu et al., 2017), however these data were obtain with multi microorganism biomes and not with single cultures. A comparison with data from caproate producing *Clostridia* in single cultures reported 0.18 g g^{-1} yield from lactate (Liu et al., 2020). The total concentration of caproate is 1.1 to 15.6-fold lower than in other microbial caproate production processes (Cavalcante et al., 2017), however most of the reported processes use undefined mixed cultures and different process modes for caproate production. The volumetric productivity of 0.6 g L^{-1} d^{-1} for example could be increased by applying fed-batch or continuous fermentation modes (Kucek et al., 2016a) and using a *in situ* product recovery technique could prevent potential inhibitory effects, leading to more cell growth and higher overall caproate yields (Jeon et al., 2013; Kucek et al., 2016b). Furthermore, the possibilities to increase the chain elongation rate from acetate to caproate by genetic engineering should be investigated, given that caproate adds up to only 23 % of the three main products, while acetate accounts for 43 %.

Table 5-2: Important process performance parameters of all batch process with *C. drakei* discussed in this chapter.

Special Set Up	OD_{max}	μ_{max}	$Y_{X/S}$	c_{Lac}	c_{cap}	q_{cap}	$Y_{P/S}$	P_{vol}	$-q_{Lac}$	c_{Ac}	c_{But}
[-]	[-]	[h^{-1}]	[$g\ g^{-1}$]	[$g\ L^{-1}$]	[$g\ L^{-1}$]	[$g\ h^{-1}$]	[$g\ g^{-1}$]	[$g\ L^{-1}\ d^{-1}$]	[$g\ h^{-1}$]	[$g\ L^{-1}$]	[$g\ L^{-1}$]
Non-adapted pre-culture	1.04	0.04	0.04	10.64	1.50	0.08	0.13	0.57	0.11	4.53	3.14
Adapted pre-culture	0.98	0.04	0.09	4.27	0.66	0.03	0.15	0.45	0.28	2.09	1.41
Low inoculation OD_{600}	0.72	0.06	0.05	10.50	0.79	0.04	0.10	0.28	0.29	3.25	2.40
AiO at t = 0 h	0.12	0.00	-	7.07	0.00	0.00	-	-	-	0.62	0.29
AiO at t = 23 h	0.96	0.08	0.06	7.17	1.25	0.06	0.16	0.68	0.42	1.76	1.78

Adaptation of *C. drakei* to Lactate in Pre-Culture

Through a step wise re-inoculation of *C. drakei* cells in pre-culture bottles with increasing lactate concentrations, the strain was adapted over time to lactate as main carbon and energy source. The success of these adaptions was shown in the growth behavior of *C. drakei* when inoculated into a bioreactor. Fermentation parameters were left unchanged, except for the lactate concentration at the beginning of the process, which was reduced to 4.3 g L^{-1}. As shown in Figure 5-18 A, no two growth phases as seen in Figure 5-17 A were observed. Cell growth took place in a continuous and linear way with a maximum growth rate of 0.04 h^{-1}, equal to the μ_{max} of the fermentation shown discussed in the previous chapter. The maximum cell density of 0.98 was reached after 37 h, adding up to an $Y_{X/S}$ of 0.11 g g^{-1}. Lactate was consumed with a rate of 0.07 g h^{-1} during the first 18 h of fermentation time, before it increased 4-fold to the maximum of 0.28 g h^{-1} during the following 17 h. After 35 h, all lactate in the fermentation medium was depleted. Low caproate concentrations were detected in the medium after 16 h. After 20 h, caproate production increased with a rate of 0.03 g h^{-1}. The maximum caproate concentration added up to 0.66 g L^{-1}, which was reached after all lactate was consumed. In the last 10 h of the fermentation, caproate concentrations stayed constant. Acetate and butyrate were produced at similar rates from the beginning of the fermentation, reaching maximum final concentrations of 2.1 and 1.4 g L^{-1}, respectively. Both acetate and butyrate concentrations were constant during the last 10 h. Both ORP and pH measured in the fermentation medium were constant at -423 ± 13 mV and 6.97 ± 0.03, respectively. Carbon balances were closed within an estimation error of 8 % and the most important process performance parameters are listed in Table 5-2.

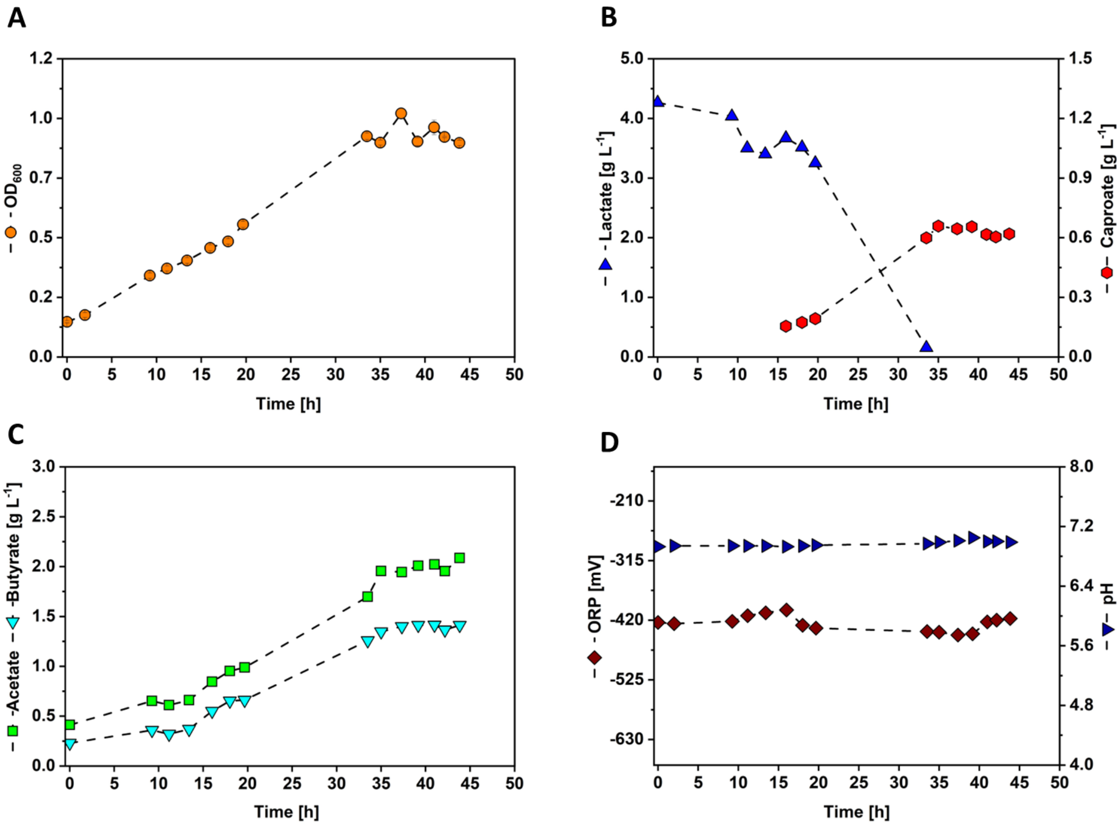

Figure 5-18: Stirred-tank batch fermentation of *C. drakei* with lactate as substrate and adapted pre-culture. (A) optical cell density (orange circles, OD_{600}); (B) concentration of lactate (blue triangles) and caproate (red hexagons, g L^{-1}); (C) concentration of acetate (green squares) and butyrate (cyan triangles, g L^{-1}); (D) ORP (brown diamonds, mV) and pH (blue triangles) measured during the cultivation. Parameters: T = 30 °C; pH = 7.0; $P\ V^{-1}$ = 0.01 W L^{-1}; V_{CO_2} = 0.003 vvm; V_0 = 1.3 L; $c_{Lac,0}$ = 4.3 g L^{-1}.

The adaptation of *C. drakei* to lactate in pre-cultures proved successful, given that in the bioreactor, the strain did not grow in two phases anymore. The constant growth furthermore happened with the same maximum growth rate of 0.04 h^{-1} as in the previous fermentation (compare data listed in Table 5-2), suggesting that this is the maximum possible growth rate of *C. drakei* using lactate as carbon source in a stirred-tank reactor. Interesting is, that $Y_{X/S}$ increased 2.3-fold compared to the non-adapted fermentation. However, this could be an indication to the assumption discussed in the previous chapter, that yeast extract was used as carbon source during the beginning of the non-adapted process. As it is difficult to quantify the components in the yeast extract which could have been consumed by *C. drakei*, the amount of carbon used for the calculation of $Y_{X/S}$ of the fermentation shown in Figure 5-17 is not the total carbon which was actually consumed. Another difference between the fermentation depicted in Figure 5-17 and

Figure 5-18 is that in the adapted fermentation process, lactate was depleted completely while in the non-adapted process, 0.22 ± 0.04 g L^{-1} of lactate were measured in the medium during the last 4 h. This could indicate that the non-adapted strain was inhibited by a metabolic component, such as caproic acid (see Chapter 3.2.1 and 5.3.1) and not by the lack of lactate as can be observed in the fermentation of the adapted strain.

5.3.3. Effect of Inoculation Cell Density and Electrical Voltage on Growth

For further characterization of *C. drakei* growth and caproate production in a stirred-tank bioreactor batch fermentation, the *C. drakei* strain was inoculated at a lower inoculation density of 0.12. Furthermore, in a parallel fermentation process, the AiO electrode was operated at 600 mV from the beginning on, to investigate possible effects of electrical voltage on the strain. Both fermentations were inoculated from the same pre-culture, which had reached an OD_{600} of 1.8 after 33 h. The results are shown in Figure 5-19. The fermentation process without the AiO electrode grew during the first 20 h with a growth rate of 0.06 h^{-1} to an OD_{600} of 0.38 while the process with the AiO electrode showed a cell density decline to 0.05 during the same time frame. After a stationary phase of 40 h, the fermentation without the AiO electrode started growing again in a second growth phase with a growth rate of 0.02 and reached a final OD_{600} of 0.72 after 66.5 h. Since the cell density of the process with the AiO electrode declined constantly, the fermentation was terminated after 40 h at an OD_{600} of 0.03. Lactate was consumed by the *C. drakei* strain in the process without the AiO electrode during the first 40 h at an uptake rate of 0.07 g h^{-1}. Afterwards, the uptake rate of lactate increased 4.3-fold to 0.30 g h^{-1} during the last 20 h. The *C. drakei* cultivation which was conducted with AiO electrode did not show any lactate consumption during the entire process. Caproate was detected in the fermentation medium of the cultivation without AiO electrode after 47 h at a concentration of 0.22 g L^{-1}. The concentration increased subsequently with a production rate of 0.04 g h^{-1} to a final value of 0.79 g L^{-1} at the end of the fermentation. Acetate was produced during the cultivation without the AiO electrode constantly, reaching a maximum value of 3.25 g L^{-1} at the end of the fermentation. Butyrate concentrations halted after 20 h at a concentration of 0.85 ± 0.05 g L^{-1}, before increasing again after 40 h. Maximum butyrate concentrations added up to 2.40 g L^{-1} at the end of the fermentation. In the cultivation with the AiO electrode, acetate concentrations stayed constant during the entire process, butyrate concentrations decreased from 0.35 g L^{-1} to 0.29 g L^{-1} until the fermentation was terminated. While the pH signal was constant in both fermentations throughout the process, the ORP signal in the fermentation without the AiO electrode decreased from -316 mV to -437 mV during the first 16 h and stayed constant at -327 ± 18 mV afterwards. The ORP in the cultivation with the AiO electrode measured 395 ± 5 mV during the first 24 h and increased subsequently to -328 mV during the final 16 h of fermentation time. Carbon balances were closed within an estimation error of 6 %. A selection of important process performance parameters is listed in Table 5-2.

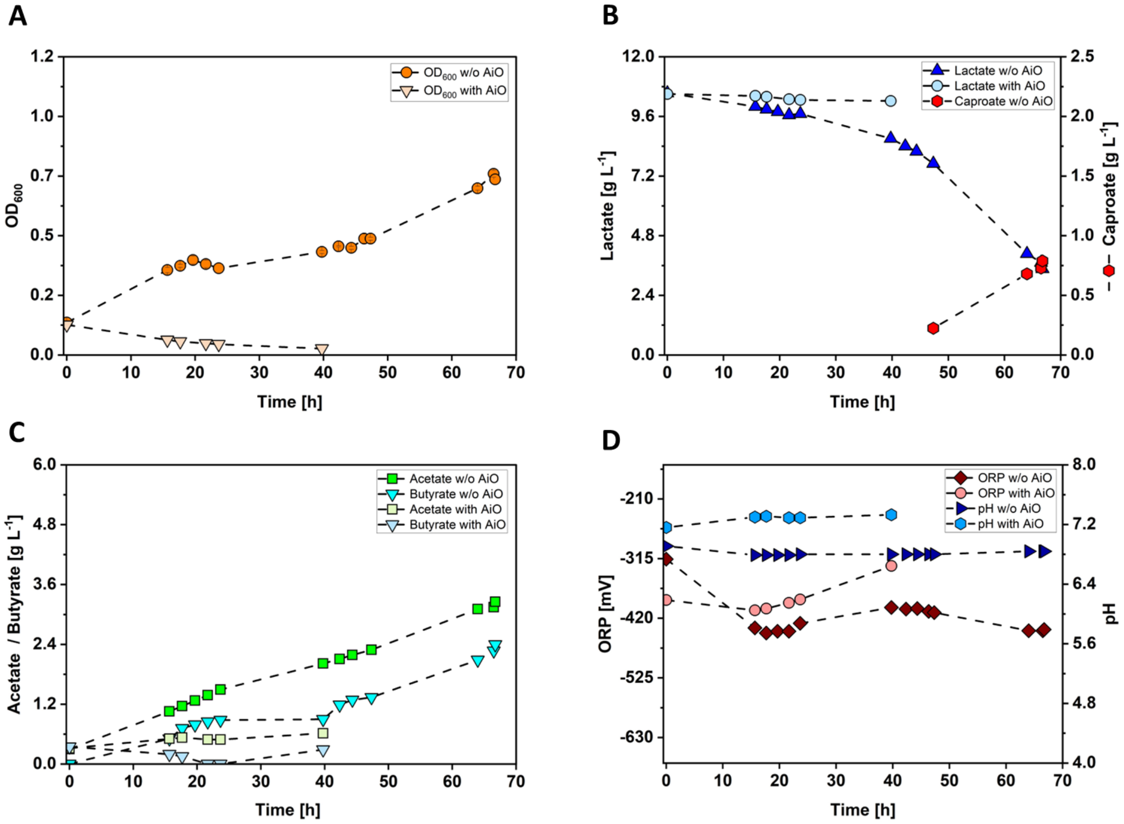

Figure 5-19: Stirred-tank batch fermentation of *C. drakei* with lactate as substrate. Darker colors show fermentation with lower inoculation cell density, lighter colors show fermentation with AiO operation. (A) optical cell density (orange circles and triangles, OD_{600}); (B) concentration of lactate (blue triangles and hexagons) and caproate (red hexagons, g L^{-1}); (C) concentration of acetate (green squares) and butyrate (cyan triangles, g L^{-1}); (D) ORP (brown diamonds and pink circles, mV) and pH (blue triangles and hexagons) measured during the cultivation. Parameters: T = 30 °C; pH = 7.0; $P\ V^{-1}$ = 0.04 W L^{-1}; V_{CO_2} = 0.003 vvm; V_0 = 1.3 L; $c_{Lac,0}$ = 10.5 g L^{-1}. I_{AiO} = 600 mA; U_{av} = 4.3 V for the fermentation conducted with the AiO electrode (represented in the lighter colors).

The influences of a lower inoculation cell density on a *C. drakei* cultivation are illustrated when comparing the results shown in Figure 5-19 and Figure 5-17 (see data Table 5-2). A lower inoculation cell density caused a 2.3-fold extension of the first stationary phase (see Figure 5-19 A); this phase lasted only 12 h during the *C. drakei* fermentation with an inoculation cell density of 0.2. Due to this delay, total cell mass, product and byproduct concentrations were expectedly lower in the process with the lower inoculation cell density. Furthermore, the volumetric productivity was reduced 50 %, which is also due to the longer stationary phase. However, the deviations of $Y_{X/S}$ and $Y_{P/S}$ where 5-fold higher and only 1.3-fold lower in comparison, which shows that the metabolic performance during this process was comparable. The influence of the AiO electrode however seems to be more substantially. The direct comparison of both fermentations, which were inoculated from the same pre-culture in the same conditions with exception for the integration of the AiO electrode, suggests a negative influence of the electrical voltage on *C. drakei*. The cells did not grow at all, cell density even declined from the start of the fermentation, suggesting cell lysis. This could fall in line with the effects described in Chapter 5.2.7, that electrical voltage can cause cell membrane perforation. Due to the non-existing cell growth, all other parameters of the fermentation were low or not analyzable, as expected. To conclude, for *C. drakei* cultivations to be successful, inoculation cell density should always exceed a value of 0.2 and the AiO electrode should not be in operation during the first hour of the process.

Effect of AiO Operation during Exponential Growth Phase

Based on the negative effects of the AiO electrode operating from the beginning of a fermentation process observed in the process described in the previous chapter, further fermentations were conducted where the AiO electrode was not turned on until a substantial growth had taken place. For the fermentation described in this chapter, the AiO electrode was turned on during the exponential growth phase, at an OD_{600} of 0.47 and a current of 400 mA. The cultivation was inoculated from a lactate adapted pre-culture with a cell density of 1.0. The results are shown in Figure 5-20. Cell growth of the *C. drakei* strain started without lag phase and reached a μ_{max} of 0.08 h^{-1} after 18 h. After phase of slower cell growth between 25 h and 38 h, the cultivation reached its maximum cell density of 0.96. Lactate consumption started with an uptake rate of 0.1 h^{-1} and increased subsequently 4.2-fold until lactate was completely consumed after 44 h. Caproate concentrations started increasing after 22 h and reached a maximum production rate of 0.06 h^{-1} after 26 h of fermentation time. The maximum caproate concentration added up to 1.25 g L^{-1} after 40 h when lactate was completely consumed. Acetate and butyrate were produced constantly at similar rates and added up to maximum concentrations of 1.76 g L^{-1} and 1.78 g L^{-1} after 40 h, respectively. pH value was constant at 7.2 ± 0.1 throughout the fermentation while the ORP decreased slowly during the first 22 h from -237 mV to -369 mV. After the AiO electrode was turned on, the ORP decreased to a minimum of -530 mV after 35 h. Carbon balances were closed within an estimation error of 7 % and important process performance parameters are listed in Table 5-2.

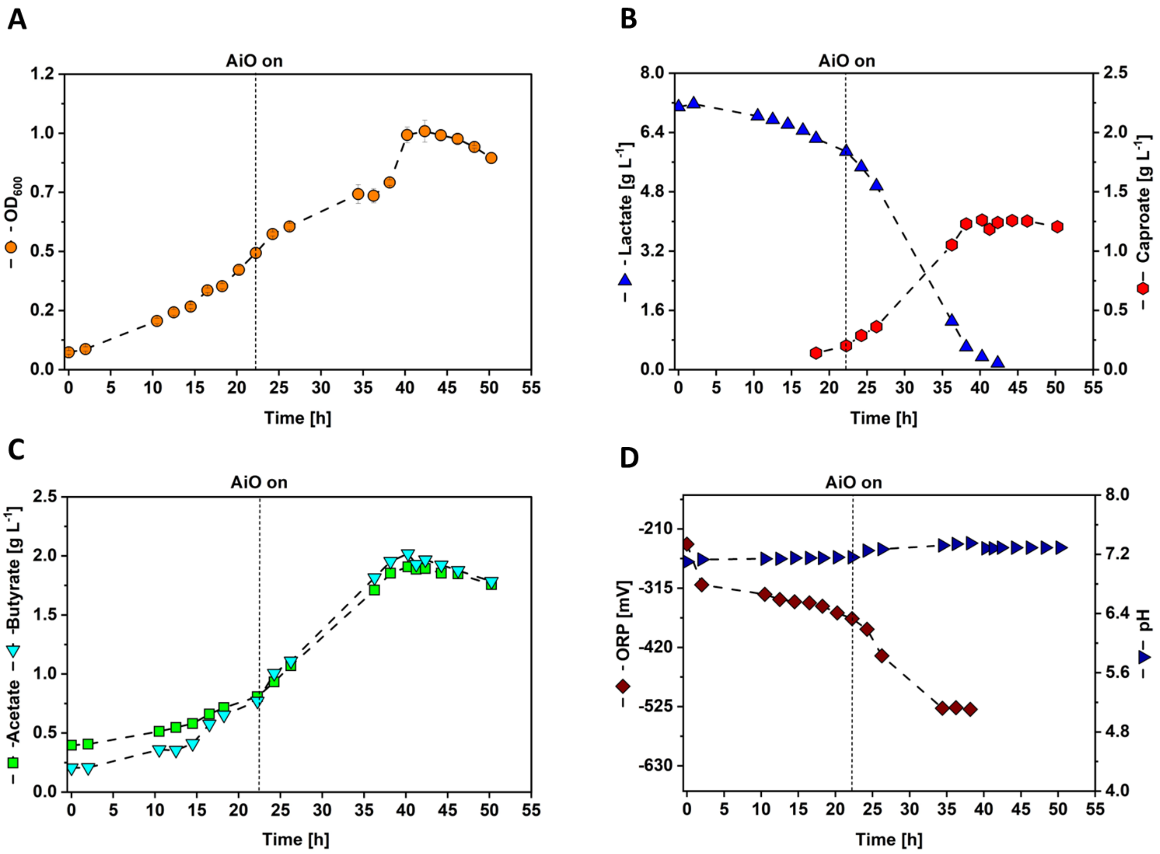

Figure 5-20: Stirred-tank batch fermentation of *C. drakei* with lactate as substrate and AiO electrode during exponential growth phase. (A) optical cell density (orange circles, OD_{600}); (B) concentration of lactate (blue triangles) and caproate (red hexagons, g L^{-1}); (C) concentration of acetate (green squares) and butyrate (cyan triangles, g L^{-1}); (D) ORP (brown diamonds, mV) and pH (blue triangles) measured during the cultivation. Parameters: T = 30 °C; pH = 7.0; $P\ V^{-1}$ = 0.04 W L^{-1}; V_{CO_2} = 0.003 vvm; V_0 = 1.3 L; $c_{Lac,0}$ = 10.5 g L^{-1}; I_{AiO} = 400 mA; U_{av} = 3.8 V.

The results shown in Figure 5-20 suggest that the electrical voltage of the AiO electrode had no influence on cell growth of *C. drakei* or its production of caproate. The growth rate did not decline significantly after the electrode was turned on and the maximum cell density was similar to the fermentation process with and without adapted pre-culture (refer to Figure 5-17 and Figure 5-18). Although biomass yield from lactate was 1.5-fold lower compared to the cultivation with the adapted pre-culture, caproate yield was very comparable. This could suggest a small effect of the electrical current on cell growth; however, it did not have an effect on caproate production, which also represents the 1.5-fold higher volumetric productivity. In conclusion, negative effects of the working AiO electrode as observed in Figure 5-19 could not be confirmed when the electrode was turned on during the exponential growth phase.

5.4. Synthetic Co-Cultures of *A. woodii* and *C. drakei*

Due to the low lactate production observed in BES fermentations of *A. woodii* [P$_{bgaL}$_*ldhD*_NFP], a first synthetic co-culture run was conducted with supplemented lactate. The results are shown in Figure 5-21. The fermentation was operated with constant electrical current of 600 mA, while the average voltage of the AiO electrode added up to 4.2 V over the course of the fermentation. The maximum H_2 production rate generated by the AiO electrode added up to 6.1 mmol L^{-1} h^{-1}. After 34 h, the pre-culture of the *A. woodii* [P$_{bgaL}$_*ldhD*_NFP] strain had reached an OD_{600} of 1.7 and the bioreactor was subsequently inoculated with 85 mL of the pre-culture broth. Cell growth of the *A. woodii* [P$_{bgaL}$_*ldhD*_NFP] strain started directly after inoculation and reached a maximum cell growth rate of 0.11 h^{-1}. After 14 h, at a cell density of 0.7, the culture was induced with 1 mM lactose for lactate production. Cell growth slowed down 5.5-fold to 0.02 h^{-1} afterwards and reached a maximum OD_{600} of 1.02 after 36 h. Subsequently the cell density decreased to 0.94. At this point, after 41 h of fermentation time, 90 mL of a *C. drakei* culture with an OD_{600} of 2 were added to the bioreactor. Based on the results discussed in Chapter 5.3.3 (refer to Figure 5-19), the AiO electrode was turned off after *C. drakei* inoculation for 7 h to prevent growth inhibition. The cell density increased shortly after the start of the co-culture phase to the maximum value of 1.09 after 47 h. Subsequently, the cell density decreased slowly to 0.97 at the end of the fermentation. Lactate was detected in the cultivation medium after 20 h and increased to 0.39 g L^{-1} at the time point of *C. drakei* addition. To prevent possible lactate limitation, 2.2 g L^{-1} of a DL-lactate solution were added at this time point to the bioreactor. Lactate concentrations decreased after *C. drakei* inoculation with a rate of 0.02 g h^{-1}. A total of 0.91 g of lactate were taken up by *C. drakei*. Caproate was detected in the medium after 56 h at a concentration of 0.04 g L^{-1} and increased towards the end of the fermentation to a maximum value of 0.08 g L^{-1}. Acetate was produced by the *A. woodii* [P$_{bgaL}$_*ldhD*_NFP] strain to 3.89 g L^{-1} when *C. drakei* was added. Afterwards, only low amounts of acetate where produced, increasing to a maximum concentration of 4.03 g L^{-1} at the end of the fermentation. Formate was produced during the first 10 h to 0.47 g L^{-1} and was then completely consumed by the *A. woodii* [P$_{bgaL}$_*ldhD*_NFP] strain again. Subsequently, formate concentrations increased again after the addition of *C. drakei*, adding up to a maximum of 0.65 g L^{-1} after 56 h. Since the *A. woodii* [P$_{bgaL}$_*ldhD*_NFP] strain does not produce butyrate, it was not measured in the medium until after *C. drakei* addition. Butyrate formation happened slowly, increasing from 0.15 to 0.35 g L^{-1} during the co-culture phase. The pH value was constant at 6.9 ± 0.1 throughout the cultivation. The ORP decreased after inoculation of *A. woodii* [P$_{bgaL}$_*ldhD*_NFP] from -270 mV to -419 mV. Subsequently, it stayed constant at -394 ± 8 mV until decreasing to -456 mV towards the time point of *C. drakei* addition. Afterwards, the ORP increased slowly towards the end of the fermentation to -271 mV.

A total of 204.6 mmol of CO_2 and 638.3 mmol of H_2 were taken up during the fermentation. Carbon balances were closed within an estimation error of 5 %. The most important process performance parameters are listed in Table 5-3.

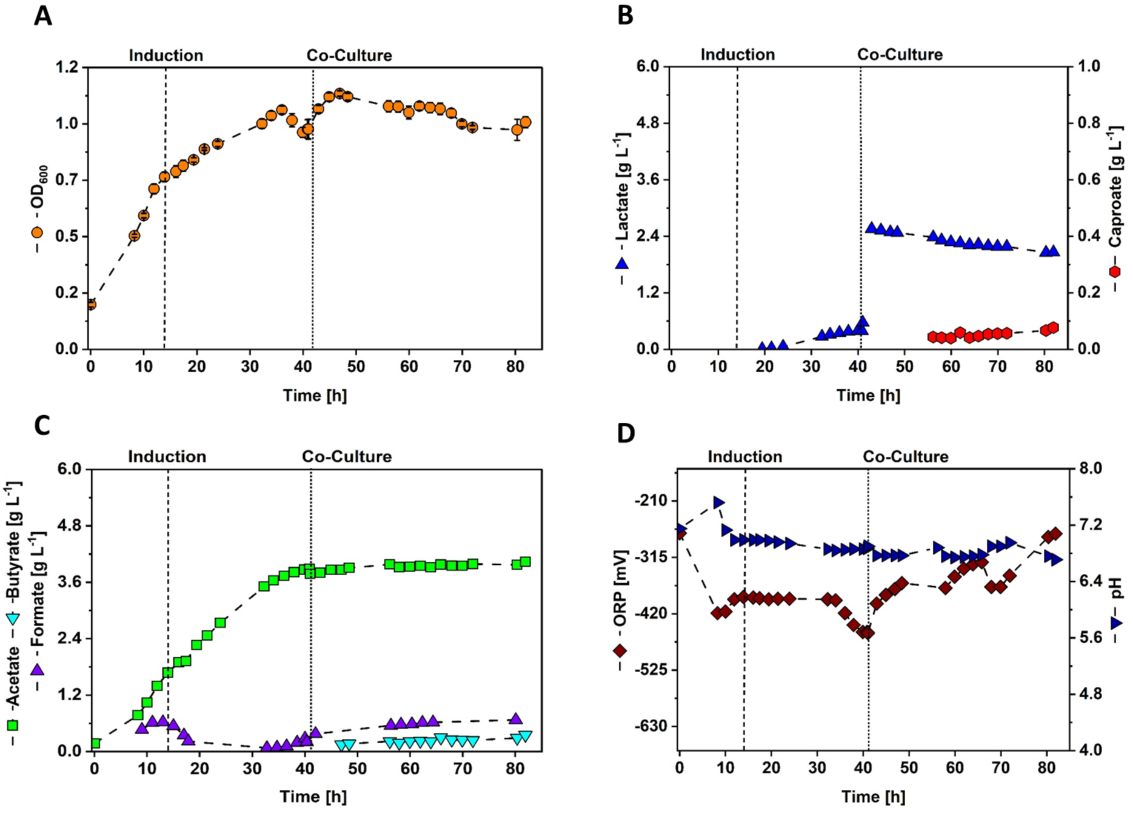

Figure 5-21: Synthetic co-culture in a stirred-tank batch fermentation of *A. woodii* [P_{bgaL}_*ldhD*_NFP] and *C. drakei* with supplemented lactate. (A) optical cell density (orange circles, OD_{600}); (B) concentration of lactate (blue triangles) and caproate (red hexagons, g L^{-1}); (C) concentration of acetate (green squares), formate (purple triangles) and butyrate (cyan triangles, g L^{-1}); (D) ORP (brown diamonds, mV) and pH (blue triangles) measured during the cultivation. The dashed vertical line indicates the time point of induction with 1mM lactose. The dotted vertical line indicates the time point of *C. drakei* and lactate addition. Parameters: $T = 30$ °C; pH = 7.0; $P\,V^{-1} = 4.6$ W L^{-1}; $V_{CO_2} = 0.01$ vvm; $I_{AiO} = 600$ mA; $U_{av} = 4.2$ V; $V_0 = 1.4$ L; $c_{Lac,suppl} = 2.2$ g L^{-1}.

The synthetic co-culture experiment illustrated in Figure 5-21, proved that a combined fermentation of *A. woodii* [P_{bgaL}_*ldhD*_NFP] and *C. drakei* to produce caproate from CO_2 and H_2 is feasible. Although no cell differentiation technique (e.g., via fluorescence tagging such as FISH (Schneider et al., 2021)) was used, the data strongly suggests that *C. drakei* was growing in the bioreactor after inoculation. As shown in Figure 5-21 B and C, the products butyrate and caproate, both unique for *C. drakei,* were measured in the cultivation medium after inoculation and increased over time. Furthermore, the lactate concentration decreased over the course of the fermentation, suggesting lactate consumption of *C. drakei*. The caproate yield from lactate of 0.10 g h^{-1} is up to 1.5-fold lower but comparable to the pure cultures of *C. drakei*: 0.13 g h^{-1} in the fermentation with the non-adapted pre-culture, and 0.15 g h^{-1} in the fermentation with the adapted pre-culture (see Figure 5-17 and Figure 5-18, respectively). The short continuous increase in OD_{600} as seen in Figure 5-21 A after the addition of *C. drakei* also suggests active growth in the bioreactor. A negative influence of the low inoculation cell density, as discussed in Chapter 5.3.3 were not observed, given that 15 h after *C. drakei* addition, caproate was measured in the medium in comparison to 47 h in the fermentation with the low inoculation density shown in Figure 5-19. *C. drakei* consumed a total of 0.50 g L^{-1} of lactate while *A. woodii* [P_{bgaL}_*ldhD*_NFP] only produced 0.40 g L^{-1}. However, even the amount of lactate produced by *A. woodii* [P_{bgaL}_*ldhD*_NFP] would have been sufficient for initial *C. drakei* growth and caproate production, so that a supplementation with lactate is not necessary for future experiments.

5.4.1. Synthetic Co-Culture Proof of Concept

For a subsequent true co-culture experiment, no lactate was supplemented to the cultivation medium. The results are depicted in Figure 5-22. The AiO electrode operated at an average voltage of 4.5 V over the course of the fermentation and generated a maximum H_2 production rate up to 8.0 mmol L^{-1} h^{-1}. The pre-culture of the *A. woodii* [P_{bgaL}_*ldhD*_NFP] strain lasted 37 h and reached an OD_{600} of 2.9. The bioreactor was subsequently inoculated with 50 mL of the pre-culture broth. The fermentation was reproduced (n = 2), the data set of the second fermentation is shown in Figure 11-3 in the appendix. The *A. woodii* [P_{bgaL}_*ldhD*_NFP] strain started growing immediately in the bioreactor, reaching the maximum cell growth rate of 0.07 h^{-1} during the first 13 h. The culture was induced for lactate production at an OD_{600} of 0.07 after 18 h with the addition of 1 mM lactose. Subsequently, the growth rate decreased 7-fold to 0.01 h^{-1}. After 42 h and at an OD_{600} of 0.97, *C. drakei* was added to the bioreactor (V = 95 mL, OD_{600} = 2.0). The AiO electrode was left on despite of the inhibiting effects observed previously (see Figure 5-19). After *C. drakei* addition, the measured cell density kept increasing for 49 h to a maximum value of 1.45. Then, during the final 10 h of the cultivation, the OD_{600} decreased to 1.39. Lactate was produced with a rate of 0.03 g h^{-1} after induction and reached a maximum concentration of 0.52 g L^{-1} at the time point of *C. drakei* addition. Subsequently, lactate was consumed with an uptake rate of 0.02 g h^{-1}. After 89 h of fermentation time, lactate was completely depleted. Caproate concentrations were first detected in the culture medium after 83 h. The maximum caproate production rate added up to 0.01 g h^{-1} and the maximum concentration of 0.1 g L^{-1} was reached after 89 h. Acetate was produced at a constant rate of 0.13 g h^{-1} before the co-culture phase. Afterwards, the rate decreased to 0.06 g h^{-1} and the maximum acetate concentration added up to 6.3 g L^{-1} at the end of the fermentation. The *A. woodii* [P_{bgaL}_*ldhD*_NFP] strain produced formate in two phases: during the first 10 h, 0.48 g L^{-1} were produced which were consumed completely in the subsequent 10 h. Then, after 35 h, the *A. woodii* [P_{bgaL}_*ldhD*_NFP] strain started accumulating formate again, reaching a maximum concentration of 0.67 g L^{-1} after 63 h of fermentation time. Butyrate was produced by *C. drakei* during the co-culture phase at low levels, reaching a maximum concentration of 0.55 g L^{-1} at the end of the fermentation. After the initial ORP reduction from -235 mV to -362 mV, the ORP remained constant at -362 ± 23 mV throughout the fermentation. The pH value showed a peak to 7.1 after 11 h of fermentation time but remained constant at 6.5 ± 0.1 in the subsequent course of the cultivation. The total CO_2 and H_2 uptake were 259.2 mmol and 531.5 mmol, respectively. Carbon balances were closed within an estimation error of 5 % and a selection of important process performance parameters are listed in Table 5-3.

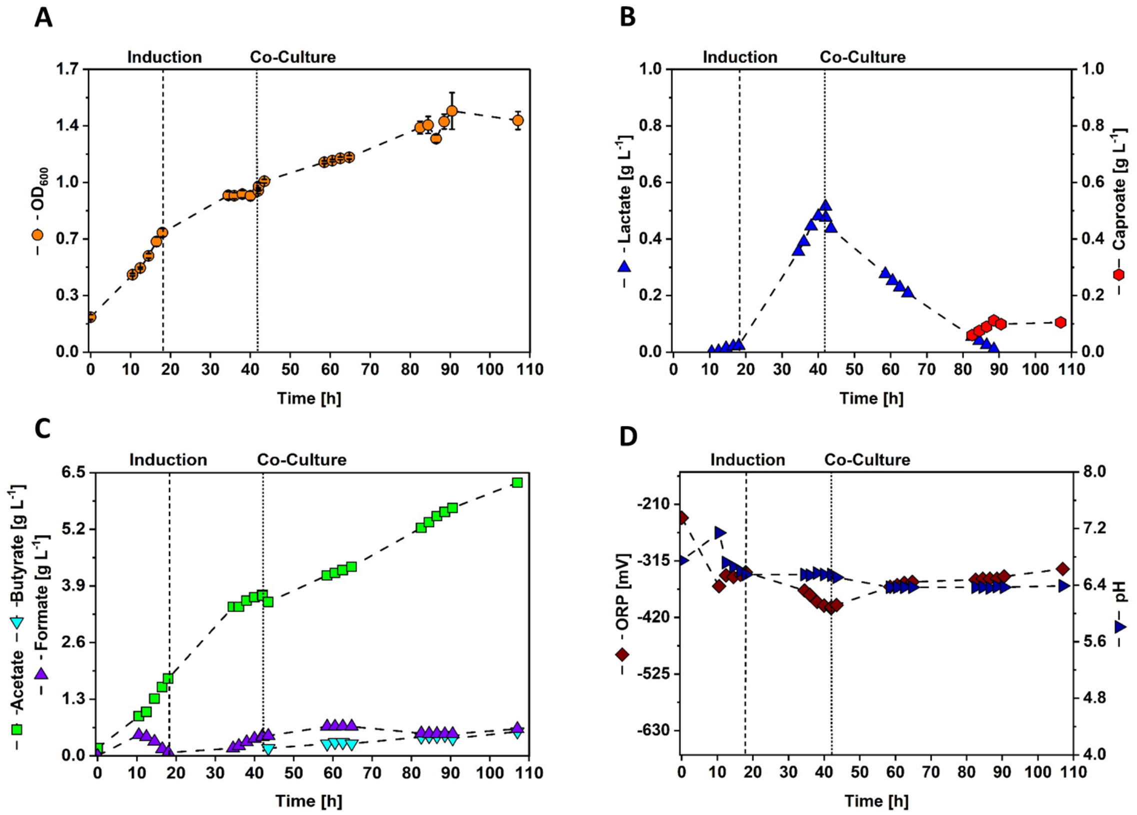

Figure 5-22: Synthetic co-culture in a stirred-tank batch fermentation of *A. woodii* [P*bgaL*_*ldhD*_NFP] and *C. drakei*. (A) optical cell density (orange circles, OD_{600}); (B) concentration of lactate (blue triangles) and caproate (red hexagons, g L^{-1}); (C) concentration of acetate (green squares), formate (purple triangles) and butyrate (cyan triangles, g L^{-1}); (D) ORP (brown diamonds, mV) and pH (blue triangles) measured during the cultivation. The dashed vertical line indicates the time point of induction with 1mM lactose. The dotted vertical line indicates the time point of *C. drakei* and lactate addition. Parameters: $T = 30$ °C; pH = 7.0; $P\ V^{-1} = 2.4$ W L^{-1}; $V_{CO_2} = 0.01$ vvm; $I_{AiO} = 600$ mA; $U_{av} = 4.5$ V; $V_0 = 1.4$ L.

The proof of concept of the synthetic co-cultivation with *A. woodii* [P*bgaL*_*ldhD*_NFP] and *C. drakei* for the production of caproate from CO_2 and H_2 was successful with the fermentation shown in Figure 5-22. It was proven, that no lactate supplementation was necessary to support growth of *C. drakei* in the co-culture set up. Furthermore, no negative effects of the AiO electrode or the low inoculation OD_{600} as discussed in Chapter 5.3.3 were observed and the caproate yield from lactate was 1.4-fold higher than in the *C. drakei* fermentation with adapted pre-culture (see Figure 5-18). This could suggest that the co-existence with *A. woodii* is beneficial for *C. drakei*, as previous publications have stated for caproic acid producing organisms (Yan and Dong, 2018). The relationship would fall in the category of commensalism, given that *A. woodii* has no observable positive effect of the co-cultivation with *C. drakei* (Ma et al., 2019). As aforementioned (refer to Figure 5-21), the data strongly suggests that *C. drakei* adapted quickly to the co-culture environment and grew in the bioreactor. Butyrate and caproate concentrations increased during the co-cultivation phase 1.6 and 1.4-fold, respectively, in comparison to the co-culture with supplemented lactate. Furthermore, lactate was consumed at the same rate as in the previous co-cultivation and cell density even increased 1.5-fold. However, lactate consumption rates were 15-fold lower than the maximum uptake rate observed in the pure *C. drakei* culture with adapted pre-culture. As seen in Figure 5-18, the lactate consumption rate increases exponentially, which suggests that lactate consumption of *C. drakei* in the co-cultivation could increase if higher autotrophic produced lactate concentrations were present in the culture medium and if fermentation times were increased. The 6-fold lower caproate formation rate in this co-cultivation compared to the pure cultures shows furthermore, that the potential for higher caproate productions in the co-culture is not yet exhausted. The overall consumed lactate does not match the produced caproate if respective carbon would be balanced. However, the simultaneous production and consumption of lactate is most likely responsible for the respective deviation. Differentiation of cells during the co-culture phase is therefore important for future co culture fermentations, to understand to what extend both bacteria contributed to the increasing cell density. As recently published by Mook et al., 2022, the expression of the D-Lactate dehydrogenase fused to an oxygen-independent fluorescence-fusion and absorption-shifting tag (FAST) could be used to analyze gene expression during the fermentation and thus give insides in cell viability and cell growth of *A. woodii* [P_{bgaL}_*ldhD*_NFP].

Table 5-3: Important process performance parameters of the synthetic co-culture batch processes with *A. woodii* [P_{bgaL}_*ldhD*_NFP] and *C. drakei* discussed in this chapter.

	Cell Growth		**Main Product**				**Byproducts**		
Lactate added	OD_{max}	μ_{max}	c_{Cap}	q_{Cap}	$Y_{P/S}$	P_{vol}	c_{Lac}	$-q_{Lac}$	c_{Ac}
[g L^{-1}]	[-]	[h^{-1}]	[g L^{-1}]	[g h^{-1}]	[g g^{-1}]	[g L^{-1} d^{-1}]	[g L^{-1}]	[g h^{-1}]	[g L^{-1}]
2.17	1.09	0.11	0.08	0.00	0.10	0.02	0.39	0.02	4.03
-	1.45	0.07	0.11	0.01	0.21	0.03	0.52	0.02	6.28

5.5. Lactate Dependent Process Control

As mentioned in Chapter 5.2.4, conventional gas fermentations use only about 2 % of the H_2 introduced into the bioreactor during the cultivation. Although the fermentations with the AiO electrode can use up to 60 %, a large part is still unused. For an efficient utilization, H_2 generation was coupled to lactate concentration measured in the medium as described in Chapter 4.5. In an ideal controlled co-cultivation process (e.g., Figure 5-22), the lactate dependent control would switch off the AiO and thus H_2 generation when sufficient lactate was produced by *A. woodii* [P_{bgaL}_*ldhD*_NFP] for consumption by *C. drakei*. Through the constant uptake of lactate, the lactate dependent control would turn on the AiO electrode again once a critical lactate threshold is reached. With this control the lactate production rate of *A. woodii* [P_{bgaL}_*ldhD*_NFP] and the lactate consumption rate of *C. drakei* could theoretically be matched, and therefore energy consumption minimized. For this to be realized, it was first necessary to investigate, if the lactate metabolism of *A. woodii* [P_{bgaL}_*ldhD*_NFP] can be turned on again after *A. woodii* [P_{bgaL}_*ldhD*_NFP] was once depleted of H_2. Therefore, a fermentation experiment was conducted, where the AiO electrode was manually turned off for an interval of 6 h, once a specific lactate concentration was reached in the cultivation medium. This experiment was compared to a reference fermentation of *A. woodii* [P_{bgaL}_*ldhD*_NFP], where the AiO kept functioning throughout the experiment. For both processes, the stirrer rate was set to 800 rpm and the AiO to 600 mA. The average voltage of the AiO electrode added up to 4.2 V. The cell density of the pre-culture for both fermentations added up to 2.5 ± 0.3 after 31 h and both cultivations were inoculated with the respective volume of pre-culture broth to reach a starting OD_{600} of 0.15. The results of the cultivations are depicted in Figure 5-23. Both *A. woodii* [P_{bgaL}_*ldhD*_NFP] strains started growing with a maximum growth rate of 0.07 h^{-1} during the initial 20 h. The cultivation where the AiO electrode was manually controlled was induced with 1 mM lactose after 15 h at an OD_{600} of 0.5, while the reference fermentation was induced at an OD_{600} of 0.6 after 20 h. Subsequently, the growth rate of the *A. woodii* [P_{bgaL}_*ldhD*_NFP] strain in the cultivation with AiO control decreased and the strain entered its stationary phase at a cell density of 0.62. For the following 40 h, the OD_{600} was constant at 0.64 ± 0.02. The growth rate of the reference fermentation did not decrease until 25 h of fermentation time and reached its stationary phase at 0.85 ± 0.02 after 39 h. After induction, both *A. woodii* [P_{bgaL}_*ldhD*_NFP] strain started producing lactate. While the maximum lactate formation rate for the strain in the controlled fermentation reached 0.02 g h^{-1}, the strain in the reference fermentation reached a production rate of 0.05 g h^{-1}. The AiO electrode was turned off as the lactate concentration in the controlled cultivation had reached 0.1 g L^{-1}. During the phase without active AiO electrode, the lactate concentration stayed constant at 0.11 ± 0.01 g L^{-1}. During the 8 h after the AiO was turned on again, the lactate concentration increased to 0.24 g L^{-1} and the final maximum value added up to 0.28 h L^{-1}. The *A. woodii* [P_{bgaL}_*ldhD*_NFP] strain in the reference cultivation continued to produce lactate, reaching a maximum value of 0.7 g L^{-1} at the end of the fermentation. While acetate was also produced constantly in the reference cultivation up to a final value of 6.8 g L^{-1}, the acetate production in the manually controlled fermentation stopped after the AiO electrode was turned off at 2.2 g L^{-1} and continued with a decreased production rate after AiO activation to a final value of 3.3 g L^{-1}. Formate was produced in low concentrations in the controlled cultivation to 0.4 g L^{-1} at the time point of AiO electrode deactivation. Then, the *A. woodii* [P_{bgaL}_*ldhD*_NFP] strain consumed all formate in the medium before producing with a higher rate again, to a final value of 1.2 g L^{-1}. The strain in the reference fermentation did not accumulate formate until 40 h, producing a total of 1.7 g L^{-1} until the end of the fermentation. pH values were constant in both cultivations at 6.5 ± 0.1 and 6.8 ± 0.1, respectively. The ORP values in both fermentations decreased during the first 15 h to -514 mV. In the controlled cultivations, the ORP increased temporarily to -354 ± 17 mV while the AiO electrode was switched off, before decreasing again after its activation. The ORP in the reference cultivation stayed at low levels of -502 ± 40 mV during the rest of the fermentation. A selection of important process parameters is listed in Table 5-4.

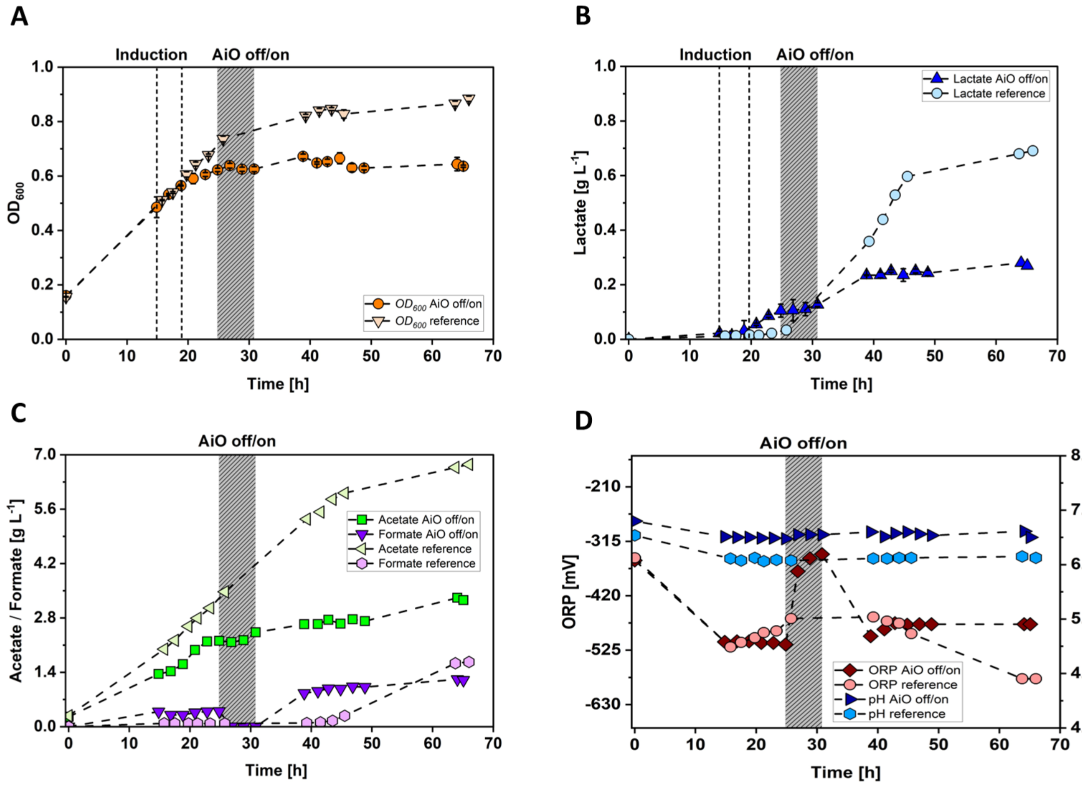

Figure 5-23: Manually controlled autotrophic stirred-tank batch BES fermentation of *A. woodii* [P$_{bgaL}$_*ldhD*_NFP]. The darker colors represent the fermentation where the AiO electrode was turned off for 6 h, the lighter colors represent the reference fermentation with constant operating AiO electrode. (A) optical cell density (orange circles and triangles, OD_{600}); (B) concentration of lactate (blue triangles and circles, g L^{-1}); (C) concentration of acetate (green squares and triangles) and formate (purple triangles and hexagons, g L^{-1}); (D) ORP (brown diamonds and pink circles, mV) and pH (blue triangles and hexagons) measured during the cultivation. The vertical dashed lines indicate the time point of induction with 1 mM lactose. The grey shaded bar represents the time interval during which the AiO electrode was turned off. Parameters: T = 30 °C; pH = 7.0; $P\,V^{-1}$ = 2.3 W L^{-1}; V_{CO_2} = 0.01 vvm; V_0 = 1.4 L; I_{AiO} = 600 mA; U_{av} = 4.2 V.

The manually controlled fermentation process depicted in Figure 5-23 showed, that the lactate metabolism of *A. woodii* [P$_{bgaL}$_*ldhD*_NFP] is controllable. The lactate concentration stayed constant during the interval where the AiO electrode was inactive and increased afterwards 2.5-fold. This was effect was also observed in the heterotrophic fermentation depicted in Figure 5-9, where lactate production was reinitiated on CO_2 and H_2 after fructose had been depleted. However, the depletion of H_2 for 6 h had negative effects on growth and production of *A. woodii* [P$_{bgaL}$_*ldhD*_NFP], given that total cell density was decreased 1.3-fold, total acetate concentration was decreased 1.4-fold and total lactate concentration even 2.5-fold. Interesting was the observation, that *A. woodii* [P_{bgaL}_*ldhD*_NFP] consumed all formate in the medium during the interval of H_2 depletion to sustain its metabolic activities. Afterwards, formate production even increased. From a biological point of view, the lactate dependent process control is possible, however AiO electrode down times should be kept small to prevent critical effects on growth and product formation.

A consecutive experiment was conducted to evaluate the function of the lactate dependent process control for feasibility during a cultivation of *A. woodii* [P_{bgaL}_*ldhD*_NFP] in a stirred-tank bioreactor. For this purpose, the lactate threshold of the control was set to 0.4 g L^{-1} and a fermentation at standard operating conditions was performed with active lactate control. The results of this cultivation are shown in Figure 5-24. The stirrer rate was set to 800 rpm and the I_{AiO} to 600 mA. The average voltage of the AiO electrode added up to 3.7 V over the course of the fermentation. After 31 h of pre-culture fermentation, 122 mL of pre-culture broth with an OD_{600} of 1.7 were transferred to the bioreactor for inoculation. Cells started growing with the maximum achieved growth rate of 0.07 h^{-1} and at an OD_{600} of 0.4, the culture was induced with 1 mM lactose for lactate production. The culture kept growing with a reduced growth rate and 8 h after induction, the *A. woodii* [P_{bgaL}_*ldhD*_NFP] strain entered stationary phase, staying constant at an average cell density of 0.49 ± 0.03 for the rest of the process. After induction, the *A. woodii* [P_{bgaL}_*ldhD*_NFP] cultivation started producing lactate reaching a maximum formation rate of 0.03 g h^{-1}. The data from the online lactate measurement system was in line with the data obtained via HPLC measurement. As the online measurement detected a concentration of 0.4 g L^{-1} after 41 h, the lactate control turned the AiO off. Subsequently, the lactate concentration stayed constant at 0.4 g L^{-1} and the process was terminated. The acetate production rate increased after induction and total acetate concentrations added up to a final value of 2.3 g L^{-1}. Formate increased up to the point of induction to a concentration of 0.4 g L^{-1}. Subsequently, *A. woodii* [P_{bgaL}_*ldhD*_NFP] consumed 0.2 g L^{-1} of formate over the following 6 h before continuing its production. Final formate concentrations added up to 0.8 g L^{-1}. The ORP decreased over the course of the fermentation, ending at a minimum value of -425 mV. Cell voltage of the AiO electrode showed a typical peak at the beginning of the process, reaching up to 13 V. After decreasing and showing a second, smaller peak up to 7 V, the voltage settled at an average value of 3.7 V until the AiO was turned off by the lactate control. A selection of the most important process performance parameters is listed in Table 5-4.

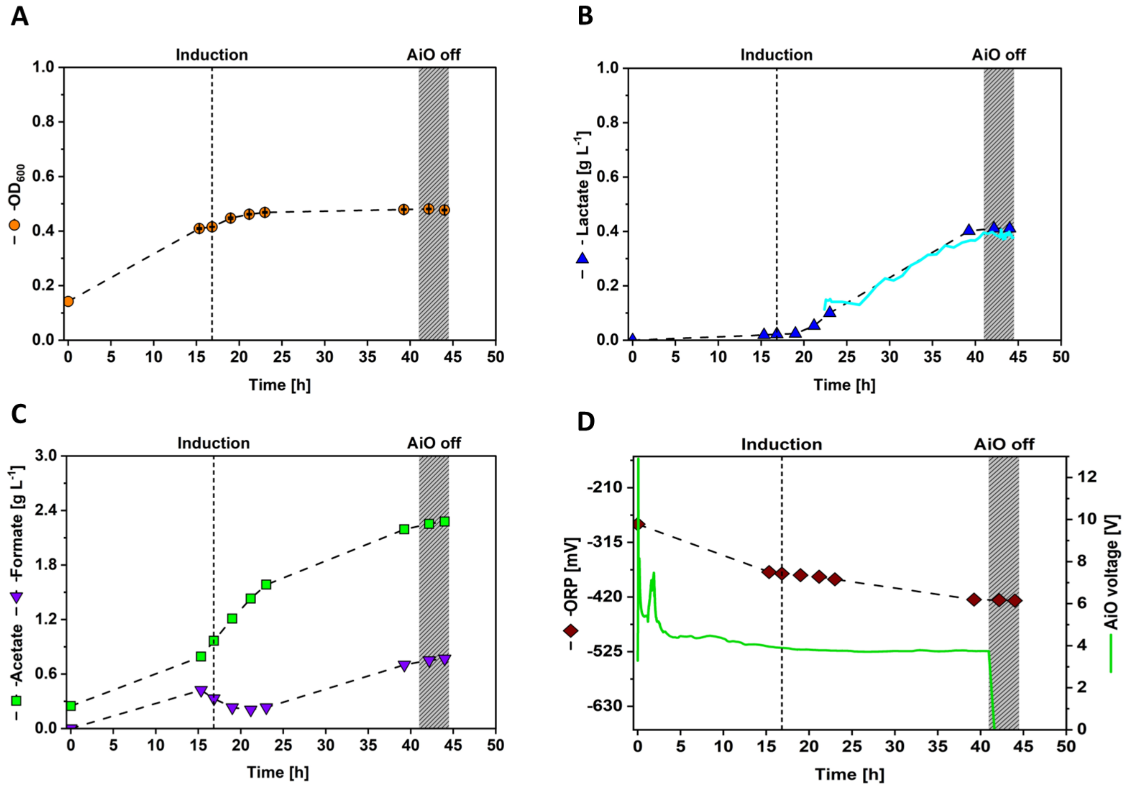

Figure 5-24: Automatically controlled autotrophic stirred-tank batch BES fermentation of *A. woodii* [P$_{bgaL}$_*ldhD*_NFP]. (A) optical cell density (orange circles, OD_{600}); (B) concentration of lactate measured via HPLC (blue triangles) and measured with the TRACE C2 (cyan line, g L^{-1}); (C) concentration of acetate (green squares) and formate (purple triangles, g L^{-1}); (D) ORP (brown diamonds, mV) and AiO voltage (green line, V) measured during the cultivation. The vertical dashed line indicates the time point of induction with 1 mM lactose. The grey shaded bar represents the time interval during which the AiO electrode was turned off automatically. Parameters: $T = 30$ °C; pH = 7.0; $P\ V^{-1} = 2.3$ W L^{-1}; $V_{CO_2} = 0.01$ vvm; $V_0 = 1.4$ L; $I_{AiO} = 600$ mA; $U_{av} = 3.7$ V; $c_{Lac,Threshold} = 0.4$ g L^{-1}.

For the final proof of concept of the lactate dependent process control, a co-cultivation of *A. woodii* [P$_{bgaL}$_*ldhD*_NFP] and *C. drakei* was conducted. The process parameters were the same as in the co-cultivation shown in Figure 5-22. The lactate threshold was set to 0.35 g L^{-1} and the addition of *C. drakei* was timed to happen 1.5 h after the control had switched off the electrode. Average cell voltages of the AiO electrode added up to 3.8 V over the course of the fermentation. The bioreactor was inoculated with 100 mL of pre-culture broth of *A. woodii* [P$_{bgaL}$_*ldhD*_NFP], with an OD_{600} of 1.2. The results of the cultivation are shown in Figure 5-25. The *A. woodii* [P$_{bgaL}$_*ldhD*_NFP] strain showed an unusual long lag phase of about 7 h before starting to grow.

The maximum growth rate of 0.1 h^{-1} was achieved after 18 h. At an OD_{600} of 0.5, the culture was induced with 1 mM lactose for lactate production and the lactate process control was activated. Afterwards, the cell growth rate declined 5-fold to 0.02 h^{-1}. At a cell density of 0.65, *C. drakei* was added to the bioreactor. Subsequently, the cell density kept increasing until reaching a final value of 1.0 after 88 h. Shortly after induction, the *A. woodii* [P_{bgaL}_*ldhD*_NFP] strain started producing lactate. At low concentrations, the online lactate measurement system did not show correct values, as seen in Figure 5-25 B. The system was therefore recalibrated after 38 h. The maximum lactate production rate added up to 0.03 g h^{-1}, and at 42.5 h, the online measurement detected values above the threshold and turned the AiO electrode off. At the time of inoculation, the pre-culture of *C. drakei* had an OD_{600} of 0.8 and not all lactate was yet consumed. For this reason, the lactate concentration increased in 0.06 g L^{-1} at the starting point of the co-culture phase. Unfortunately, 1.5 h after *C. drakei* addition, the online lactate measurement system showed strong fluctuations in the measured values. Given that these false values were below the set threshold, the AiO electrode was turned on again after 45.5 h of fermentation time. Subsequently, lactate was consumed by *C. drakei* with a consumption rate of 0.02 g h^{-1}. After 86 h of fermentation time, lactate was depleted in the medium. Caproate concentrations were first detected at 63 h at 0.05 g L^{-1}. Subsequently, *C. drakei* produced caproate at a rate of 0.01 g h^{-1}, reaching a final value of 0.08 g L^{-1} at the end of the process. Acetate concentrations increased once the *A. woodii* [P_{bgaL}_*ldhD*_NFP] strain had entered the exponential growth phase and kept increasing with similar rates after the addition of *C. drakei*. Final acetate concentrations added up to 7.3 g L^{-1}. Formate concentrations showed a first peak after 16 h at 0.4 g L^{-1} and after decreasing, a second concentration peak at 0.5 g L^{-1} just before the AiO electrode was turned off. Then, *A. woodii* [P_{bgaL}_*ldhD*_NFP] consumed all formate in the fermentation medium. During the co-culture phase, formate concentrations increased to 0.7 after 70 h and decreased again subsequently. Butyrate was produced by *C. drakei* during the co-culture phase at low concentrations, reaching a maximum value of 0.6 g L^{-1} at the end of the process. The ORP decreased after the start of the fermentation to -476 mV after 20 h and decreased again to -544 mV after 43 h. Then, the AiO electrode was turned off and the ORP increased to -427 mV. During the co-cultivation, the ORP decreased at first to -512 mV after 63 h before increasing constantly until the end of the fermentation to -371 mV. The current of the AiO was maintained constant at 600 mA throughout the fermentation until it was turned off by the lactate control. During the co-culture phase at about 60 h and 65 h, gas started accumulating inside the CE channel, causing the cell voltage to increase and the current was not able to be maintained at its set point. Refilling the CE channel with culture medium resolved the issue. See Table 5-4 for a list of relevant process performance parameters.

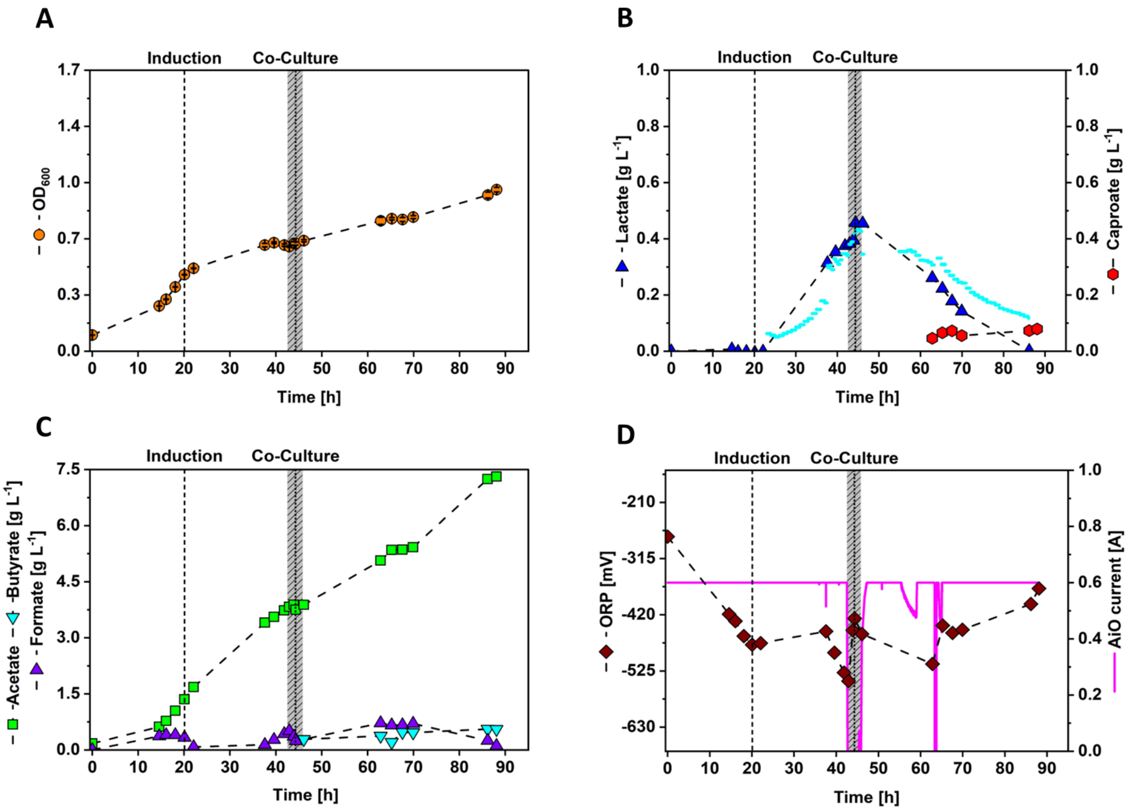

Figure 5-25: Automatically controlled synthetic co-culture of *A. woodii* [P_{bgaL}_*ldhD*_NFP] and *C. drakei* in a stirred-tank batch BES fermentation. (A) optical cell density (orange circles, OD_{600}); (B) concentration of lactate measured via HPLC (blue triangles) and measured with the TRACE C2 (cyan line, g L^{-1}); (C) concentration of acetate (green squares), formate (purple triangles) and butyrate (cyan triangles, g L^{-1}); (D) ORP (brown diamonds, mV) and AiO current (magenta line, A) measured during the cultivation. The vertical dashed line indicates the time point of induction with 1 mM lactose. The dotted lines represent the time point of *C. drakei* addition. The grey shaded bar represents the time interval during which the AiO electrode was turned off. Parameters: $T = 30$ °C; pH = 7.0; $P\ V^{-1} = 2.3$ W L^{-1}; $V_{CO_2} = 0.01$ vvm; $V_0 = 1.4$ L; $I_{AiO} = 600$ mA; $U_{av} = 3.8$ V; $c_{Lac,Threshold} = 0.35$ g L^{-1}.

The lactate dependent process control as demonstrated in the fermentations shown in Figure 5-24 and Figure 5-25 was implemented successfully and prove to be feasible. If the online measurement system communicates correct values, it can control the process exactly to a desired lactate concentration (see Figure 5-24 B). Unfortunately, incorrect measured values can cause an early shut down or reactivation of the AiO electrode (see Figure 5-25 B). However, the early reactivation of the AiO electrode had no negative influence on the process itself and dynamic reaction of the control system was proven despite that. The co-cultivation shown in Figure 5-25 furthermore demonstrated, that short down times of the AiO electrode have no negative effects on process performance as observed in the manually controlled fermentation shown in Figure 5-23. In comparison to the co-cultivations discussed in Chapter 5.4, caproate production and lactate consumption rates were the same (0.01 g h^{-1} and 0.02 g h^{-1} respectively), suggesting that *C. drakei* was as active as in the previous reported co-cultivation. Given that, acetate and cell density both increased during the co-culture phase, also suggests that the *A. woodii* [P_{bgaL}_*ldhD*_NFP] strain was still active. In this chapter we discussed the implementation of the lactate process control to ideally match lactate production rate to the maximum lactate consumption rate of *C. drakei* in a co-culture process. Comparing the maximum lactate production rate of *A. woodii* [P_{bgaL}_*ldhD*_NFP] determined at 0.05 g h^{-1} (see Figure 5-23 B, reference fermentation) with the maximum lactate consumption rate of *C. drakei* of 0.42 g h^{-1} (see Figure 5-20 B), it seems, that controlling lactate production is not necessary given that *C. drakei* could consume lactate faster than *A. woodii* [P_{bgaL}_*ldhD*_NFP] produces. However, the maximum lactate consumption rate of *C. drakei* is reached only in the last third of the fermentation, while during the initial 15 h of the process, the lactate uptake rate was 4.2-fold lower. Furthermore, as already discussed in Chapter 5.4, lactate uptake rates of *C. drakei* have reached a maximum of only 0.02 g h^{-1} in a co-cultivation (see Table 5-4). The data of co-cultivations presented in this study suggests, that at least during the first 45 h of a co-cultivation of *C. drakei* and *A. woodii* [P_{bgaL}_*ldhD*_NFP], the lactate process control could reduce the amount of H_2 being produced via electrolysis without limiting the availability of lactate for *C. drakei*. Moreover, if conducting a co-cultivation in a conventional gas fermentation as presented in Chapter 5.2.4 (see Figure 5-10) the maximum possible lactate production rate of *A. woodii* [P_{bgaL}_*ldhD*_NFP] reaches up to 0.21 g h^{-1}. As the amount of unused H_2 in these conventional gas fermentations is even greater than in the BES set up, such processes would benefit even more from the lactate process control presented in this study.

Table 5-4: Important process performance parameters of all batch processes with lactate dependent process control discussed in this chapter.

Cultivation	**Control**	OD_{max}	μ_{max}	c_{Lac}	q_{Lac}	$-q_{Lac}$	c_{Cap}	q_{Cap}	$Y_{P/S}$	c_{Ac}	c_{Form}
[-]	[-]	[-]	[h^{-1}]	[$g\,L^{-1}$]	[$g\,h^{-1}$]	[$g\,h^{-1}$]	[$g\,L^{-1}$]	[$g\,h^{-1}$]	[$g\,g^{-1}$]	[$g\,L^{-1}$]	[$g\,L^{-1}$]
Pure	-	0.88	0.07	0.69	0.05	-	-	-	0.11	6.75	1.67
Pure	Manual	0.67	0.07	0.28	0.02	-	-	-	0.05	3.26	1.20
Pure	Auto	0.54	0.07	0.41	0.03	-	-	-	0.09	2.28	0.77
Co-Culture	Auto	0.98	0.10	0.39	0.03	0.02	0.08	0.01	0.19	7.31	0.72

6 Conclusion

The goal of this study was to establish a synthetic co-culture of *A. woodii* and *C. drakei* for the production of caproic acid from CO_2 and H_2. The H_2 for this process was generated *in situ* from the AiO electrode. For the development of this process, it was necessary to investigate cell growth and product formation in a stirred-tank bioreactor of both bacterial strains separately, to reach a deeper understanding of the metabolic processes and to adjust technical parameters if necessary to optimize cell growth and product formation. Furthermore, an automatic process control system was developed to adjust the H_2 generation rate of the AiO electrode based on the concentration of the intermediate lactate in the cultivation medium.

A major part of this study was to establish and optimize the cultivation of *A. woodii* in the BES. Although the cultivation of *A. woodii* on H_2 and CO_2 has been subject of extensive research over the past decades, and the AiO electrode has been used for a variety of assisted electro-fermentations, an *A. woodii* cultivation on H_2 generated via *in situ* electrolysis has not been published before. First, a comparison of different *A. woodii* strains was performed to choose the most suitable candidate for the co-cultivation. The recombinant strains *A. woodii* [P_{bgaL}_*ldhD*_NFP] and *A. woodii* P_{tet}_*ldhD*$_{\mathrm{CI}}$ were furthermore compared to the *A. woodii* WT strain. In autotrophic BES fermentations, the *A. woodii* [P_{bgaL}_*ldhD*_NFP] strain outperformed the *A. woodii* P_{tet}_*ldhD*$_{\mathrm{CI}}$ strain, reaching a 1.5-fold higher volumetric productivity and a 2.0-fold higher maximum lactate production. This showed that the *A. woodii* [P_{bgaL}_*ldhD*_NFP] strain developed by Mook et al. (2022) proved to be more suitable for application in the BES. The major drawback of the *A. woodii* P_{tet}_*ldhD*$_{\mathrm{CI}}$ strain was assumed to be the inoculation agent anhydrotetracycline, which has a reported low toxic effect on microorganisms.

All BES fermentations with *A. woodii* showed a reduced performance in comparison to literature and to the conventional gas fermentations conducted with the *A. woodii* [P_{bgaL}_*ldhD*_NFP] strain. The data shown in this study strongly suggest H_2 limitation as reason for the underperformance. While the *A. woodii* [P_{bgaL}_*ldhD*_NFP] strain cultivated in the conventional gas fermentation accumulated a 16-fold higher lactate concentration with a 12-fold higher volumetric productivity than the same strain cultivated in the BES, the gas fermentation also showed a 137-fold higher H_2 gassing rate. Regarding the data from the conventional gas fermentations, a reduction of H_2 gassing rate from 971 mmol L^{-1} h^{-1} to 60 mmol L^{-1} h^{-1} caused already a reduction of total lactate concentration of 2.3-fold, suggesting the sensitivity of *A. woodii* towards lower H_2 availability. Another indicator for a H_2 and thus energy limitation in the BES cultivations is the observed accumulation of formate. The BES fermentations reported here show a 7.5-fold increased formate to lactate concentration ratio in comparison to the conventional gas fermentations. For *A. woodii* to metabolize formate, it needs to be first converted to formyl-THF, a step which is dependent on ATP. The shortage of energy and thus ATP may cause the metabolism to stop at formate, thus causing accumulation.

The increase in H_2 by the AiO electrode could in theory be possible by increasing WE surface areas, to increase possible currents and thus H_2 production while maintaining the current density at 8 mA cm^{-2}. Most BES use even lower current densities and higher current densities are considered not to be feasible. To match the H_2 production rate of the gas fermentation with 60 mmol L^{-1} h^{-1}, the WE surface area would have to be increased by a factor of 8. Given that some BES reach specific cathode area to liquid volumes of 810 m² m^{-3}, while the BES used in this study only accounts for 5.3 m² m^{-3}, this is regarded as technically feasible. However, the observed growth inhibiting effect of high cell voltages in this study have to be considered for a new electrode design. The designs with a higher cathode surface area presented in this study showed high operating voltages and showed not to be feasible for cell growth.

Further BES fermentations with *A. woodii* [P$_{bgaL}$_*ldhD*_NFP] showed that a higher induction cell density results in higher lactate concentrations and volumetric productivities. Presumably, this is due to the forced redirecting of redox energies towards lactate.

This study was the first to characterize *C. drakei* growing in a bioreactor on lactate as substrate. Maximum caproate yields from lactate of 0.16 g g^{-1} fall in line with comparable processes with other *Clostridia*, however caproate concentrations are too low at the moment considering a possible industrial application. Yet, the maximum caproate concentration of 1.5 g L^{-1} was also identified as the inhibition concentration of caproic acid for *C. drakei*. This suggests the reason for the comparable low caproic acid concentrations is growth inhibition due to the product itself. The initial observation of cell growth in the bioreactor in two phases was assumed to be due to the yeast extract in the cultivation medium. However, various pre-culture cycles with an increasing lactate concentration led to an adaptation of *C. drakei* and to constant cell growth in the bioreactor. In preparation for co-culture experiments, inhibiting effects of low inoculation cell density and electrical voltages applied from the beginning of cell growth were observed. The voltages however did not affect the cells once they had started to grow.

Synthetic co-cultures of *A. woodii* [P$_{bgaL}$_*ldhD*_NFP] and *C. drakei* were established and proved to be feasible. The available data showing caproate production and lactate consumption strongly suggest that *C. drakei* adapted well to the proximity of *A. woodii*. Given that no negative effects of voltages from the AiO electrode or the low inoculation OD_{600} as observed in the pure cultures were noticed, it is suggested that the co-existence with *A. woodii* was even beneficial for

C. drakei. However, caproate yield from lactate and lactate consumption rates were significantly lower than in the pure cultivations of *C. drakei*, due to the overall low lactate concentrations supplied by *A. woodii*.

The lactate dependent process control was successfully implemented and proved to be feasible. It was shown, that the lactate metabolism of *A. woodii* [P_{bgaL}_*ldhD*_NFP] was controllable, given that the *A. woodii* [P_{bgaL}_*ldhD*_NFP] strain produced lactate again after being deprived of H_2 for 6 h. However, it was also shown, that longer AiO deactivation times could cause negative effects on cell growth and product formation. The lactate control was able to react in a dynamic way during a co-cultivation of *A. woodii* [P_{bgaL}_*ldhD*_NFP] and *C. drakei* and showed that it has the potential to adjust the lactate production rate to the maximum lactate consumption rate of *C. drakei* in a co-culture process. Although the comparison of the maximum lactate production rate of *A. woodii* [P_{bgaL}_*ldhD*_NFP] in a BES with the maximum lactate consumption rate of *C. drakei* determined in pure cultures could question the necessity of such a control system, these maximum lactate consumption rates were never met during the co-cultivation. Thus, the lactate dependent process control has the potential to reduce the amount of H_2 being produced via electrolysis without limiting the availability of lactate for *C. drakei* in this fermentation set up.

7 Outlook

The co-cultivation of *A. woodii* and *C. drakei* for the production of caproic acid from CO_2 and H_2 in a BES was successful but also demonstrated optimization potential. Especially the H_2 limitation of the BES as primary bottleneck for caproate production should be approached with priority, given that the *A. woodii* [P_{bgaL}_*ldhD*_NFP] strain showed a high potential for lactate production if supplied with sufficient H_2. Increasing cathode surface areas for the application of higher electrical currents at constant current densities could be an option, however only if considering the reduction of Faradaic losses in the new design to prevent growth inhibiting voltage levels. This could be done by screening new separator materials to reduce the cathodic O_2 reduction or by decreasing the distance between the anode and cathode even further. Another option could be using external commercial electrolyzers for H_2 supply. This would remove the current advantage of enhanced mass transfer through the fine bubbles generated by the AiO electrode, however the higher H_2 input would probably compensate this loss. Higher lactate production of the *A woodii* [P_{bgaL}_*ldhD*_NFP] strain could also be accomplished via strain engineering by redirecting metabolic routes towards lactate instead of acetate, which is still the main product for the current *A. woodii* strain. Implementing a cell differentiation technique via fluorescence tagging (e.g., FISH or FAST) would be key in gaining a deeper insight of the processes happening during the co-cultivation. Such a technique could clarify to what extend both bacteria contributed to the observed increasing cell density and give insides in cell viability and cell growth. It could possibly even help to understand if the *A woodii* [P_{bgaL}_*ldhD*_NFP] strain keeps producing lactate while *C. drakei* is consuming it. Once higher lactate concentrations are reached with *A. woodii* [P_{bgaL}_*ldhD*_NFP], longer fermentation times should be applied during the co-cultivation phase, to possibly reach the higher caproate production rates as observed in the *C. drakei* pure cultures. Furthermore, when higher caproate concentrations can be produced, an *in situ* product removal technique for caproate such as pertraction should be implemented, to prevent inhibitory concentrations in the cultivation medium and potentially increase caproate concentrations even further.

8 References

Abrini, J., Naveau, H., and Nyns, E.-J. (1994). *Clostridium autoethanogenum*, sp. nov., an anaerobic bacterium that produces ethanol from carbon monoxide. *Arch. Microbiol.* 161, 345–351. doi: 10.1007/BF00303591

Abubackar, H. N., Veiga, M. C., and Kennes, C. (2011). Biological conversion of carbon monoxide: rich syngas or waste gases to bioethanol. *Biofuels, Bioprod. Bioref.* 5, 93–114. doi: 10.1002/bbb.256

Agler, M. T., Wrenn, B. A., Zinder, S. H., and Angenent, L. T. (2011). Waste to bioproduct conversion with undefined mixed cultures: the carboxylate platform. *Trends Biotechnol.* 29, 70–78. doi: 10.1016/j.tibtech.2010.11.006

Ahamed, A., and Vermette, P. (2008). Enhanced enzyme production from mixed cultures of *Trichoderma reesei* RUT-C30 and *Aspergillus niger* LMA grown as fed batch in a stirred tank bioreactor. *Biochem. Eng. J.* 42, 41–46. doi: 10.1016/j.bej.2008.05.007

Arbter, P., Sabra, W., Utesch, T., Hong, Y., and Zeng, A.-P. (2021). Metabolomic and kinetic investigations on the electricity-aided production of butanol by *Clostridium pasteurianum* strains. *Eng. Life Sci.* 21, 181–195. doi: 10.1002/elsc.202000035

Arbter, P., Sinha, A., Troesch, J., Utesch, T., and Zeng, A.-P. (2019). Redox governed electro-fermentation improves lipid production by the oleaginous yeast *Rhodosporidium toruloides*. *Bioresour. Technol*. doi: 10.1016/j.biortech.2019.122122.

Arbter, P., Widderich, N., Utesch, T., Hong, Y., and Zeng, A.-P. (2022). Control of redox potential in a novel continuous bioelectrochemical system led to remarkable metabolic and energetic responses of *Clostridium pasteurianum* grown on glycerol. *Microb. Cell Fact.* 21, 178. doi: 10.1186/s12934-022-01902-5

Arrhenius, S. (1896). On the Influence of Carbonic Acid in the Air upon the Temperature on the Ground. *Philos. Mag. J. Sci.* 41, 237–276.

Asimakopoulos, K., Gavala, H. N., and Skiadas, I. V. (2018). Reactor systems for syngas fermentation processes: A review. *Chem. Eng. J.* 348, 732–744. doi: 10.1016/j.cej.2018.05.003

Bache, R., and Pfennig, N. (1981). Selective isolation of *Acetobacterium woodii* on methoxylated aromatic acids and determination of growth yields. *Arch. Microbiol.* 130, 255–261. doi: 10.1007/BF00459530

Bagby, M. O., Johnson, R. W., Daniels, R. W., Contrell, R. R., Sauer, E. T., Keenan, M. J., et al. (2000). “Carboxylic Acids” in *Kirk‐Othmer Encyclopedia of Chemical Technology*, ed. I. John Wiley & Sons (Wiley). doi: 10.1002/0471238961

Bagotsky, V. S. (2006). *Fundamentals of electrochemistry*. Hoboken N.J. Wiley-Interscience. ISBN: 978-0-471-70058-6

Balch, W. E., Schoberth, S., Tanner, R. S., and Wolfe, R. S. (1977). *Acetobacterium*, a New Genus of Hydrogen-Oxidizing, Carbon Dioxide-Reducing, Anaerobic Bacteria. *Int. J. Syst. Bacteriol.* 27, 355–361. doi: 10.1099/00207713-27-4-355

Bard, A. J., ed (2008). *Electrochemical dictionary*. Berlin, Heidelberg: Springer.

Bäumler, M., Schneider, M., Ehrenreich, A., Liebl, W., and Weuster-Botz, D. (2021). Synthetic co-culture of autotrophic Clostridium carboxidivorans and chain elongating *Clostridium kluyveri* monitored by flow cytometry. *Microb. Biotechnol.* 0, 1–15. doi: 10.1111/1751-7915.13941

Beck, M. H. (2020). *Biological conversion of CO_2 into the platform chemicals lactate and 3-hydroxypropionate using recombinant strains of Acetobacterium woodii*. Doctoral dissertation. Faculty of Natural Sciences, University of Ulm. doi: 10.18725/OPARU-28743

Beck, M. H., Flaiz, M., Bengelsdorf, F. R., and Dürre, P. (2020). Induced heterologous expression of the arginine deiminase pathway promotes growth advantages in the strict anaerobe *Acetobacterium woodii. Appl. Microbiol. Biotechnol.* 104, 687–699. doi: 10.1007/s00253-019-10248-9

Bengelsdorf, F. R., and Dürre, P. (2017). Gas fermentation for commodity chemicals and fuels. *Microb. Biotechnol.* 10, 1167–1170. doi: 10.1111/1751-7915.12763

Bertsch, J., and Müller, V. (2015). CO Metabolism in the Acetogen *Acetobacterium woodii*. *Appl. Environ. Microbiol.* 81, 5949–5956. doi: 10.1128/AEM.01772-15

Bo, T., Zhu, X., Zhang, L., Tao, Y., He, X., Li, D., et al. (2014). A new upgraded biogas production process: Coupling microbial electrolysis cell and anaerobic digestion in single-chamber, barrel-shape stainless steel reactor. *Electrochem. Commun.* 45, 67–70. doi: 10.1016/j.elecom.2014.05.026

Boga, H. I., and Brune, A. (2003). Hydrogen-dependent oxygen reduction by homoacetogenic bacteria isolated from termite guts. *Appl. Environ. Microbiol.* 69, 779–786. doi: 10.1128/AEM.69.2.779-786.2003

Braun, K., and Gottschalk, G. (1981). Effect of molecular hydrogen and carbon dioxide on chemo-organotrophic growth of *Acetobacterium woodii* and *Clostridium aceticum*. *Arch. Microbiol.* 128, 294–298. doi: 10.1007/BF00422533

Bredwell, Srivastava, and Worden (1999). Reactor Design Issues for Synthesis-Gas Fermentations. *Biotechnol. Prog.* 15, 834–844. doi: 10.1021/bp990108m

Bredwell, M. D., and Worden, R. M. (1998). Mass-transfer properties of microbubbles. 1. Experimental studies. *Biotechnol. Prog.* 14, 31–38. doi: 10.1021/bp970133x

Brown, T. R., and Brown, R. C. (2013). A review of cellulosic biofuel commercial-scale projects in the United States. *Biofuels, Bioprod. Bioref.* 7, 235–245. doi: 10.1002/bbb.1387

Bueno, C., Villegas, M. L., Bertolotti, S. G., Previtali, C. M., Neumann, M. G., and Encinas, M. V. (2002). The Excited-State Interaction of Resazurin and Resorufin with Aminesin Aqueous Solutions. Photophysics and Photochemical Reaction. *Photochem. and Photobiol.* 76, 385–390. doi: 10.1562/0031-8655(2002)0760385TESIOR2.0.CO2

Call, D. F., Merrill, M. D., and Logan, B. E. (2009). High surface area stainless steel brushes as cathodes in microbial electrolysis cells. *Environ. Sci. Technol.* 43, 2179–2183. doi: 10.1021/es803074x

Cao, X., Huang, X., Liang, P., Xiao, K., Zhou, Y., Zhang, X., et al. (2009). A new method for water desalination using microbial desalination cells. *Environ. Sci. Technol.* 43, 7148–7152. doi: 10.1021/es901950j

Cavalcante, W. d. A., Leitão, R. C., Gehring, T. A., Angenent, L. T., and Santaella, S. T. (2017). Anaerobic fermentation for n-caproic acid production: A review. *Process Biochem.* 54, 106–119. doi: 10.1016/j.procbio.2016.12.024

Charney, J. G., Arakawa, A., Baker, J. D., Bolin, B., Dickinson, R. E., Goody, R. M., et al. (1979). *Carbon Dioxide and Climate: A Scientific Assessment: Report of an Ad Hoc Study Group on Carbon Dioxide and Climate*. Woods Hole, Massachusetts. Accessed online 26.03.2023. https://web.archive.org/web/20161221211339/http://www.ecd.bnl.gov/steve/charney_report1979.pdf

Che, S., and Men, Y. (2019). Synthetic microbial consortia for biosynthesis and biodegradation: promises and challenges. *J. Ind. Microbiol. Biotechnol.* 46, 1343–1358. doi: 10.1007/s10295-019-02211-4

Chen, J. L., Steele, T. W. J., and Stuckey, D. C. (2015). Modeling and Application of a Rapid Fluorescence-Based Assay for Biotoxicity in Anaerobic Digestion. *Environ. Sci. Technol.* 49, 13463–13471. doi: 10.1021/acs.est.5b03050

Chen, W.-S., Strik, D. P. B. T. B., Buisman, C. J. N., and Kroeze, C. (2017). Production of Caproic Acid from Mixed Organic Waste: An Environmental Life Cycle Perspective. *Environ. Sci. Technol.* 51, 7159–7168. doi: 10.1021/acs.est.6b06220

Cheng, K. Y., Ho, G., and Cord-Ruwisch, R. (2011). Novel methanogenic rotatable bioelectrochemical system operated with polarity inversion. *Environ. Sci. Technol.* 45, 796–802. doi: 10.1021/es102482j

Chmiel, H., Takors, R., and Weuster-Botz, D. (2018). *Bioprozesstechnik*. Berlin, Heidelberg: Springer Berlin Heidelberg. doi: 0.1007/978-3-662-54042-8

Choi, K., Jeon, B. S., Kim, B.-C., Oh, M.-K., Um, Y., and Sang, B.-I. (2013). *In situ* biphasic extractive fermentation for hexanoic acid production from sucrose by *Megasphaera elsdenii* NCIMB 702410. *Appl. Biochem. Biotechnol.* 171, 1094–1107. doi: 10.1007/s12010-013-0310-3

Choi, O., and Sang, B.-I. (2016). Extracellular electron transfer from cathode to microbes: application for biofuel production. *Biotechnol. Biofuels* 9, 11. doi: 10.1186/s13068-016-0426-0

Cusick, R. D., Bryan, B., Parker, D. S., Merrill, M. D., Mehanna, M., Kiely, P. D., et al. (2011). Performance of a pilot-scale continuous flow microbial electrolysis cell fed winery wastewater. *Appl. Microbiol. Biotechnol.* 89, 2053–2063. doi: 10.1007/s00253-011-3130-9

Dalton, J. (1802). Essay IV. On the expansion of elastic fluids by heat. *Memoirs of the Literary and Philosophical Society of Manchester* 5, 595–602.

Daniell, J., Köpke, M., and Simpson, S. (2012). Commercial Biomass Syngas Fermentation. *Energies* 5, 5372–5417. doi: 10.3390/en5125372

Das, A., Coulter, E. D., Kurtz, D. M., and Ljungdahl, L. G. (2001). Five-gene cluster in *Clostridium thermoaceticum* consisting of two divergent operons encoding rubredoxin oxidoreductase- rubredoxin and rubrerythrin-type A flavoprotein- high-molecular-weight rubredoxin. *J. Bacteriol.* 183, 1560–1567. doi: 10.1128/JB.183.5.1560-1567.2001

Das, A., and Ljungdahl, L. G. (1997). Composition and primary structure of the F1F0 ATP synthase from the obligately anaerobic bacterium *Clostridium thermoaceticum*. *J. Bacteriol.* 179, 3746–3755. doi: 10.1128/jb.179.11.3746-3755.1997

Das, A., Silaghi-Dumitrescu, R., Ljungdahl, L. G., and Kurtz, D. M. (2005). Cytochrome bd oxidase, oxidative stress, and dioxygen tolerance of the strictly anaerobic bacterium *Moorella thermoacetica*. *J. Bacteriol.* 187, 2020–2029. doi: 10.1128/JB.187.6.2020-2029.2005

Demler, M., and Weuster-Botz, D. (2011). Reaction engineering analysis of hydrogenotrophic production of acetic acid by *Acetobacterium woodii*. *Biotechnol. Bioeng.* 108, 470–474. doi: 10.1002/bit.22935

Devarapalli, M., and Atiyeh, H. K. (2015). A review of conversion processes for bioethanol production with a focus on syngas fermentation. *Biofuel Research Journal*, 268–280. doi: 10.18331/BRJ2015.2.3.5

Di Min, Cheng, L., Zhang, F., Huang, X.-N., Li, D.-B., Liu, D.-F., et al. (2017). Enhancing Extracellular Electron Transfer of *Shewanella oneidensis* MR-1 through Coupling Improved Flavin Synthesis and Metal-Reducing Conduit for Pollutant Degradation. *Environ. Sci. Technol.* 51, 5082–5089. doi: 10.1021/acs.est.6b04640

Diekert, G., and Ritter, M. (1982). Nickel Requirement of *Acetobacterium woodii*. *J. Bacteriol.* 151, 1043–1045. doi: 10.1128/jb.151.2.1043-1045.1982

Diender, M., Stams, A. J. M., and Sousa, D. Z. (2016). Production of medium-chain fatty acids and higher alcohols by a synthetic co-culture grown on carbon monoxide or syngas. *Biotechnol. Biofuels* 9. doi: 10.1186/s13068-016-0495-0

Ding, A., Yang, Y., Sun, G., and Wu, D. (2016). Impact of applied voltage on methane generation and microbial activities in an anaerobic microbial electrolysis cell (MEC). *Chem. Eng. J.*283, 260–265. doi: 10.1016/j.cej.2015.07.054

Ditzig, J., Liu H., and Logan, B. E. (2007). Production of hydrogen from domestic wastewater using a bioelectrochemically assisted microbial reactor (BEAMR). *Int. J. Hydrogen Energy* 32, 2296–2304. doi: 10.1016/j.ijhydene.2007.02.035

Doran, P. M. (2013). *Bioprocess engineering principles*. Waltham, MA: Academic Press. ISBN: 0080917704

Drake, H. L. (1995). “Acetogenesis, Acetogenic Bacteria, and the Acetyl-CoA “Wood/Ljungdahl” Pathway: Past and Current Perspectives,” in *Acetogenesis*, ed. H. L. Drake (Boston, MA: Springer US), 3–60. ISBN: 978-1-4613-5716-2

Drake, H. L., Gössner, A. S., and Daniel, S. L. (2008). Old acetogens, new light. *Ann. N. Y. Acad. Sci.* 1125, 100–128. doi: 10.1196/annals.1419.016

Drake, H. L., Küsel, K., and Matthies, C. (2006). “Acetogenic Prokaryotes,” in *The Prokaryotes*, eds. M. Dworkin, S. Falkow, E. Rosenberg, K.-H. Schleifer, and E. Stackebrandt (New York, NY: Springer New York), 354–420. doi: 10.1007/0-387-30742-7_13

Dunn, I. J. (2003). *Biological reaction engineering: Dynamic modelling fundamentals with simulation examples*. Wienheim: VCH. ISBN: 3-527-30759-1

Dürre, P., and Eikmanns, B. J. (2015). C1-carbon sources for chemical and fuel production by microbial gas fermentation. *Curr. Opin. Biotechnol.* 35, 63–72. doi: 10.1016/j.copbio.2015.03.008

Eggerth, A. H. (1935). The Gram-positive Non-spore-bearing Anaerobic *Bacilli* of Human Feces. *J. Bacteriol.* 30, 277–299. doi: 10.1128/jb.30.3.277-299.1935

Faraday, M. (1834). VI. Experimental researches in electricity.-Seventh Series. *Phil. Trans. R. Soc.* 124, 77–122. doi: 10.1098/rstl.1834.0008

Farias, D., and Maugeri Filho, F. (2019). Co-culture strategy for improved 2G bioethanol production using a mixture of sugarcane molasses and bagasse hydrolysate as substrate. *Biochem. Eng. J.* 147, 29–38. doi: 10.1016/j.bej.2019.03.020

Fast, A. G., Schmidt, E. D., Jones, S. W., and Tracy, B. P. (2015). Acetogenic mixotrophy: novel options for yield improvement in biofuels and biochemicals production. *Curr. Opin. Biotechnol.* 33, 60–72. doi: 10.1016/j.copbio.2014.11.014

Faust, K., and Raes, J. (2012). Microbial interactions: from networks to models. *Nat. Rev. Microbiol.* 10, 538–550. doi: 10.1038/nrmicro2832

Fontaine, F. E., Peterson, W. H., McCoy, E., Johnson, M. J., and Ritter, G. J. (1942). A New Type of Glucose Fermentation by *Clostridium thermoaceticum*. *J. Bacteriol.* 43, 701–715. doi: 10.1128/jb.43.6.701-715.1942

Fruehauf, H. M., Enzmann, F., Harnisch, F., Ulber, R., and Holtmann, D. (2020). Microbial Electrosynthesis-An Inventory on Technology Readiness Level and Performance of Different Process Variants. *Biotechnol. J.* 15, e2000066. doi: 10.1002/biot.202000066

Ge, S., Usack, J. G., Spirito, C. M., and Angenent, L. T. (2015). Long-Term n-Caproic Acid Production from Yeast-Fermentation Beer in an Anaerobic Bioreactor with Continuous Product Extraction. *Environ. Sci. Technol.* 49, 8012–8021. doi: 10.1021/acs.est.5b00238

Gildemyn, S., Molitor, B., Usack, J. G., Nguyen, M., Rabaey, K., and Angenent, L. T. (2017). Upgrading syngas fermentation effluent using *Clostridium kluyveri* in a continuous fermentation. *Biotechnol. Biofuels* 10, 83. doi: 10.1186/s13068-017-0764-6

Gong, Z., Yu, H., Zhang, J., Li, F., and Song, H. (2020). Microbial electro-fermentation for synthesis of chemicals and biofuels driven by bi-directional extracellular electron transfer. *Synth. Syst. Biotechnol.* 5, 304–313. doi: 10.1016/j.synbio.2020.08.004

Gossen, M., and Bujard, H. (1993). Anhydrotetracycline, a novel effector for tetracycline controlled gene expression systems in eukaryotic cells. *Nucleic Acids Res.* 21, 4411–4412. doi: 10.1093/nar/21.18.4411

Gössner, A. S., Picardal, F., Tanner, R. S., and Drake, H. L. (2008). Carbon metabolism of the moderately acid-tolerant acetogen *Clostridium drakei* isolated from peat. *FEMS Microbiol. Lett.* 287, 236–242. doi: 10.1111/j.1574-6968.2008.01313.x

Gostin, P. F., Helth, A., Voss, A., Sueptitz, R., Calin, M., Eckert, J., et al. (2013). Surface treatment, corrosion behavior, and apatite-forming ability of Ti-45Nb implant alloy. *J. Biomed. Mater. Res. B. Appl. Biomater* 101, 269–278. doi: 10.1002/jbm.b.32836

Gottwald, M., Andreesen, J. R., LeGall, J., and Ljungdahl, L. G. (1975). Presence of Cytochrome and Menaquinone in *Clostridium formicoaceticum* and *Clostridium thermoaceticum*. *J. Bacteriol.*122, 325–328. doi: 10.1128/jb.122.1.325-328.1975

Greening, R. C., and Leedle, J. A. (1989). Enrichment and isolation of *Acetitomaculum ruminis*, gen. nov., sp. nov. acetogenic bacteria from the bovine rumen. *Arch. Microbiol.* 151, 399–406. doi: 10.1007/BF00416597

Griffin, D. W., and Schultz, M. A. (2012). Fuel and chemical products from biomass syngas: A comparison of gas fermentation to thermochemical conversion routes. *Environ. Prog. Sustain. Energy* 31, 219–224. doi: 10.1002/ep.11613

Groher, A., and Weuster-Botz, D. (2016). Comparative reaction engineering analysis of different acetogenic bacteria for gas fermentation. *J. Biotechnol.* 228, 82–94. doi: 10.1016/j.jbiotec.2016.04.032

Guo, K., Tang, X., Du, Z., and Li, H. (2010). Hydrogen production from acetate in a cathode-on-top single-chamber microbial electrolysis cell with a mipor cathode. *Biochem. Eng. J.* 51, 48–52. doi: 10.1016/j.bej.2010.05.001

Haas, T., Krause, R., Weber, R., Demler, M., and Schmid, G. (2018). Technical photosynthesis involving CO_2 electrolysis and fermentation. *Nat. Catal.* 1, 32–39. doi: 10.1038/s41929-017-0005-1

Haghighi Mood, S., Hossein Golfeshan, A., Tabatabaei, M., Salehi Jouzani, G., Najafi, G. H., Gholami, M., et al. (2013). Lignocellulosic biomass to bioethanol, a comprehensive review with a focus on pretreatment. *Renew. Sustain. Energy Rev.* 27, 77–93. doi: 10.1016/j.rser.2013.06.033

Hamann, C. H., and Vielstich, W. (2005). *Elektrochemie*. Wiley-VCH.

Harnisch, F., and Holtmann, D., eds (2019). *Bioelectrosynthesis*. Cham: Springer International Publishing. doi: 10.1007/978-3-030-03299-9

Harnisch, F., Rosa, L. F. M., Kracke, F., Virdis, B., and Krömer, J. O. (2015). Electrifying white biotechnology: engineering and economic potential of electricity-driven bio-production. *ChemSusChem* 8, 758–766. doi: 10.1002/cssc.201402736

Harnisch, F., and Schröder, U. (2009). Selectivity versus mobility: separation of anode and cathode in microbial bioelectrochemical systems. *ChemSusChem* 2, 921–926. doi: 10.1002/cssc.200900111

Harvey, B. G., and Meylemans, H. A. (2014). 1-Hexene: a renewable C6 platform for full-performance jet and diesel fuels. *Green Chem.* 16, 770–776. doi: 10.1039/c3gc41554f

Heise, R., Müller, V., and Gottschalk, G. (1989). Sodium dependence of acetate formation by the acetogenic bacterium *Acetobacterium woodii*. *J. Bacteriol.* 171, 5473–5478. doi: 10.1128/jb.171.10.5473-5478.1989

Henry, W. (1803). III. Experiments on the quantity of gases absorbed by water, at different temperatures, and under different pressures. *Phil. Trans. R. Soc.* 93, 29–274. doi: 10.1098/rstl.1803.0004

Herzog, J., Mook, A., Guhl, L., Bäumler, M., Beck, M. H., Weuster‐Botz, D., Bengelsdorf, F.R., and Zeng, A.-P. (2022). Novel synthetic co-culture of *Acetobacterium woodii* and

Clostridium drakei using CO_2 and *in situ* generated H_2 for the production of caproic acid via lactic acid. *Eng. Life Sci.*, 1–13. doi: 10.1002/elsc.202100169

Hess, V., Schuchmann, K., and Müller, V. (2013). The ferredoxin:NAD+ oxidoreductase (Rnf) from the acetogen *Acetobacterium woodii* requires Na^+ and is reversibly coupled to the membrane potential. *J. Biol. Chem.* 288, 31496–31502. doi: 10.1074/jbc.M113.510255

Hiegemann, H., Herzer, D., Nettmann, E., Lübken, M., Schulte, P., Schmelz, K.-G., et al. (2016). An integrated 45L pilot microbial fuel cell system at a full-scale wastewater treatment plant. *Bioresour. Technol.* 218, 115–122. doi: 10.1016/j.biortech.2016.06.052

Hiller, H., Reimert, R., and Stönner, H.-M. (2003). "Gas Production," in *Ullmann's encyclopedia of industrial chemistry*, eds. M. Bohnet, and F. Ullmann (Weinheim: Wiley-VCH). doi: 10.1002/14356007.a12_169.pub3

Ho, C.-Y., Chang, J.-J., Lee, S.-C., Chin, T.-Y., Shih, M.-C., Li, W.-H., et al. (2012). Development of cellulosic ethanol production process via co-culturing of artificial cellulosomal *Bacillus* and kefir yeast. *Appl. Energy* 100, 27–32. doi: 10.1016/j.apenergy.2012.03.016

Hoffmeister, S., Gerdom, M., Bengelsdorf, F. R., Linder, S., Flüchter, S., Öztürk, H., et al. (2016). Acetone production with metabolically engineered strains of *Acetobacterium woodii*. *Metab. Eng.* 36, 37–47. doi: 10.1016/j.ymben.2016.03.001

Huang, C. B., Alimova, Y., Myers, T. M., and Ebersole, J. L. (2011). Short- and medium-chain fatty acids exhibit antimicrobial activity for oral microorganisms. *Arch. Oral Biol.* 56, 650–654. doi: 10.1016/j.archoralbio.2011.01.011

Humphreys, C. M., McLean, S., Schatschneider, S., Millat, T., Henstra, A. M., Annan, F. J., et al. (2015). Whole genome sequence and manual annotation of *Clostridium autoethanogenum*, an industrially relevant bacterium. *BMC Genomics* 16, 1085. doi: 10.1186/s12864-015-2287-5

Hunting, E. R., and Kampfraath, A. A. (2013). Contribution of bacteria to redox potential (E h) measurements in sediments. *Int. J. Environ. Sci. Technol.* 10, 55–62. doi: 10.1007/s13762-012-0080-4

IEA (2022). *Global Hydrogen Review 2022*. Paris. Accessed online 27.03.2023. https://www.iea.org/reports/global-hydrogen-review-2022

IEA, Paris (2022). *Chemicals*. Accessed online 27.03.2023 https://www.iea.org/reports/chemicals.

Isaksson, J., Asblad, A., and Berntsson, T. (2013). Influence of different pretreatment methods on biomass gasification and production of fischer-tropsch crude integrated with a pulp and paper mill. *Chem. Eng. Trans.* 35, 559–564. doi: 10.3303/CET1335093

Jackson, R. (2020). Eunice Foote, John Tyndall and a question of priority. *Notes Rec.* 74, 105–118. doi: 10.1098/rsnr.2018.0066

Jacob, H. E. (1970). Influence of pretreatment of the redoxpotential electrode on the determination of oxygen pressure in bacterial cultures. *Pathol. Microbiol. (Basel)* 36, 57–62. doi: 10.1159/000162420

Jeon, B. S., Moon, C., Kim, B.-C., Kim, H., Um, Y., and Sang, B.-I. (2013). *In situ* extractive fermentation for the production of hexanoic acid from galactitol by *Clostridium* sp. BS-1. *Enzyme Microb. Technol.* 53, 143–151. doi: 10.1016/j.enzmictec.2013.02.008

Jeong, Y., Song, Y., Shin, H. S., and Cho, B.-K. (2014). Draft Genome Sequence of Acid-Tolerant *Clostridium drakei* SL1T, a Potential Chemical Producer through Syngas Fermentation. *Genome Announc.* 2. doi: 10.1128/genomeA.00387-14

Kamlage, B., Boelter, A., and Blaut, M. (1993). Spectroscopic and potentiometric characterization of cytochromes in two *Sporomusa* species and their expression during growth on selected substrates. *Arch. Microbiol.* 159, 189–196. doi: 10.1007/BF00250281

Kantzow, C., Mayer, A., and Weuster-Botz, D. (2015). Continuous gas fermentation by *Acetobacterium woodii* in a submerged membrane reactor with full cell retention. *J. Biotechnol.* 212, 11–18. doi: 10.1016/j.jbiotec.2015.07.020

Kantzow, C., and Weuster-Botz, D. (2016). Effects of hydrogen partial pressure on autotrophic growth and product formation of *Acetobacterium woodii*. *Bioprocess Biosyst. Eng.* 39, 1325–1330. doi: 10.1007/s00449-016-1600-2

Karnholz, A., Küsel, K., Gössner, A., Schramm, A., and Drake, H. L. (2002). Tolerance and metabolic response of acetogenic bacteria toward oxygen. *Appl. Environ. Microbiol.* 68, 1005–1009. doi: 10.1128/AEM.68.2.1005-1009.2002

Kenealy, W. R., Cao, Y., and Weimer, P. J. (1995). Production of caproic acid by cocultures of ruminal cellulolytic bacteria and *Clostridium kluyveri* grown on cellulose and ethanol. *Appl. Microbiol. Biotechnol.* 44, 507–513. doi: 10.1007/BF00169952

Khor, W. C., Andersen, S., Vervaeren, H., and Rabaey, K. (2017). Electricity-assisted production of caproic acid from grass. *Biotechnol. Biofuels* 10, 180. doi: 10.1186/s13068-017-0863-4

Kipf, E., Koch, J., Geiger, B., Erben, J., Richter, K., Gescher, J., et al. (2013). Systematic screening of carbon-based anode materials for microbial fuel cells with *Shewanella oneidensis* MR-1. *Bioresour. Technol.* 146, 386–392. doi: 10.1016/j.biortech.2013.07.076

Kobayashi, H., Saito, N., Fu, Q., Kawaguchi, H., Vilcaez, J., Wakayama, T., et al. (2013). Bio-electrochemical property and phylogenetic diversity of microbial communities associated with bioelectrodes of an electromethanogenic reactor. *J. Biosci. Bioeng.* 116, 114–117. doi: 10.1016/j.jbiosc.2013.01.001

Köpke, M., Mihalcea, C., Liew, F., Tizard, J. H., Ali, M. S., Conolly, J. J., et al. (2011). 2,3-butanediol production by acetogenic bacteria, an alternative route to chemical synthesis, using industrial waste gas. *Appl. Environ. Microbiol.* 77, 5467–5475. doi: 10.1128/AEM.00355-11

Kotsyurbenko, O. R., Simankova, M. V., Not Available, A. N. N., Zhilina, T. N., Bolotina, N. P., Lysenko, A. M., et al. (1995). New species of psychrophilic acetogens: *Acetobacterium bakii* sp. nov., *A. paludosum* sp. nov., *A. fimetarium* sp. nov. *Arch. Microbiol.* 163, 29–34. doi: 10.1007/s002030050167

Kraume, M. (2003). *Mischen und Rühren: Grundlagen und moderne Verfahren*. Weinheim: Wiley-VCH. ISBN: 9783527307098

Kremp, F., Poehlein, A., Daniel, R., and Müller, V. (2018). Methanol metabolism in the acetogenic bacterium *Acetobacterium woodii*. *Environ. Microbiol.* 20, 4369–4384. doi: 10.1111/1462-2920.14356

Kremp, F., Roth, J., and Müller, V. (2022). A Third Way of Energy Conservation in Acetogenic Bacteria. *Microbiol. Spectr.* 10, e0138522. doi: 10.1128/spectrum.01385-22

Krieg, T., Madjarov, J., Rosa, Luis F.M., Enzmann, Franziska, Harnisch, F., Holtmann, D., and Rabaey, K. (2019). "Reactors for Microbial Electrobiotechnology," in *Bioelectrosynthesis*, eds. F. Harnisch, and D. Holtmann (Cham: Springer International Publishing), 231–272. doi: 10.1007/10_2017_40

Krieg, T., Sydow, A., Schröder, U., Schrader, J., and Holtmann, D. (2014). Reactor concepts for bioelectrochemical syntheses and energy conversion. *Trends Biotechnol.* 32, 645–655. doi: 10.1016/j.tibtech.2014.10.004

Kucek, L. A., Nguyen, M., and Angenent, L. T. (2016a). Conversion of L-lactate into n-caproate by a continuously fed reactor microbiome. *Water Res.* 93, 163–171. doi: 10.1016/j.watres.2016.02.018

Kucek, L. A., Spirito, C. M., and Angenent, L. T. (2016b). High n-caprylate productivities and specificities from dilute ethanol and acetate: chain elongation with microbiomes to upgrade products from syngas fermentation. *Energy Environ. Sci.* 9, 3482–3494. doi: 10.1039/C6EE01487A

Küsel, K., Dorsch, T., Acker, G., Stackebrandt, E., and Drake, H. L. (2000). *Clostridium scatologenes* strain SL1 isolated as an acetogenic bacterium from acidic sediments. *Int. J. Syst. Evol. Microbiol.* 50, 537–546. doi: 10.1099/00207713-50-2-537

Küsel, K., Karnholz, A., Trinkwalter, T., Devereux, R., Acker, G., and Drake, H. L. (2001). Physiological ecology of *Clostridium glycolicum* RD-1, an aerotolerant acetogen isolated from sea grass roots. *Appl. Environ. Microbiol.* 67, 4734–4741. doi: 10.1128/AEM.67.10.4734-4741.2001

Lee, H., Calvin, K., Dasgupat, D., Krinner, G., Mukherji, A., Thorne, P., et al. (2023). *Synthesis Report of the IPCC Sixth Assessment Report (AR6): Summary for Policymakers*. Accessed online 27.03.2023. https://report.ipcc.ch/ar6syr/pdf/IPCC_AR6_SYR_SPM.pdf

Li, H., Opgenorth, P. H., Wernick, D. G., Rogers, S., Wu, T.-Y., Higashide, W., et al. (2012). Integrated electromicrobial conversion of CO_2 to higher alcohols. *Science* 335, 1596. doi: 10.1126/science.1217643

Liew, F., Martin, M. E., Tappel, R. C., Heijstra, B. D., Mihalcea, C., and Köpke, M. (2016). Gas Fermentation-A Flexible Platform for Commercial Scale Production of Low-Carbon-Fuels and Chemicals from Waste and Renewable Feedstocks. *Front. Microbiol.* 7, 694. doi: 10.3389/fmicb.2016.00694

Liew, F. E., Nogle, R., Abdalla, T., Rasor, B. J., Canter, C., Jensen, R. O., et al. (2022). Carbon-negative production of acetone and isopropanol by gas fermentation at industrial pilot scale. *Nat. Biotechnol.* 40, 335–344. doi: 10.1038/s41587-021-01195-w

Lin, T., Ding, W., Sun, L., Wang, L., Liu, C.-G., and Song, H. (2018). Engineered *Shewanella oneidensis*-reduced graphene oxide biohybrid with enhanced biosynthesis and transport of flavins enabled a highest bioelectricity output in microbial fuel cells. *Nano. Energy* 50, 639–648. doi: 10.1016/j.nanoen.2018.05.072

Liou, J. S.-C., Balkwill, D. L., Drake, G. R., and Tanner, R. S. (2005). *Clostridium carboxidivorans* sp. nov., a solvent-producing *clostridium* isolated from an agricultural settling lagoon, and reclassification of the acetogen *Clostridium scatologenes* strain SL1 as *Clostridium drakei* sp. nov. *Int. J. Syst. Evol. Microbiol.* 55, 2085–2091. doi: 10.1099/ijs.0.63482-0

Liu, B., Popp, D., Müller, N., Sträuber, H., Harms, H., and Kleinsteuber, S. (2020). Three Novel *Clostridia* Isolates Produce n-Caproate and iso-Butyrate from Lactate: Comparative Genomics of Chain-Elongating Bacteria. *Microorganisms* 8. doi: 10.3390/microorganisms8121970

Liu, H., and Logan, B. E. (2004). Electricity generation using an air-cathode single chamber microbial fuel cell in the presence and absence of a proton exchange membrane. *Environ. Sci. Technol.* 38, 4040–4046. doi: 10.1021/es0499344

Ljungdahl, L., Irion, E., and Wood, H. G. (1966). Role of corrinoids in the total synthesis of acetate from CO_2 by *Clostridium thermoaceticum*. *Fed Proc* 25, 1642–1648. doi: 10.1146/annurev.mi.23.100169.002503

Ljungdahl, L., and Wood, H. G. (1969). Total Synthesis of Acetate from CO_2 by Heterotrophic Bacteria. *Annu. Rev. Microbiol.*23, 515–538. doi: 10.1146/annurev.mi.23.100169.002503

Logan, B. E. (2008). *Microbial fuel cells*. Hoboken, N.J. Wiley-Interscience. ISBN: 9780470239483

Logan, B. E., Hamelers, B., Rozendal, R., Schröder, U., Keller, J., Freguia, S., et al. (2006). Microbial fuel cells: methodology and technology. *Environ. Sci. Technol.* 40, 5181–5192. doi: 10.1021/es0605016

Luo, Q., Wang, H., Zhang, X., and Qian, Y. (2005). Effect of direct electric current on the cell surface properties of phenol-degrading bacteria. *Appl. Environ. Microbiol.* 71, 423–427. doi: 10.1128/AEM.71.1.423-427.2005

Ma, Q., Bi, Y.-H., Wang, E.-X., Zhai, B.-B., Dong, X.-T., Qiao, B., et al. (2019). Integrated proteomic and metabolomic analysis of a reconstructed three-species microbial consortium for one-step fermentation of 2-keto-L-gulonic acid, the precursor of vitamin C. *J. Ind. Microbiol. Biotechnol.* 46, 21–31. doi: 10.1007/s10295-018-2096-3

Masson-Delmotte, V., Zhai, P., Pirani, A., Connors, S. L., Péan, C., Berger, S., et al. (2021). *Climate change 2021: the physical science basis: contribution of working group I to the sixth assessment report of the intergovernmental panel on climate change*. IPCC 2021. Cambridge University Press. Accessed online 26.03.2023 https://www.ipcc.ch/report/ar6/wg1/

Merchuk, J. C., and Garcia Camacho, F. (2010). “Bioreactors: Airlift Reactors,” in *Encyclopedia of industrial biotechnology, bioprocess, bioseparation, and cell technology*, ed. M. C. Flickinger (Hoboken, NJ: Wiley). doi: 10.1002/9780470054581.eib144

Mittermeier, F., Bäumler, M., Arulrajah, P., García Lima, J. d. J., Hauke, S., Stock, A., et al. (2023). Artificial microbial consortia for bioproduction processes. *Eng. Life Sci.* 23, e2100152. doi: 10.1002/elsc.202100152

Mizuno, A., and Hori, Y. (1988). Destruction of living cells by pulsed high-voltage application. *IEEE Trans. on Ind. Applicat.* 24, 387–394. doi: 10.1109/28.2886

Mohammadi, M., Najafpour, G. D., Younesi, H., Lahijani, P., Uzir, M. H., and Mohamed, A. R. (2011). Bioconversion of synthesis gas to second generation biofuels: A review. *Renew. Sust. Energy Rev.* 15, 4255–4273. doi: 10.1016/j.rser.2011.07.124

Möller, B., Omer, R., Howard, B. H., Gottschalk, G., and Hippe, H. (1984). *Sporomusa*, a new genus of gram-negative anaerobic bacteria including *Sporomusa sphaeroides* spec. nov. and *Sporomusa ovata* spec. nov. *Arch. Microbiol.* 139, 388–396. doi: 10.1007/BF00408385

Monod, J. (1949). The growth of bacterial cultures. *Annu. Rev. Microbiol.* 3, 371–394. doi: 10.1146/annurev.mi.03.100149.002103

Mook, A., Beck, M. H., Baker, J. P., Minton, N. P., Dürre, P., and Bengelsdorf, F. R. (2022). Autotrophic lactate production from H_2 + CO_2 using recombinant and fluorescent FAST-tagged *Acetobacterium woodii*. *Appl. Microbiol. Biotechnol.*, 1447–1458. doi: 10.1007/s00253-022-11770-z

Moon, J., Dönig, J., Kramer, S., Poehlein, A., Daniel, R., and Müller, V. (2021). Formate metabolism in the acetogenic bacterium *Acetobacterium woodii*. *Environ. Microbiol.* 23, 4214–4227. doi: 10.1111/1462-2920.15598

Moscoviz, R., Toledo-Alarcón, J., Trably, E., and Bernet, N. (2016). Electro-Fermentation: How To Drive Fermentation Using Electrochemical Systems. *Trends Biotechnol.* 34, 856–865. doi: 10.1016/j.tibtech.2016.04.009

Müller, V. (2003). Energy conservation in acetogenic bacteria. *Appl. Environ. Microbiol.* 69, 6345–6353. doi: 10.1128/AEM.69.11.6345-6353.2003

Müller, V., Aufurth, S., and Rahlfs, S. (2001). The Na(+) cycle in *Acetobacterium woodii*: identification and characterization of a Na(+) translocating F(1)F(0)-ATPase with a mixed oligomer of 8 and 16 kDa proteolipids. *Biochem. Biophys. Acta.* 1505, 108–120. doi: 10.1016/s0005-2728(00)00281-4

Müller, V., Imkamp, F., Biegel, E., Schmidt, S., and Dilling, S. (2008). Discovery of a ferredoxin:NAD+-oxidoreductase (Rnf) in *Acetobacterium woodii*: a novel potential coupling site in acetogens. *Ann. N. Y. Acad. Sci.* 1125, 137–146. doi: 10.1196/annals.1419.011

Naik, S. N., Goud, V. V., Rout, P. K., and Dalai, A. K. (2010). Production of first and second generation biofuels: A comprehensive review. *Renew. Sust. Energy Rev.* 14, 578–597. doi: 10.1016/j.rser.2009.10.003

Neuendorf, C. S., Vignolle, G. A., Derntl, C., Tomin, T., Novak, K., Mach, R. L., et al. (2021). A quantitative metabolic analysis reveals *Acetobacterium woodii* as a flexible and robust host for formate-based bioproduction. *Metab. Eng.* 68, 68–85. doi: 10.1016/j.ymben.2021.09.004

Nevin, K. P., Woodard, T. L., Franks, A. E., Summers, Z. M., and Lovley, D. R. (2010). Microbial electrosynthesis: feeding microbes electricity to convert carbon dioxide and water to multicarbon extracellular organic compounds. *mBio* 1. doi: 10.1128/mBio.00103-10

Oswald, F., Stoll, I. K., Zwick, M., Herbig, S., Sauer, J., Boukis, N., et al. (2018). Formic Acid Formation by *Clostridium ljungdahlii* at Elevated Pressures of Carbon Dioxide and Hydrogen. *Front. Bioeng. Biotechnol.* 6, 6. doi: 10.3389/fbioe.2018.00006

Pace, R. T., and Burg, K. J. L. (2015). Toxic effects of resazurin on cell cultures. *Cytotechnology* 67, 13–17. doi: 10.1007/s10616-013-9664-1

Poehlein, A., Cebulla, M., Ilg, M. M., Bengelsdorf, F. R., Schiel-Bengelsdorf, B., Whited, G., et al. (2015). The Complete Genome Sequence of *Clostridium aceticum*: a Missing Link between Rnf- and Cytochrome-Containing Autotrophic Acetogens. *mBio* 6, e01168-15. doi: 10.1128/mBio.01168-15

Poehlein, A., Schmidt, S., Kaster, A.-K., Goenrich, M., Vollmers, J., Thürmer, A., et al. (2012). An ancient pathway combining carbon dioxide fixation with the generation and utilization of a sodium ion gradient for ATP synthesis. *PLoS ONE* 7, e33439. doi: 10.1371/journal.pone.0033439

Potter, M. C. (1911). Electrical effects accompanying the decomposition of organic compounds. *Proc. R. Soc. Lond. B.* 84, 260–276. doi: 10.1098/rspb.1911.0073

PW Consulting Agency (2021). *pmarketresearch predicts that global sales of 2024 acid will reach 12,456 tonnes*. Accessed 08.02.2023, https://pmarketresearch.com/2024-will-sell-12456-tons-of-caproic-acid-worldwide-pmarketresearch-predicts/

Rader, G. K., and Logan, B. E. (2010). Multi-electrode continuous flow microbial electrolysis cell for biogas production from acetate. *Int. J. Hydrogen Energy* 35, 8848–8854. doi: 10.1016/j.ijhydene.2010.06.033

Rasmussen, M., Abdellaoui, S., and Minteer, S. D. (2016). Enzymatic biofuel cells: 30 years of critical advancements. *Biosens. Bioelectron.* 76, 91–102. doi: 10.1016/j.bios.2015.06.029

Reguera, G., McCarthy, K. D., Mehta, T., Nicoll, J. S., Tuominen, M. T., and Lovley, D. R. (2005). Extracellular electron transfer via microbial nanowires. *Nature* 435, 1098–1101. doi: 10.1038/nature03661

Reidlinger, J., and Müller, V. (1994). Purification of ATP synthase from *Acetobacterium woodii* and identification as a Na(+)-translocating F1F0-type enzyme. *Eur. J. Biochem.* 223, 275–283. doi: 10.1111/j.1432-1033.1994.tb18992.x

Rieu-Lesme, F., Morvan, B., Collins, M. D., Fonty, G., and Willems, A. (1996). A new H_2 / CO_2-using acetogenic bacterium from the rumen: Description of *Ruminococcus schinkii* sp. nov. *FEMS Microbiol Lett* 140, 281–286. doi: 10.1111/j.1574-6968.1996.tb08350.x

Roell, G. W., Zha, J., Carr, R. R., Koffas, M. A., Fong, S. S., and Tang, Y. J. (2019). Engineering microbial consortia by division of labor. *Microb Cell Fact* 18, 35. doi: 10.1186/s12934-019-1083-3

Rosenbaum, F. P., and Müller, V. (2021). Energy conservation under extreme energy limitation: the role of cytochromes and quinones in acetogenic bacteria. *Extremophiles* 25, 413–424. doi: 10.1007/s00792-021-01241-0

Rostrup-Nielsen, J. R. (2000). New aspects of syngas production and use. *Catal Today* 63, 159–164. doi: 10.1016/S0920-5861(00)00455-7

Rozendal, R. A., Hamelers, H. V. M., and Buisman, C. J. N. (2006). Effects of membrane cation transport on pH and microbial fuel cell performance. *Environ Sci Technol* 40, 5206–5211. doi: 10.1021/es060387r

Russell, J. B. (1992). Another explanation for the toxicity of fermentation acids at low pH: anion accumulation versus uncoupling. *J Appl Bacteriol* 73, 363–370. doi: 10.1111/j.1365-2672.1992.tb04990.x

Sabra, W., Dietz, D., Tjahjasari, D., Zeng, A.-P. (2010). Biosystems analysis and engineering of microbial consortia for industrial biotechnology. *Eng. Life Sci.* 10, 407-421. doi: 10.1002/elsc.201000111

Sabra, W., Dietz, D., Zeng, A.-P. (2013). Substrate-limited co-culture for efficient production of propionic acid from flour hydrolysate. *Appl. Microbiol. Biotechnol.* 97, 5771-5777. doi: 10.1007/s00253-013-4913-y

Sander, R. (2015). Compilation of Henry's law constants (version 4.0) for water as solvent. *Atmos. Chem. Phys.* 15, 4399–4981. doi: 10.5194/acp-15-4399-2015

San-Valero, P., Fernández-Naveira, Á., Veiga, M. C., and Kennes, C. (2019). Influence of electron acceptors on hexanoic acid production by *Clostridium kluyveri*. *J Environ Manage* 242, 515–521. doi: 10.1016/j.jenvman.2019.04.093

Schmidt, V. M. (2003). *Elektrochemische Verfahrenstechnik: Grundlagen, Reaktionstechnik, Prozeßoptimierung*. Weinheim: Wiley-VCH. ISBN: 3527299580

Schneider, M., Bäumler, M., Lee, N. M., Weuster-Botz, D., Ehrenreich, A., and Liebl, W. (2021). Monitoring co-cultures of *Clostridium carboxidivorans* and *Clostridium kluyveri* by fluorescence *in situ* hybridization with specific 23S rRNA oligonucleotide probes. *Syst Appl Microbiol* 44, 126271. doi: 10.1016/j.syapm.2021.126271

Schoelmerich, M. C., Katsyv, A., Sung, W., Mijic, V., Wiechmann, A., Kottenhahn, P., et al. (2018). Regulation of lactate metabolism in the acetogenic bacterium *Acetobacterium woodii. Environ Microbiol* 20, 4587–4595. doi: 10.1111/1462-2920.14412

Schoelmerich, M. C., and Müller, V. (2019). Energy conservation by a hydrogenase-dependent chemiosmotic mechanism in an ancient metabolic pathway. *Proc Natl Acad Sci U S A* 116, 6329–6334. doi: 10.1073/pnas.1818580116

Schoelmerich, M. C., and Müller, V. (2020). Energy-converting hydrogenases: the link between H_2 metabolism and energy conservation. *Cell Mol Life Sci* 77, 1461–1481. doi: 10.1007/s00018-019-03329-5

Schröder, U., Harnisch, F., and Angenent, L. T. (2015). Microbial electrochemistry and technology: terminology and classification. *Energy Environ. Sci.* 8, 513–519. doi: 10.1039/C4EE03359K

Schuchmann, K., and Müller, V. (2013). Direct and reversible hydrogenation of CO_2 to formate by a bacterial carbon dioxide reductase. *Science* 342, 1382–1385. doi: 10.1126/science.1244758

Schuchmann, K., and Müller, V. (2014). Autotrophy at the thermodynamic limit of life: a model for energy conservation in acetogenic bacteria. *Nat Rev Microbiol* 12, 809–821. doi: 10.1038/nrmicro3365

Schwarz, F. M., Moon, J., Oswald, F., and Müller, V. (2022). Biological hydrogen storage and release through multiple cycles of bi-directional hydrogenation of CO_2 to formic acid in a single process unit. *Joule* 6, 1304–1319. doi: 10.1016/j.joule.2022.04.020

Selder, L., Sabra, W., Jürgensen, N., Lakshmanan, A., and Zeng, A.-P. (2020). Co-cultures with integrated *in situ* product removal for lactate-based propionic acid production. *Bioprocess Biosyst Eng* 43, 1027–1035. doi: 10.1007/s00449-020-02300-0

Serhan, M., Mattar, J., and Debs, L. (2016). Concentrated yogurt (Labneh) made of a mixture of goats' and cows' milk: Physicochemical, microbiological and sensory analysis. *Small Rumi Res* 138, 46–52. doi: 10.1016/j.smallrumres.2016.04.003

Shen, Y., Brown, R., and Wen, Z. (2014). Syngas fermentation of *Clostridium carboxidivoran* P7 in a hollow fiber membrane biofilm reactor: Evaluating the mass transfer coefficient and ethanol production performance. *Biochem Eng J.* 85, 21–29. doi: 10.1016/j.bej.2014.01.010

Shima, S., and Ataka, K. (2011). Isocyanides inhibit Fe-hydrogenase with very high affinity. *FEBS Lett* 585, 353–356. doi: 10.1016/j.febslet.2010.12.014

Skidmore, B. E., Baker, R. A., Banjade, D. R., Bray, J. M., Tree, D. R., and Lewis, R. S. (2013). Syngas fermentation to biofuels: Effects of hydrogen partial pressure on hydrogenase efficiency. *Biomass and Bioenergy* 55, 156–162. doi: 10.1016/j.biombioe.2013.01.034

Song, Y., Lee, J. S., Shin, J., Lee, G. M., Jin, S., Kang, S., et al. (2020). Functional cooperation of the glycine synthase-reductase and Wood-Ljungdahl pathways for autotrophic growth of *Clostridium drakei*. *Proc Natl Acad Sci U S A* 117, 7516–7523. doi: 10.1073/pnas.1912289117

Soussan, L., Riess, J., Erable, B., Delia, M.-L., and Bergel, A. (2013). Electrochemical reduction of CO_2 catalysed by *Geobacter sulfurreducens* grown on polarized stainless steel cathodes. *Electrochem Commun,* 28, 27–30. doi: 10.1016/j.elecom.2012.11.033

Spirito, C. M., Richter, H., Rabaey, K., Stams, A. J. M., and Angenent, L. T. (2014). Chain elongation in anaerobic reactor microbiomes to recover resources from waste. *Curr Opin Biotechnol* 27, 115–122. doi: 10.1016/j.copbio.2014.01.003

Stackebrandt, E., Kramer, I., Swiderski, J., and Hippe, H. (1999). Phylogenetic basis for a taxonomic dissection of the genus *Clostridium*. *FEMS Immunol Med Microbiol* 24, 253–258. doi: 10.1111/j.1574-695X.1999.tb01291.x

Stanley, D., Bandara, A., Fraser, S., Chambers, P. J., and Stanley, G. A. (2010). The ethanol stress response and ethanol tolerance of *Saccharomyces cerevisiae*. *J Appl Microbiol* 109, 13–24. doi: 10.1111/j.1365-2672.2009.04657.x

Strätz, M., Sauer, U., Kuhn, A., and Dürre, P. (1994). Plasmid Transfer into the Homoacetogen *Acetobacterium woodii* by Electroporation and Conjugation. *Appl Environ Microbiol* 60, 1033–1037. doi: 10.1128/aem.60.3.1033-1037.1994

Sun, G., Thygesen, A., Ale, M. T., Mensah, M., Poulsen, F. W., and Meyer, A. S. (2014). The significance of the initiation process parameters and reactor design for maximizing the efficiency of microbial fuel cells. *Appl Microbiol Biotechnol* 98, 2415–2427. doi: 10.1007/s00253-013-5486-5

Takors, R., Kopf, M., Mampel, J., Bluemke, W., Blombach, B., Eikmanns, B., et al. (2018). Using gas mixtures of CO, CO_2 and H_2 as microbial substrates: the do's and don'ts of successful technology transfer from laboratory to production scale. *Microb Biotechnol* 11, 606–625. doi: 10.1111/1751-7915.13270

Tanaka, K., and Pfennig, N. (1988). Fermentation of 2-methoxyethanol by *Acetobacterium malicum* sp. nov. and *Pelobacter venetianus*. *Arch. Microbiol.* 149, 181–187. doi: 10.1007/BF00422003

Tanner, R. S. (2007). “Cultivation of Bacteria and Fungi,” in *Manual of environmental microbiology*, eds. C. J. Hurst, and R. L. Crawford (Washington, D.C: ASM Press), 69–78. doi: 10.1128/9781555815882.ch6

Tanner, R. S., Miller, L. M., and Yang, D. (1993). *Clostridium ljungdahlii* sp. nov., an acetogenic species in clostridial rRNA homology group I. *Int J Syst Bacteriol* 43, 232–236. doi: 10.1099/00207713-43-2-232

Tanner, R. S., Stackebrandt, E., Fox, G. E., and Woese, C. R. (1981). A phylogenetic analysis of *Acetobacterium woodii*, *Clostridium barkeri*, *Clostridium butyricum*, *Clostridium lituseburense*, *Uubacterium limosum*, and *Eubacterium tenue*. *Curr Microbiol* 5, 35–38. doi: 10.1007/BF01566595

Tremblay, P.-L., Zhang, T., Dar, S. A., Leang, C., and Lovley, D. R. (2012). The Rnf complex of *Clostridium ljungdahlii* is a proton-translocating ferredoxin:NAD+ oxidoreductase essential for autotrophic growth. *mBio* 4, e00406-12. doi: 10.1128/mBio.00406-12

Tschech, A., and Pfennig, N. (1984). Growth yield increase linked to caffeate reduction in *Acetobacterium woodii*. *Archives of Microbiology*, 163–167. doi: 10.1007/BF00414460

Turner, A. P. F. (2013). Biosensors: sense and sensibility. *Chem Soc Rev* 42, 3184–3196. doi: 10.1039/C3CS35528D

Ungerman, A. J., and Heindel, T. J. (2007). Carbon monoxide mass transfer for syngas fermentation in a stirred tank reactor with dual impeller configurations. *Biotechnol Prog* 23, 613–620. doi: 10.1021/bp060311z

United Nations (2015). *Paris Agreement*. Accessed online 26.03.2023. https://unfccc.int/sites/default/files/english_paris_agreement.pdf

Utesch, T. (2019). *Entwicklung einer neuen Elektroden- und Bioreaktoranordnung für elektrochemisch unterstützte Bioprozesse*. Doctoral dissertation. Hamburg: Institute of Bioprocess and Biosystems Engineering, Hamburg University of Technology. ISBN: 978-3-8439-4196-9

Utesch, T., Sabra, W., Prescher, C., Baur, J., Arbter, P., and Zeng, A.-P. (2019). Enhanced electron transfer of different mediators for strictly opposite shifting of metabolism in *Clostridium pasteurianum* grown on glycerol in a new electrochemical bioreactor. *Biotechnol Bioeng* 116, 1627–1643. doi: 10.1002/bit.26963

Utesch, T., and Zeng, A.-P. (2018). A novel All-in-One electrolysis electrode and bioreactor enable better study of electrochemical effects and electricity-aided bioprocesses. *Eng. Life Sci.* 18, 600–610. doi: 10.1002/elsc.201700198

Valle, A., Zanardini, E., Abbruscato, P., Argenzio, P., Lustrato, G., Ranalli, G., et al. (2007). Effects of low electric current (LEC) treatment on pure bacterial cultures. *J Appl Microbiol* 103, 1376–1385. doi: 10.1111/j.1365-2672.2007.03374.x

van Immerseel, F., Buck, J. de, Boyen, F., Bohez, L., Pasmans, F., Volf, J., et al. (2004). Medium-chain fatty acids decrease colonization and invasion through hilA suppression shortly after infection of chickens with *Salmonella enterica* serovar Enteritidis. *Appl Environ Microbiol* 70, 3582–3587. doi: 10.1128/AEM.70.6.3582-3587.2004

Villadsen, J., Nielsen, J., and Lidén, G. (2011). “Gas–Liquid Mass Transfer,” in *Bioreaction Engineering Principles*, eds. J. Villadsen, J. Nielsen, and G. Lidén (Boston, MA: Springer US), 459–496. ISBN: 978-1-4419-9687-9

Villano, M., Aulenta, F., Ciucci, C., Ferri, T., Giuliano, A., and Majone, M. (2010). Bioelectrochemical reduction of CO(2) to CH(4) via direct and indirect extracellular electron transfer by a hydrogenophilic methanogenic culture. *Bioresour Technol* 101, 3085–3090. doi: 10.1016/j.biortech.2009.12.077

Wainaina, S., Horváth, I. S., and Taherzadeh, M. J. (2018). Biochemicals from food waste and recalcitrant biomass via syngas fermentation: A review. *Bioresour Technol* 248, 113–121. doi: 10.1016/j.biortech.2017.06.075

Wang, G., and Wang, D. I. (1984). Elucidation of Growth Inhibition and Acetic Acid Production by *Clostridium thermoaceticum*. *Appl Environ Microbiol* 47, 294–298. doi: 10.1128/aem.47.2.294-298.1984

Wang, L., York, S. W., Ingram, L. O., and Shanmugam, K. T. (2019). Simultaneous fermentation of biomass-derived sugars to ethanol by a co-culture of an engineered *Escherichia coli* and *Saccharomyces cerevisiae*. *Bioresour Technol* 273, 269–276. doi: 10.1016/j.biortech.2018.11.016

Wasewar, K. L., and Shende, D. Z. (2011). Reactive Extraction of Caproic Acid Using Tri-n-butyl Phosphate in Hexanol, Octanol, and Decanol. *J. Chem. Eng. Data* 56, 288–297. doi: 10.1021/je100974f

Weghoff, M. C., Bertsch, J., and Müller, V. (2015). A novel mode of lactate metabolism in strictly anaerobic bacteria. *Environ Microbiol* 17, 670–677. doi: 10.1111/1462-2920.12493

Wiegel, J., Braun, M., and Gottschalk, G. (1981). *Clostridium thermoautotrophicum* species novum, a thermophile producing acetate from molecular hydrogen and carbon dioxide. *Curr Microbiol.* 5, 255–260. doi: 10.1007/BF01571158

Wieringa, K. T. (1936). Over het verdwijnen van waterstof en koolzuur onder anaerobe voorwaarden. *Antonie van Leeuwenhoek* 3, 263–273.

Wilhelm, E., Battino, R., and Wilcock, R. J. (1977). Low-pressure solubility of gases in liquid water. *Chem. Rev.* 77, 219–262. doi: 10.1021/cr60306a003

Wirth, S., and Dürre, P. (2021). Investigation of putative genes for the production of medium-chained acids and alcohols in autotrophic acetogenic bacteria. *Metab Eng* 66, 296–307. doi: 10.1016/j.ymben.2021.04.010

Wolin, E. A., Wolin, M. J., and Wolfe, R. S. (1963). Formation of methane by bacterial extracts. *J. Biol. Chem.* 238, 2882–2886. doi: 1016/S0021-9258(18)67912-8

Wood, H. G. (1991). Life with CO or CO_2 and H_2 as a source of carbon and energy. *FASEB J* 5, 156–163. doi: 10.1096/fasebj.5.2.1900793

Wu, G., Yan, Q., Jones, J. A., Tang, Y. J., Fong, S. S., and Koffas, M. A. G. (2016). Metabolic Burden: Cornerstones in Synthetic Biology and Metabolic Engineering Applications. *Trends Biotechnol* 34, 652–664. doi: 10.1016/j.tibtech.2016.02.010

Xu, J., Guzman, J. J. L., Andersen, S. J., Rabaey, K., and Angenent, L. T. (2015). In-line and selective phase separation of medium-chain carboxylic acids using membrane electrolysis. *Chem Commun (Camb)* 51, 6847–6850. doi: 10.1039/c5cc01897h

Yan, S., and Dong, D. (2018). Improvement of caproic acid production in a *Clostridium kluyveri* H068 and Methanogen 166 co-culture fermentation system. *AMB express* 8, 175. doi: 10.1186/s13568-018-0705-1

Yang, J. S., Liu, C., Wang, G. Y., Zhao, X. Y., Li, B. Z., and Yuan, H. L. (2010). The effect of low direct current on *Pseudomonas aeruginosa* PKE117's enzyme production and degradable ability. *Biotechnol. Bull* 6, 185–188.

Young Jeon, B., Lae Jung, I., and Hyun Park, D. (2012). Conversion of Carbon Dioxide to Metabolites by *Clostridium acetobutylicum* KCTC1037 Cultivated with Electrochemical Reducing Power. *AiM* 02, 332–339. doi: 10.4236/aim.2012.23040

Zaldivar, J., and Ingram, L. O. (1999). Effect of organic acids on the growth and fermentation of ethanologenic *Escherichia coli* LY01. *Biotechnol Bioeng* 66, 203–210. doi: 10.1002/(SICI)1097-0290(1999)66:4<203:AID-BIT1>3.0.CO;2-#

Zeng, K., and Zhang, D. (2010). Recent progress in alkaline water electrolysis for hydrogen production and applications. *Prog Energy Comb Sci* 36, 307–326. doi: 10.1016/j.pecs.2009.11.002

Zentek, J., Buchheit-Renko, S., Ferrara, F., Vahjen, W., van Kessel, A. G., and Pieper, R. (2011). Nutritional and physiological role of medium-chain triglycerides and medium-chain fatty acids in piglets. *Anim Health Res Rev* 12, 83–93. doi: 10.1017/S1466252311000089

Zhang, C., Traitrongsat, P., Zeng, A.-P. (2023). Electrochemically mediated bioconversion and integrated purification greatly enhanced co-production of 1,3-propanediol and organic acids from glycerol in an industrial bioprocess. *Bioprocess Biosyst. Eng.* 46, 565-575. doi: 10.1007/s00449-022-02841-6

Zhu, X., Zhou, Y., Wang, Y., Wu, T., Li, X., Li, D., et al. (2017). Production of high-concentration n-caproic acid from lactate through fermentation using a newly isolated *Ruminococcaceae* bacterium CPB6. *Biotechnol Biofuels* 10. doi: 10.1186/s13068-017-0788-y

Zoski, C. G., ed (2007). *Handbook of electrochemistry*. Amsterdam: Elsevier. ISBN: 9780080469300

9 List of Figures

10 List of Tables

11 Appendix

11.1. Additional Figures

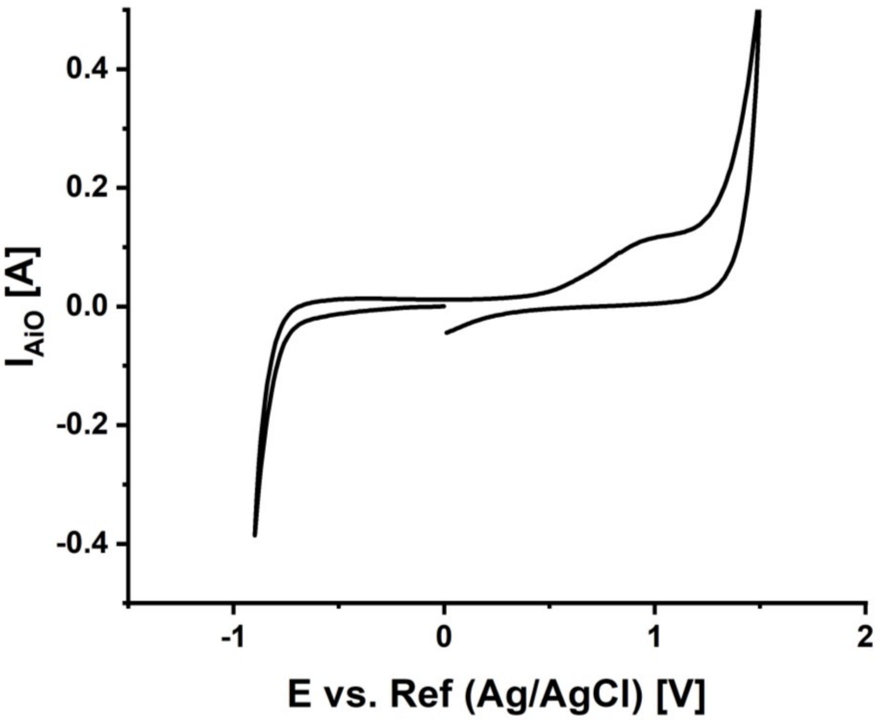

Figure 11-1: CV of the AiO electrode in cultivation medium between -1 V and 1.5 V vs. Ag/AgCl.

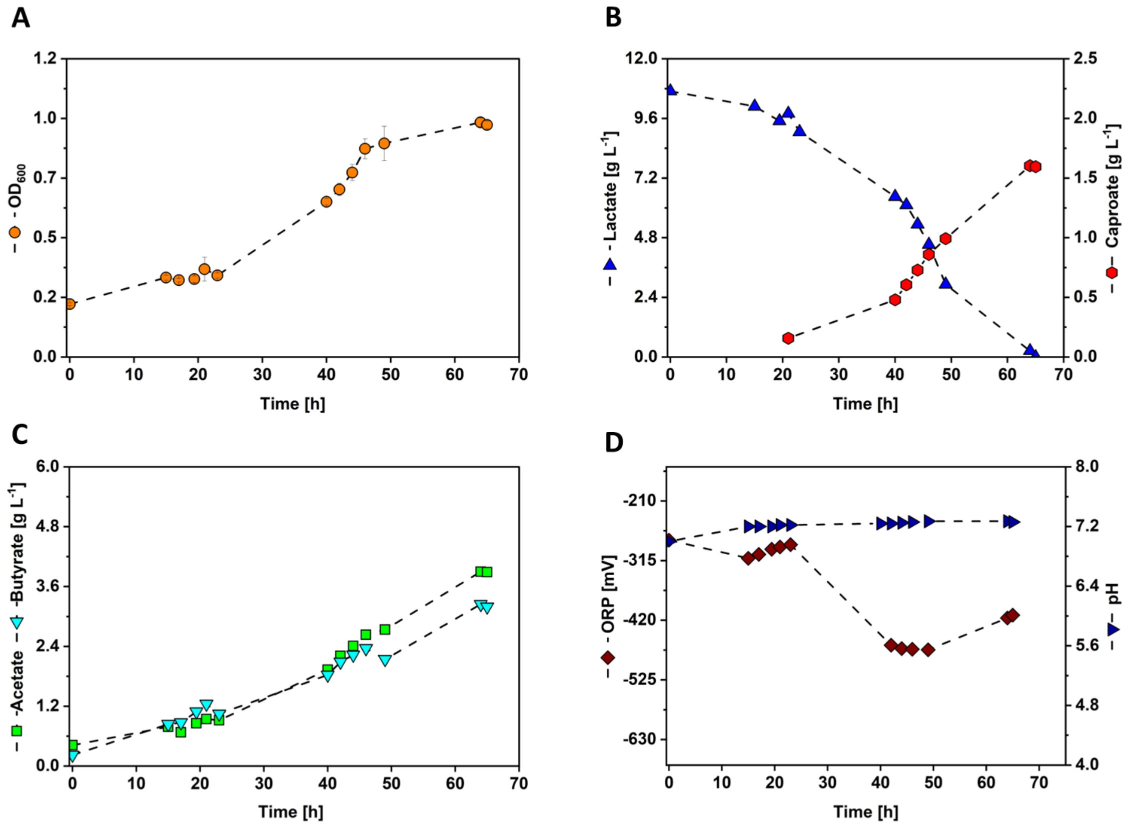

Figure 11-2: Stirred-tank batch fermentation of *C. drakei* with lactate as substrate. Repetition of Figure 5-17. (A) optical cell density (orange circles, OD_{600}); (B) concentration of lactate (blue triangles) and caproate (red hexagons, g L^{-1}); (C) concentration of acetate (green squares) and butyrate (cyan triangles, g L^{-1}); (D) ORP (brown diamonds, mV) and pH (blue triangles) measured during the cultivation. Parameters: $T = 30$ °C; pH = 7.0; $P\ V^{-1} = 0.04$ W L^{-1}; $V_{CO_2} = 0.003$ vvm; $V_0 = 1.4$ L; $c_{Lac,0} = 10.7$ g L^{-1}.

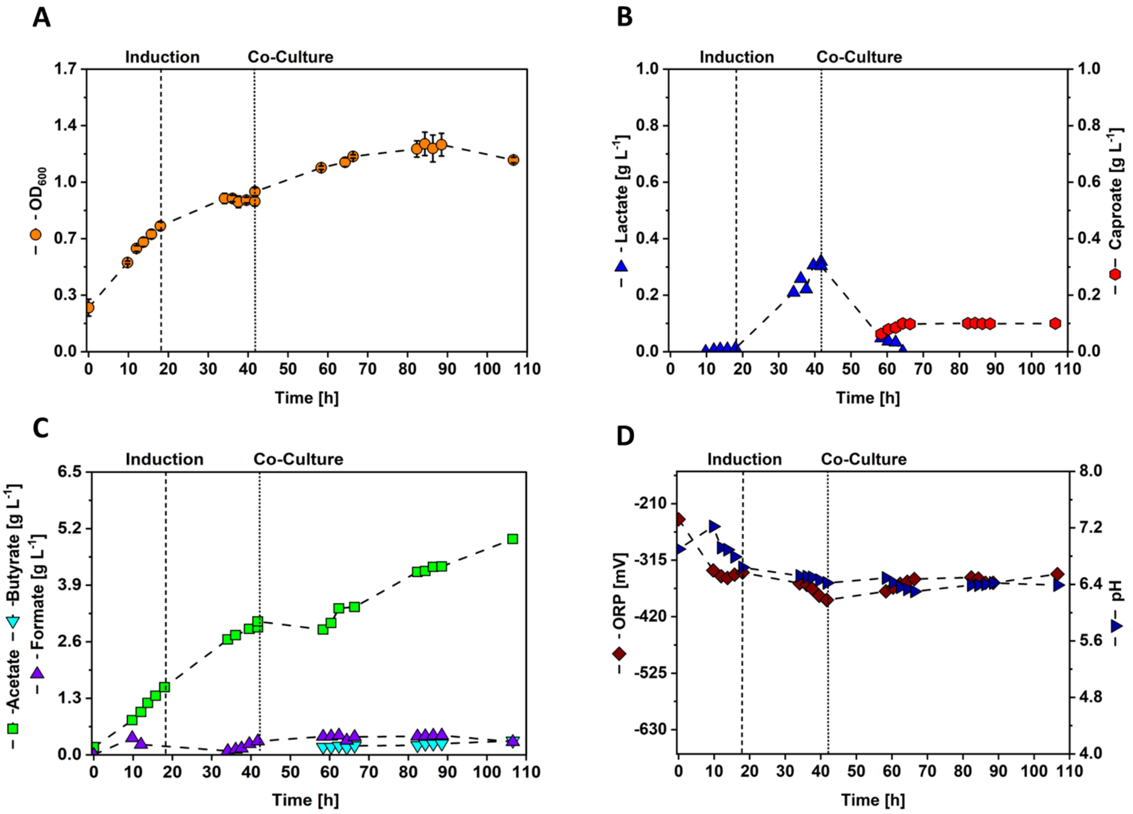

Figure 11-3: Synthetic co-culture in a stirred-tank batch fermentation of *A. woodii* [P_{bgaL}_*ldhD*_NFP] and *C. drakei*, repetition of Figure 5-22. (A) optical cell density (orange circles, OD_{600}); (B) concentration of lactate (blue triangles) and caproate (red hexagons, g L^{-1}); (C) concentration of acetate (green squares), formate (purple triangles) and butyrate (cyan triangles, g L^{-1}); (D) ORP (brown diamonds, mV) and pH (blue triangles) measured during the cultivation. The dashed vertical line indicates the time point of induction with 1mM lactose. The dotted vertical line indicates the time point of *C. drakei* and lactate addition. Parameters: T = 30 °C; pH = 7.0; $P\,V^{-1}$ = 2.4 W L^{-1}; V_{CO_2}= 0.01 vvm; I_{AiO} = 600 mA; U_{av} = 4.2 V; V_0 = 1.4 L.

11.2. Equipment

Table 11-1: General equipment list

Equipment	Type	Manufacturer
Analytical balance	Practum 224-1S	Sartorius AG
Autoclave	FNR 9699	Integra Biosciences
Balance	PRS 20-3	Kern & Sohn GmbH
Centrifuge (tabletop)	Heraeus Fresco 17	Thermo Fischer Scientific
Clean bench	HERA Safe	Thermo Fischer Scientific
Drying cabinet	BE 60	Memmert GmbH
Incubator	WB 120	Mytron
Magnetic stirrer plate	IKAMAG RCT	Artisan Technology Group
pH-meter	pH 1100 L	VWR international GmbH
Pipettes	Reference	Eppendorf SE
Spectrophotometer	V3000PC	VWR international GmbH
Spectrophotometer	Genesys 150	Thermo Fischer Scientific
Vortexer	1719	VWR international GmbH

Table 11-2: Equipment list for the operation of the anaerobic chamber

Equipment	Manufacturer
Airlock	COY Laboratory Products inc.
Anaerobic chamber	COY Laboratory Products inc.
Gas meter	COY Laboratory Products inc.
Oven for catalyst	COY Laboratory Products inc.

Table 11-3: Equipment list for the operation of the HPLC

Equipment	Type	Manufacturer
Autosampler	Autosampler 3950	KNAUER GmbH
Column	Aminex HPX-87H	Biorad Laboratories Inc.
Pump module	Smartline Pump 1000	KNAUER GmbH
Oven	Jetstream 2 Plus	KNAUER GmbH
UV-detector	UV Detector 2500	KNAUER GmbH
RI-detector	RI Detector 2300	KNAUER GmbH
Software	ChromGate V3.3.1	KNAUER GmbH
System	Smartline	KNAUER GmbH

Table 11-4: Equipment list for the operation of the stirred-tank reactor

Equipment	Type	Manufacturer
AiO-Electrode	-	Dr. Utesch / METAKEM GmbH
Gas flow controller	Model 5876	Brook Instruments
Lactate measurement	TRACE C2 control	TRACE Analytics GmbH
Mass spectrometer for exhaust gas	Omnistar GDS 300	Pfeiffer Vacuum GmbH
Mass flow meter for inlet gas	EL-FLOW	Bronkhorst High-Tech B.V
Mass flow meter for exhaust gas	EL-FLOW Prestige	Bronkhorst High-Tech B.V
ORP-sensor	Pt4805-DPAS-SC-K8S/225	Mettler Toledo GmbH
Peristaltic pump	101U/R	Watson-Marlow limited
pH-sensor	405-DPAS-SC-K8S/225	Mettler Toledo GmbH
Potentiostat	Interface 1000	Gamry Instruments
Power source	2231A-30-3	Keithly
Reactor vessel and control	KSF2000	Bioengineering AG
Reference electrode	RE-1B (Ag/AgCl)	ALS Co. Ltd
Thermostat MS inlet gas cooling	E100 + Ecoline RE107	LAUDA-Brinkmann

11.3. Chemicals, Gases and Consumables

Table 11-5: List of chemicals and buffers used in this study

Compound	Formula	Supplier
2-Mercaptoethansulfonate	$C_2H_5O_3S_2$	Sigma Life Science
α-Aminobenzoic acid	$C_7H_7NO_2$	Sigma Life Science
α-Lactose monohydrate	$C_{12}H_{22}O_{11}$ x H_2O	Sigma Life Science
Ammonium chloride	NH_4Cl	Carl Roth
Ammonium iron(II) sulfate hexahydrate	$(NH_4)_2Fe(SO_4)_2$ x 6 H_2O	Carl Roth
Ammonium sulfate	$(NH_4)_2SO_4$	Carl Roth
Anhydrotetracycline hydrochloride	$C_{22}H_{23}ClN_2O_7$-HCl	Cayman Chemical
Biotin	$C_{10}H_{16}N_2O_3S$	Sigma Life Science
Boric acid	H_3BO_3	Carl Roth
Calcium chloride dihydrate	$CaCl_2$ x 2 H_2O	Carl Roth
Calibration standard glucose/lactate	-	TRACE Analytics
Cobalt chloride hexahydrate	$CoCl_2$ x 6 H_2O	Carl Roth
Copper chloride dihydrate	$CuCl_2$ x 2 H_2O	Carl Roth
Cyanocobalamine	$C_{63}H_{88}CoN_{14}O_{14}P$	Sigma Life Science
Cysteine hydrochloride monohydrate	$C_3H_7NO_2S$-HCl x H_2O	Carl Roth
D-Ca-pantothenate	$C_9H_{17}NO_5Ca$	Sigma Life Science
D-glucose	$C_6H_{12}O_6$	Merck
Dimethyl sulfoxide	C_2H_6OS	Sigma Life Science
Dipotassium dihydrogen phosphate	K_2HPO_4	Carl Roth
Ethanol	C_2H_6O	Carl Roth
Folic acid	$C_{19}H_{19}N_7O_6$	Carl Roth
Fructose	$C_6H_{12}O_6$	Carl Roth
Iron(II) chloride tetrahydrate	$FeCl_2$ x 4 H_2O	Carl Roth
Lipoic acid	$C_8H_{14}O_2S_2$	Sigma Life Science
Magnesium sulfate heptahydrate	$MgSO_4$ x 7 H_2O	Merck
Manganese(II) chloride dihydrate	$MnCl_2$ x 2 H_2O	Merck
Manganese(II) sulfate monohydrate	$MnSO_4$ x H_2O	Merck
MOPS	$C_7H_{15}NO_4S$	Carl Roth
Nickel(II) chloride hexahydrate	$NiCl_2$ x 6 H_2O	Sigma Life Science
Nicotinic acid	$C_6H_5NO_2$	Sigma Life Science

Compound	Formula	Supplier
Nitrilotriacetic acid	$C_6H_9NO_6$	Sigma Life Science
Peptone from meat	-	Thermo Fisher
Phosphoric acid	H_3PO_4	Carl Roth
Potassium chloride	KCl	Carl Roth
Potassium dihydrogen phosphate	KH_2PO_4	Carl Roth
Potassium hydroxide	KOH	Carl Roth
Pyridoxine hydrochloride	$C_8H_{11}NO_3$-HCl	Sigma Life Science
Sodium bicarbonate	$NaHCO_3$	Carl Roth
Sodium chloride	$NaCl$	Carl Roth
Sodium DL-lactate	$NaC_3H_5O_3$	Sigma Life Science
Sodium hexanoate	$NaC_6H_{11}O_2$	Sigma Life Science
Sodium hydroxide	$NaOH$	Merck
Sodium molybdate dihydrate	Na_2MoO_4 x 2 H_2O	Merck
Sodium selenite pentahydrate	Na_2SeO_3 x 5 H_2O	Merck
Sodium sulfide	Na_2S	Riedel-de Haën
Sodium tungstate dihydrate	Na_2WO_4 x 2 H_2O	Sigma Life Science
Thiamine hydrochloride	$C_{12}H_{17}N_4OS$-HCl	Sigma Life Science
Transport buffer TRACE C2	-	TRACE Analytics
Trifluoroacetic acid	$C_2HF_3O_2$	Carl Roth
Trypticase peptone	-	Thermo Fisher
Resazurin	$C_{12}H_7NO_4$	Merck
Riboflavin	$C_{17}H_{20}N_4O_6$	Sigma Life Science
Uracil	$C_4H_4N_2O_2$	Sigma Life Science
Yeast extract	-	Carl Roth
Zinc chloride	$ZnCl_2$	Carl Roth
Zinc sulfate heptahydrate	$ZnSO_4$ x 7 H_2O	Carl Roth

Table 11-6: List of gases used in this study

Gas	Composition	Supplier
Calibration gas for MS	10 v% H_2 / 90 v% Ar	Westfalen Gas
Calibration gas for MS	10 v% CO_2 / 90 v% Ar	Westfalen Gas
Carbon dioxide	99.99 v% CO_2	Westfalen Gas
Forming gas	10 v% H_2 / 90 v% N_2	Westfalen Gas
Nitrogen	99.99 v% N_2	Westfalen Gas

Table 11-7: List of consumables used in this study

Consumable	Type	Manufacturer
Butyl septum	N20	Glasgerätebau Ochs
Centrifuge tubes	15 and 50 mL	Sarstedt
Cryo vials	2 mL	Carl Roth
Cuvettes	Polystyrene 10 x 4 x 45 mm	Sarstedt
Dialysis membranes	Application glucose/lactate	TRACE Analytics
Diaphragms Bioreactor	Silicone DN12	Bioengineering
Flared caps	Aluminum, 20 mm	Glasgerätebau Ochs
Gas filter	Midisart 2000, 0.2 µm	Sartorius
Gas filter	Millex-FG. PTFE, 0.2 µm	Millipore
Glass bottles HPLC	12 x 32 mm, 1.5 mL	CZT
Luer stopper	-	B. Braun
Needles Sterican®	Short bevel facet 1.20 x 40 mm	B. Braun
Pipette tips	200 and 1000 µL	Sarstedt
SafeSeal reaction tube	1.5 and 5 mL	Sarstedt
Syringe	1 mL	Dispomed
Syringe filters Rotilabo®	PVDF, 0.22 µm pore size	Carl Roth
Syringe filters		
Syringes Omnifix®	3, 5, 10, 20, 30 and 50 mL	B. Braun
Tubing set TRACE C2	Dialysis (glucose/lactate)	TRACE Analytics